Master's thesis

NTNU
Norwegian University of Science and Technology
Faculty of Natural Sciences
Department of Physics

Frida Marie Ihle Julbø

MR-based radiotherapy dose painting: modelling studies

Master's thesis in Applied Physics and Mathematics

Supervisor: Kathrine Røe Redalen

June 2020

NTNU
Norwegian University of
Science and Technology

Frida Marie Ihle Julbø

MR-based radiotherapy dose painting: modelling studies

Master's thesis in Applied Physics and Mathematics
Supervisor: Kathrine Røe Redalen
June 2020

Norwegian University of Science and Technology
Faculty of Natural Sciences
Department of Physics

NTNU
Kunnskap for en bedre verden

Preface

This Master's thesis was conducted as part of the study program Biophysics and Medical Technology at the Norwegian University of Science and Technology (NTNU) in Trondheim. The work was performed during the spring of 2020, and builds on a Master's thesis carried out in 2018.

The work is based on image materials and patient data from the OxyTarget study, which aimed to develop new functional MRI protocols for assessing tumor aggressiveness in rectal cancer patients.

I would like to thank my supervisor, Kathrine Røe Redalen, for being supportive and available for questions and guidance throughout these months. I also want to thank her for including me in her research group, and for the opportunity to learn more about this interesting field. Further, I would like to thank René Winter for calculating the ADC maps, helping me prepare the dose painting plans for RayStation, and for helpful input and advice. Finally, I would like to thank Anne Beate Langeland Marthinsen at St. Olavs hospital for all her efforts trying to implement the dose plans into RayStation.

Frida Marie Ihle Julbø
Trondheim, June 2020

Abstract

Background: The outcomes of chemoradiotherapy (CRT) in rectal cancer patients are highly variable depending on the tumor aggressiveness. The tumor is usually irradiated with a uniform dose distribution, even though most tumors have a spatial variation in radiation sensitivity due to factors such as hypoxia. R_2^*-AUC derived from dynamic susceptibility contrast (DSC)-MRI is shown to be significantly associated with the CRT response, and may be used to detect aggressive tumor regions that could benefit from a dose escalation. The aim of this thesis was to individually adapt the radiation dose by creating three-dimensional dose painting by contours (DPBC) prescriptions based on R_2^*-AUC tumor maps.

Materials and methods: 35 rectal cancer patients who underwent DSC-MRI prior to CRT and surgery were analyzed. First, noise filtration and spatial smoothing were performed on the R_2^*-AUC tumor maps. A threshold value, R_2^*-AUC_{CUT} was used to divide the tumor into a radioresistant region, R, and a radiosensitive region, S. DPBC dose prescription maps were then created by assigning a standard dose to S, and an escalated dose to R. R-regions smaller than 1 cm^3 were neglected and considered as a part of S. The relationship between the volume of R and tumor regression grade (TRG) was statistically analyzed by using the Mann-Whitney U-test. A Poisson-based linear quadratic (LQ) tumor control probability (TCP) model was applied to assess the potential advantage of the DPBC prescriptions compared to a uniform dose boost to the whole tumor. The TCP modelling was done both with α and β values found in the literature, and with α values fitted to the TCP for the patient cohort. The tumor cell density was estimated based on apparent diffusion coefficient (ADC) maps calculated from diffusion weighted MRI (DWI), and included in the TCP modelling. Finally, an attempt was made to incorporate the DPBC prescriptions into RayStation to generate dose volume histograms (DVHs).

Results: Three-dimensional DPBC maps were successfully generated based on R_2^*-AUC tumor maps. 16 of the patients had subvolumes larger than 1 cm^3. Patients with TRG3 had significantly larger resistant volumes compared to patients with TRG1 and TRG2. TCP modelling predicted a higher TCP for DPBC than for a uniform dose boost. Overall, the TCP values ended up very low when using the sug-

gested α values from the literature. More realistic TCP values were observed when α was fitted to the cohort TCP. The cell densities estimated from ADC maps were higher than the constant cell density first assumed. When adjusting the constant cell density to 10^7 cells/cm^3, the TCP for the ADC-based cell densities ended up being very similar to the TCP for a constant cell density. Because of issues related to the import of the MR images and subvolume structures into RayStation, DVHs could not be generated.

Conclusion: DPBC based on R_2^*-AUC tumor maps has the potential to escalate the dose to radioresistant regions, and increase the probability of a good radiotherapy treatment outcome. However, further work on including the DPBC plans in RayStation is crucial to investigate the impact on organs at risks (OAR), and the clinical potential of this method. The TCP modelling predicted similar outcomes when using non-uniform, patient-specific cell densities and a constant cell density of 10^7 cells/cm^3. It may therefore be sufficient to assume a constant cell density across the tumor.

Sammendrag

Bakgrunn: Effekten av kjemoradiasjonsterapi (CRT) hos pasienter med endetarmskreft er svært varierende, og er avhengig av aggressiviteten til tumoren. Tumoren bestråles vanligvis med en uniform dosefordeling, selv om de fleste tumorer har varierende strålingsfølsomhet på grunn av faktorer som hypoksi. R_2^*-AUC fra dynamisk susceptibilitetskontrast (DSC) MR har vist seg å være assosiert med tumorrespons ved CRT, og kan potensielt brukes til å oppdage aggressive tumorregioner som kunne dratt nytte av en høyere dose. Målet med dette arbeidet var å individuelt tilpasse stråledosen ved å lage tredimensjonale "dose painting by contours" (DPBC)-planer basert på tumorkart av R_2^*-AUC.

Materialer og metode: 35 pasienter med endetarmskreft som gjennomgikk DSC MR-avbildning før CRT og kirurgi ble analysert. Først ble støyfiltrering og Gaussisk utjevning brukt på R_2^*-AUC tumorkartene. Terskelverdien R_2^*-AUC_{CUT} ble brukt for å dele tumoren inn i et strålingsresistent område, R, og et strålingsfølsomt område, S. DPBC-planer ble deretter lagd ved å tilordne en standard dose til S, og en eskalert dose til R. R-regioner mindre enn 1 cm^3 ble neglisjert og betraktet som en del av S. Korrelasjonen mellom volumet av R og tumorregresjonsgrad (TRG) ble statistisk analysert ved bruk av Mann-Whitney U-testen. En Poisson-basert lineær kvadratisk (LQ) modell for tumorkontroll (TCP) ble anvendt for å vurdere den potensielle fordelen med DPBC-planene sammenlignet med en uniform doseøkning til hele tumoren. TCP-modelleringen ble gjort både med α- og β-verdier funnet i litteraturen, og med α-verdier tilpasset TCP for pasientkohorten. Celletettheten i tumoren ble estimert basert på ADC-kart beregnet fra diffusjonsvektet MR (DWI), og inkludert i TCP-modelleringen. Til slutt ble det gjort et forsøk på å inkludere DPBC-planene i RayStation for å generere dosevolumhistogrammer.

Resultater: Tredimensjonale DPBC-planer ble generert basert på R_2^*-AUC tumorkart. 16 av pasientene hadde subvolumer større enn 1 cm^3. Pasienter med TRG3 hadde signifikant større resistente volum sammenlignet med pasienter med TRG1 og TRG2. TCP-modellering predikerte en høyere TCP for DPBC enn for uniform doseøkning. Alt i alt var TCP-verdiene veldig lave når α-verdiene som var forslått i litteraturen ble brukt. Mer realistiske TCP-verdier ble observert når α

ble tilpasset TCP for pasientkohorten. Celletetthetene estimert fra ADC-kart var høyere enn den konstante celletettheten først antatt. Når den konstante celletettheten ble justert til 10^7 celler/cm^3, endte TCP for ADC-basert celletetthet opp med å være veldig lik som TCP for konstant celletetthet. På grunn av problemer med importering av MR-bildene og subvolum-strukturene i RayStation, kunne ikke dosevolumhistogrammer bli generert.

Konklusjon: DPBC basert på R_2^*-AUC tumorkart har potensial til å øke stråledosen til strålingsresistente regioner, og til å forbedre sannsynligheten for et godt utfall av strålebehandling. Videre arbeid med å inkludere DPBC planene i RayStation er derimot avgjørende for å undersøke effekten på risikoorganer (OAR), og det kliniske potensialet til denne metoden. TCP-modelleringen forutså lignende utfall ved bruk av ikke-uniforme, pasientspesifikke celletettheter og en konstant celletetthet på 10^7 celler/cm^3. Det kan derfor være tilstrekkelig å anta en konstant celletetthet over tumoren.

Contents

Abbreviations

ADC	Apparent diffusion coefficient
AUC	Area under the curve
CRT	Chemoradiotherapy
CT	Computed tomography
CTV	Clinical target volume
DPBC	Dose painting by contours
DPBN	Dose painting by numbers
DSC-MRI	Dynamic susceptibility contrast MRI
DVH	Dose volume histograms
DWI	Diffusion weighted MRI
EPI	Echo planar imaging
fMRI	Functional MRI
FSE	Fast spin echo
Gd	Gadolinium
GTV	Gross tumor volume
HIF	Hypoxia-inducible factor
IMRT	Intensity-modulated radiation therapy
LARC	Locally advanced rectal cancer
LET	Linear energy transfer
LQ	Linear-quadratic
MRI	Magnetic resonance imaging
NTCP	Normal tissue complication probability
OAR	Organs at risk

OER	Oxygen enhancement ratio
PTV	Planning target volume
RF	Radio frequency
ROI	Region of interest
TCP	Tumor control probability
TE	Echo time
TME	Total mesorectal excision
TNM	Tumor node metastasis
TR	Repetition time
TRG	Tumor regression grade

1 Introduction

Modern surgical approaches, as well as preoperative chemoradiotherapy (CRT), have improved the outcomes for rectal cancer patients the last decades [1]. However, rectal cancer is still one of the most frequently diagnosed cancers, and the second most common cause of cancer deaths worldwide [2].

Solid tumors are characterized by a hostile microenvironment containing regions of hypoxia, various blood flow, and uncontrolled cell proliferation [3]. These factors are primarily caused by disorganized tumor vascular networks, and give rise to variable efficiency of radiation and chemotherapy. It has therefore been suggested to irradiate the radioresistant regions of the tumor with an escalated dose, so-called biologically adapted radiotherapy or dose painting [4]. The goal is to increase local control by individually adapting the radiation dose to biological factors of the tumor.

Recent advances in functional imaging and radiotherapy techniques have made it possible to identify radioresistant regions of the tumor, and to deliver a non-uniform dose distribution. Functional MRI (fMRI) is considered a promising tool in dose painting, as it enables visualization of radiobiologically relevant tumor parameters, such as vasculature and oxygenation levels [5, 6]. These characteristics are related to the radioresistance of the tumor, and can hence serve as guidance maps for dose painting. The delivery of a heterogeneous dose distribution is done by using one of two approaches; dose painting by contours (DPBC) or dose painting by numbers (DPBN) [7]. DPBN assigns a specific dose for each tumor voxel according to the voxel value in the corresponding biological image. DPBC, on the other hand, segments radioresistant regions based on a threshold value, and prescribes a uniform dose escalation to these.

Reliable biological tumor maps are essential in dose painting. The OxyTarget study investigated detection of tumor hypoxia by the use of fMRI techniques, including dynamic susceptibility contrast (DSC)-MRI [8]. Moreover, the DSC-MRI-derived parameter R_2^*-AUC was found to be significantly associated with the CRT response in rectal cancer patients, and thus has the potential to be used as a biomarker in hypoxia-targeted dose painting [9].

The main objectives of this thesis were:

1. To create three-dimensional DPBC prescriptions based on pre-CRT R_2^*-AUC tumor maps, and assess the potential advantage of these prescriptions with tumor control probability (TCP) modelling.

2. To estimate the tumor cell density based on apparent diffusion coefficient (ADC) maps, and evaluate the implication on the TCP model.

3. To incorporate the DPBC plans into RayStation, the radiotherapy treatment planning system used at St. Olavs hospital, to create dose volume histograms (DVHs) in order to investigate if the dose delivered to organs at risk (OAR) are changed with the DPBC strategy.

2 Theory

2.1 Magnetic resonance imaging

This section gives a brief introduction to the fundamental principles of magnetic resonance imaging (MRI) relevant for the analyses in this thesis. Subsections 2.1.1 and 2.1.2 are based on similar sections in the author's project thesis [10], which in turn were based on Westbrook et al. [11].

2.1.1 Basic principles

MRI is the observation of nuclear spins. A nucleus has a net spin or angular momentum if it consists of an odd number of protons or neutrons. Hydrogen (^{1}H) has spin $\frac{1}{2}$, and is the nucleus most commonly used in medical imaging. This is because it is abundant in the human body, and because it has a relatively large magnetic moment, μ, due to its solitary proton. When looking at an ensemble of hydrogen nuclei, ^{1}H is classically described as a spinning charged sphere, illustrated in figure 2.1a. The spins are usually randomly orientated, but when an external magnetic field, B_0, is applied, they align to be either parallel or anti-parallel with the magnetic field. This represents the two possible energy states of hydrogen, and is shown in figure 2.1b. Low-energy nuclei align their magnetic moments parallel with B_0 and are termed spin-up nuclei, while high-energy nuclei align their magnetic moments in the anti-parallel direction and are termed spin-down nuclei. There is a slight preference of low-energy nuclei, which results in a small net magnetization vector, M, illustrated in figure 2.1c. It is the interaction of M with B_0 that creates the basis of MRI.

When B_0 is applied, the magnetic moments of hydrogen get an additional spin that makes them follow a circular path around B_0. This is called precession, and the precessional frequency is known as the Larmor frequency, ω_0. ω_0 is determined by the Larmor equation

$$\omega_0 = B_0\gamma, \tag{2.1}$$

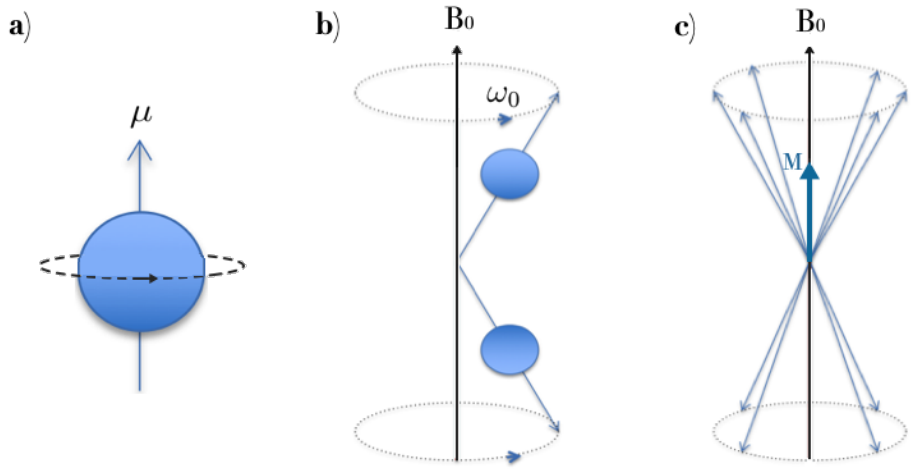

Figure 2.1: a) The hydrogen nucleus can be thought of as a small spinning sphere, inducing a magnetic moment, μ. b) When B_0 is applied, the spins starts precessing around the axis of the external magnetic field with the Larmor frequency, ω_0, and align either parallel or anti-parallel with B_0. c) There is a slight preference of spins aligned parallel to B_0, which results in a small net magnetization vector, M.

where γ is the gyromagnetic ratio. The gyromagnetic ratio describes the relationship between the magnetic moment and the angular momentum, and is characteristic for every MR active nucleus. For a given B_0, each nucleus will therefore precess at a specific ω_0, which makes it possible to only image the substance of interest (often ^{1}H). In order to produce a detectable MR signal, the net magnetization vector needs to move out of alignment with B_0. This is done by applying a second external field, B_1, also called a radio frequency (RF) pulse, with energy equal to the Larmor frequency of hydrogen. The RF pulse is usually described by the flip angle, α, which is the angle between M and B_0. The plane perpendicular to B_0 is called the transverse plane, and the amount of magnetization present in this plane affects the magnitude of the signal.

When the RF pulse is turned off, M tries to realign with B_0, and relaxation occurs. There are two types of relaxation: T_1 recovery and T_2 decay. The relaxation processes happen at the same time, but are independent of each other. T_1 relaxation is the recovery of longitudinal magnetization, and is caused by loss of energy to the surrounding lattice. This relaxation is characterized by the time constant T_1. T_2 relaxation occurs due to interaction between the magnetic fields of neighbouring

nuclei. This makes individual spins experience small magnetic field differences, and gradually start to dephase in the transverse plane. T_2 decay is characterized by the transverse relaxation time T_2, or by the relaxation rate R_2, which is inversely proportional to T_2. In practice, transverse magnetization decays much faster than predicted due to inhomogeneities in the magnetic field. This relaxation rate is denoted R_2^*, and described by:

$$R_2^* = R_2 + R_2', \tag{2.2}$$

where R_2' is the relaxation rate contribution from magnetic field inhomogeneities.

2.1.2 Pulse sequences and spatial encoding

The MRI signal is recorded by receiving coils that induce a current when exposed to an area of a moving magnetic field. To create an image, the signal needs to be spatially localized in three dimensions. This is done by applying magnetic field gradients, one for each direction x, y and z. The gradients alter B_0 in a linear way by adding or subtracting magnetic field strength to B_0 relative to the isocentre to generate a specific resonance frequency for every point along the axis of the gradient. A new effective magnetic field, B_{eff}, is then created as illustrated in figure 2.2. The gradients make it possible to only excite spins in selected areas by matching the frequency of the excitation pulse with the Larmor frequency at the desired position.

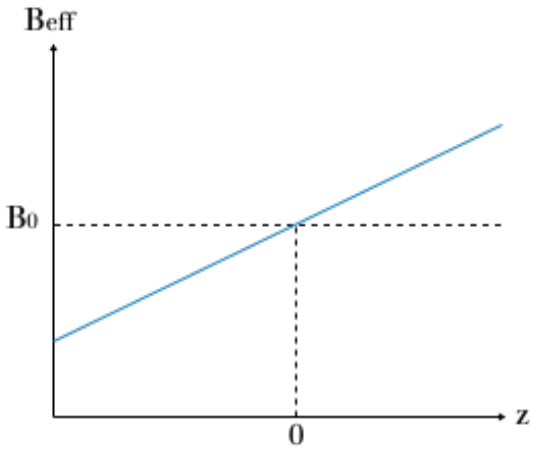

Figure 2.2: The gradient alters B_0 in a linear way, and creates a new effective magnetic field, B_{eff}, that is dependent on the position along the gradient axis.

The spatial frequencies of the signals are stored as an array of numbers in a 2D matrix called k-space. The k-space is filled during the scan, usually one line per acquisition. Each point in k-space contains information about every pixel in the final MR image. The center of the k-space contains low spatial frequency information, and provide information on the general shape, contrast and brightness of the image. The outer parts of the k-space contain high spatial frequency information, and provide information on details, edges and contours. By applying inverse Fourier transform on the k-space, an MR image of the object can be obtained.

Pulse sequences are combinations of RF pulses and gradients that make it possible to record an MR signal with the desired information. A pulse sequence is classified as T_2 weighted if it acquires MR images with a contrast depending on the tissues' T_2 relaxation. T_2 weighted MRI is fundamental for visualising anatomy and detecting abnormalities, and is often acquired with a spin echo sequence. To regenerate the signal loss created by the T_2^* decay, the spin echo sequence utilizes a 180° refocusing pulse to rephase the spins, as illustrated in figure 2.3. The rephasing is called a spin echo, and the time it occurs at is defined as the echo time (TE).

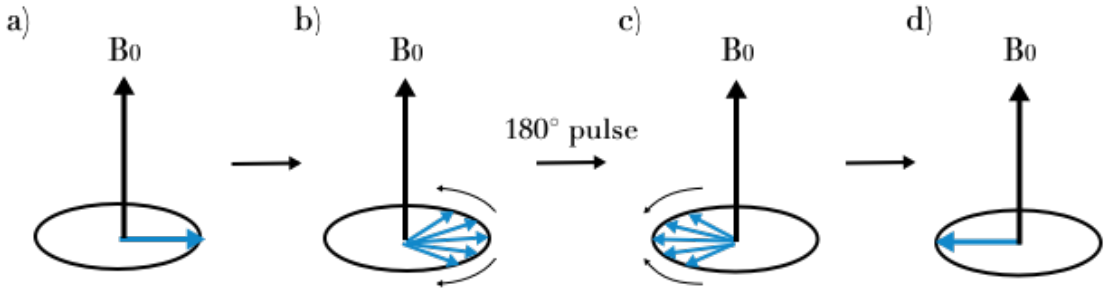

Figure 2.3: Illustration of a spin echo. a) Immediately after the excitation pulse is applied, the spins are in the same phase. b) The spins starts to dephase due to T_2^* decay. c) The dephasing gets reversed by applying a 180° pulse that flips the spins. d) When all the spins are in the same phase again, at t=TE, a spin echo occurs.

A spin echo sequence along with the timing of the different gradients are shown in figure 2.4. First, a slice selection gradient, G_{slice}, is applied simultaneously as the 90° excitation pulse. The slice thickness is determined by the frequency range of the exciting RF pulse, called the transmit bandwidth. When the image slice has been selected, the signal needs to be located along both axes of the slice. This is done by using frequency and phase encoding gradients. The frequency encoding gradient

produces a frequency shift along one axis of the image, and is applied when the signal is received. It is therefore often called the readout gradient, G_{ro}. The phase encoding gradient, G_{phase}, is applied after the excitation pulse, and produces a phase shift along the remaining axis. Multiple phase-encoding steps must be used, one for each acquisition, in order to sort out spatial information in this direction. The time between each 90° excitation pulse is called the repetition time (TR).

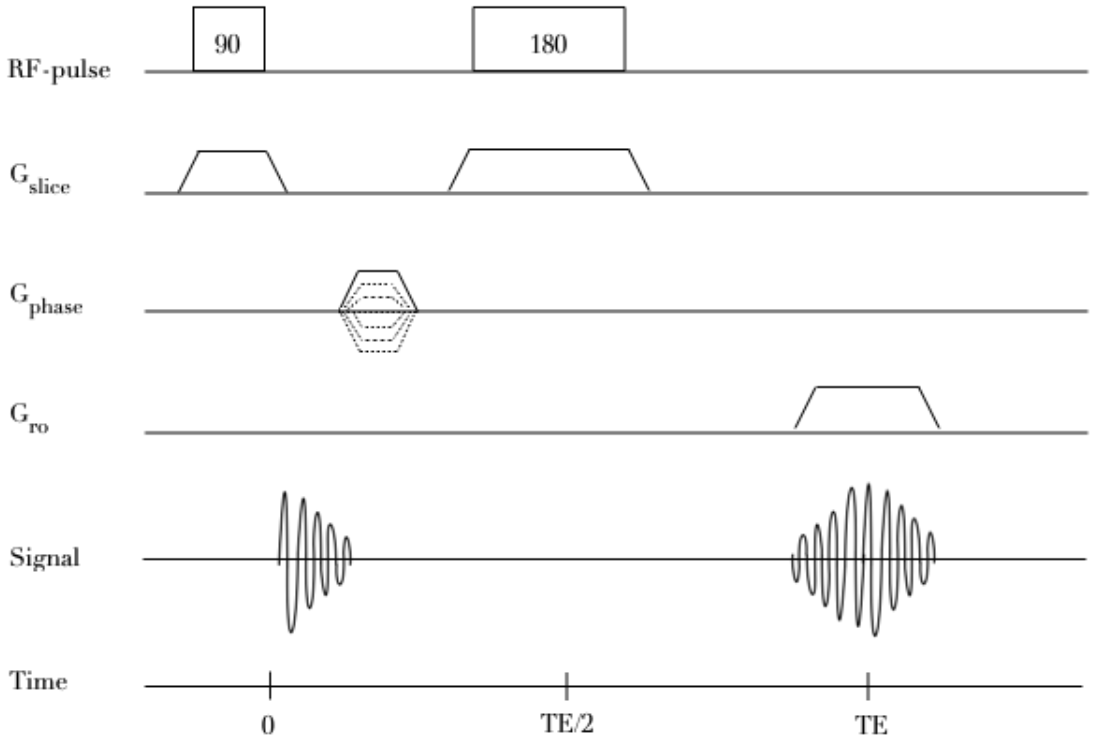

Figure 2.4: Schematic illustration of a spin echo pulse sequence. G_{slice} and the 90° excitation pulse are applied simultaneously, followed by G_{phase} and G_{ro}. A 180° pulse is applied at t=TE/2, and creates a spin echo at t=TE.

T_2 weighting is achieved when both the TR and TE are long (typically 2000 ms and 90 ms, respectively). Fast spin echo (FSE) sequences are often used to shorten the acquisition times. FSE sequences use multiple 180°-refocusing pulses after the excitation pulse to generate a train of echoes. This makes it possible to sample several k-space lines per excitation.

2.1.3 Functional MRI

Unlike conventional anatomical imaging, functional MRI (fMRI) enables assessment of tissue structures that can be used to characterize physiological processes of a tumor, such as oxygenation levels and perfusion related parameters [12, 13].

2.1.3.1 Dynamic susceptibility contrast MRI

Dynamic susceptibility contrast MRI (DSC-MRI) is a dynamic contrast based imaging method, which is useful to describe vascular characteristic of a tumor [14, 15]. The signal change in each image voxel is measured as a function of time by acquiring MR images before, during, and after injecting an MR contrast agent [16]. Gadolinium (Gd)-based contrast agents are most commonly used, and normally given as a single bolus intravenous injection [14]. The Gd-component is paramagnetic, and possesses a large magnetic moment which alters the local magnetic susceptibility [13]. As the Gd flushes through the blood vessels, it creates microscopic disturbances of the magnetic field causing the spins to precess at different rates and rapidly dephase [14]. The relaxation for nearby protons is hence enhanced, and R_2^* increased. This can be seen as a signal loss in tissues where the contrast agent is distributed, as shown in Figure 2.5. DSC-MRI will also enhance T_1 relaxation, but this effect can be neglected if the contrast agent does not leak out of the intravascular area.

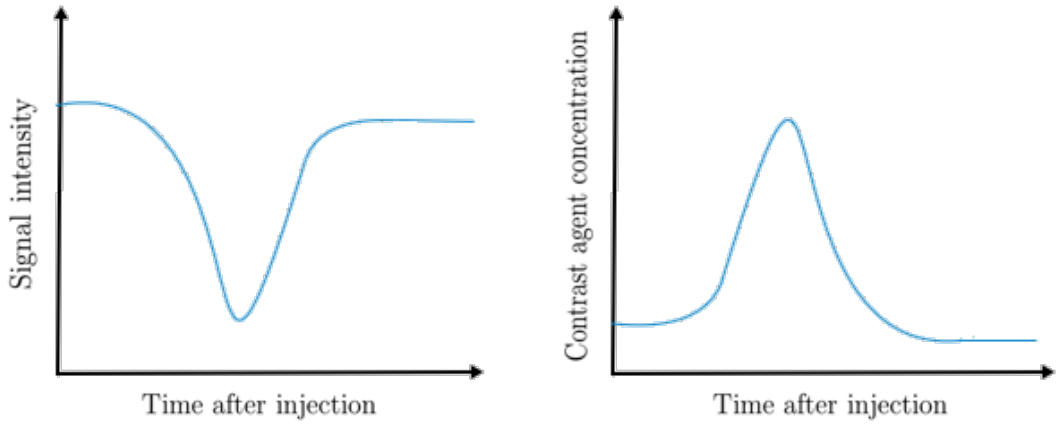

Figure 2.5: Signal intensity and contrast agent concentration as a function of time after the contrast agent has been injected. In tissues where the contrast agent is distributed, a signal loss is seen due to enhanced T_2^* effects. The signal intensity increases again as the contrast agent concentration decreases.

DSC-MRI data can be acquired by using an echo planar imaging (EPI) sequence

[13]. The EPI technique is rapid and provides high temporal resolution as it collects data from multiple k-space lines following a single RF excitation pulse. The number of k-space lines (echoes) acquired per excitation is called the EPI-factor [17]. In tumors, the contrast agent can easily leak out of the vessels, and T_1 effects can not be neglected. To avoid contamination from T_1 relaxation, it can be beneficial to use a 3D T_1-weighted multi-echo EPI sequence [18]. The dynamic change in R_2^* can then be estimated by assuming a mono-exponential signal intensity decay as a function of TE [14]:

$$S(t, TE_n) = S_{PD}(t)e^{-TE_n \cdot R_2^*(t)}, \tag{2.3}$$

where n labels the echo number, and $S_{PD}(t)$ is the peak signal intensity in the absence of T_2^*-effects (TE=0). The resulting R_2^*-information can be used to derive parameters from each voxel, and to assess characteristics about the tumor, such as the vasculature and hypoxia [9].

2.1.3.2 Diffusion weighted MRI

Diffusion weighted MRI (DWI) is a functional MRI technique that generates signal contrast based on differences in Brownian motion of water molecules [19]. Different tissues of the human body have characteristic diffusion properties, due to differences in the cellular architecture such as cell size, organization and packing density. The diffusion is also affected by the water exchange between intracellular and extracellular compartments [20].

DWI is used to evaluate the molecular function and micro-architecture, and provides both qualitative and quantitative information about the diffusion properties without using intravenous contrast media [19]. DWI data is commonly acquired with an EPI sequence, based on a spin echo sequence where symmetric diffusion-sensitizing gradients are applied on either side of the 180°-pulse. Stationary spins are unaffected by the gradients, while diffusing spins dephase and cause signal loss. Areas with a large amount of diffusion along the gradient axis, such as blood vessels, will therefore appear dark in a diffusion-weighted image, and areas with limited diffusion will appear bright. The DWI parameter b decides the diffusion weighting and is expressed

as:

$$b = \gamma^2 G^2 \delta^2 \big(\Delta - \delta/3\big), \tag{2.4}$$

where γ is the gyromagnetic ratio, G is the diffusion gradient strength, δ is the duration of the diffusion gradient, and Δ is the time between the start of the first and second gradient [13]. $b = 0$ corresponds to no diffusion-weighting, while increasing b-values lead to increased diffusion-weightings. Figure 2.6a shows an example of a diffusion weighted image with $b = 1000$ s/mm^2.

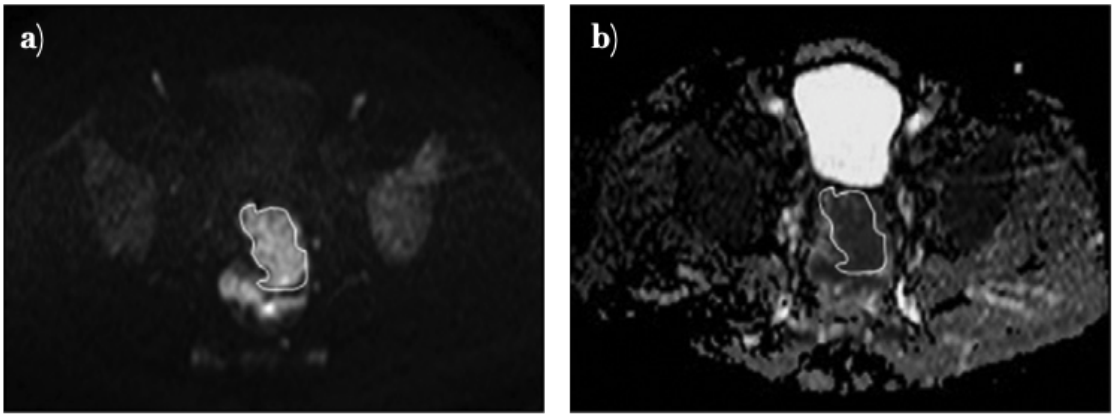

Figure 2.6: Pre-CRT images of a patient with rectal cancer. a) Diffusion weighted image where the tumor is seen as a bright mass. b) The corresponding ADC map, where the signal intensity of the tumor is lower compared to the surrounding tissue. The images are from [21].

In order to get quantitative information about the diffusion, apparent diffusion coefficient (ADC) maps can be calculated. The ADC value in one voxel is defined as:

$$\text{ADC} = \frac{\ln[S_2(x,y,z)/S_1(x,y,z)]}{b_1 - b_2}, \tag{2.5}$$

and can in theory be estimated from measuring the signal intensity for two b values. However, generally more than two b values are applied in order to get more accurate ADC values. Tumors have lower ADC compared to surrounding normal tissue, as seen in figure 2.6b. The low diffusivity in tumors is not fully understood, but

is probably related to the higher cellularity in addition to a more chaotic tissue structure in the tumor [20].

2.2 Cancer

Normal tissues have a net production of new cells that balances the loss of cells from the tissue. Cancer arises when the production of new cells exceeds cell loss, which happens because of uncontrolled cell division and failure for self-elimination [22]. The development of normal cells to tumor cells involves a stepwise progression of molecular and morphologic changes, where oncogenes are activated and tumor suppressor genes are inactivated. Hanahan and Weinberg suggested to organize these traits into ten essential alterations in cell physiology [23, 24]:

1. Self-sufficiency in growth signals
2. Insensitivity to anti-growth signals
3. Evading apoptosis
4. Limitless replicative potential
5. Sustained angiogenesis
6. Tissue invasion and metastasis
7. Genome instability and mutation
8. Tumor-promoting inflammation
9. Reprogramming energy metabolism
10. Evading immune destruction

These capabilities are called the hallmarks of cancer, and are according to Hanahan and Weinberg shared in common by the majority and perhaps all types of cancer.

2.2.1 Tumor vasculature

The vasculature in tumors develops very differently than in normal tissue, and is associated with an abnormal microenvironment including limited oxygen and nutrient supply, increased interstitial fluid pressure and disorganized blood flow, as seen in figure 2.7 [3, 25]. Hostile tumor microenvironmental parameters, such as hypoxia,

can directly or indirectly influence the resistance to irradiation and chemotherapy [26].

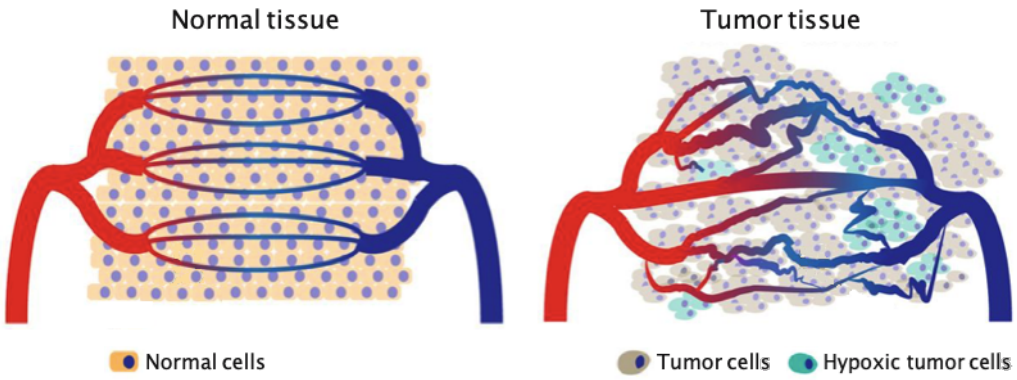

Figure 2.7: Normal tissues have a well-organized vessel network that ensures sufficient oxygen and nutrient supply. The blood vessels in tumor tissues, on the other hand, are irregular and chaotic, resulting in a disorganized blood flow that make oxygen and nutrient supply inefficient. Figure based on [27].

The vasculature is essential for tumor growth and metastatic spread [25, 28]. Tumor cells must be close to a nutritive blood vessel to survive and proliferate, which requires the tumor to develop its own blood supply from adjacent tissues. This process is known as angiogenesis, and is triggered by signalling molecules released by the tumor cells. Normal cells restrain angiogenesis by releasing a balanced amount of inhibitors and activators. Tumors, however, have an increased production of activators as well as a downregulation of inhibitors that causes an uncontrolled growth of new blood vessels [29]. The newly formed blood vessels are irregular and have branching patterns that tend to make the them leaky [26]. The chaotic vessel organization along with the leakiness causes a variable blood flow that make the delivery of oxygen and nutrients to the tumor inefficient [28].

2.2.2 Tumor hypoxia

Tumor cells may become hypoxic due to the irregular vasculature that frequently reduces the oxygen delivery to the expanding tumor. Healthy tissues normally have a median oxygen pressure in the range 40–60 mmHg (pO_2), while half of all solid tumors have pO_2 values lower than 10 mmHg [30]. Tissues that are completely depleted of oxygen are called anoxic. Hypoxia in tumors can result from two different

mechanisms, shown in figure 2.8 [31]. Chronic hypoxia results from limited diffusion of oxygen to the tumor cells because of increasing distance to a nutritive blood vessel. If the cells get farther away than a distance of about 70 μm from the capillaries, they will receive less oxygen than needed [3, 31]. The oxygen delivery may also be perfusion-limited due to temporary closing or blockage of a tumor blood vessel. This condition is often transient, and is called acute hypoxia.

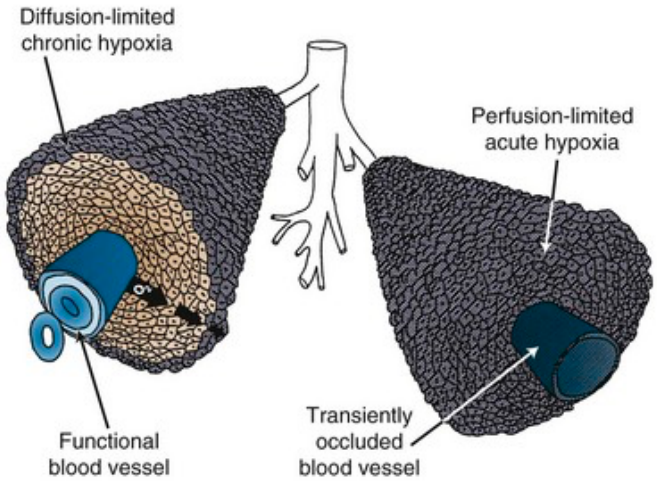

Figure 2.8: Chronic hypoxia occurs when cells are too far away from a blood vessel to get sufficient oxygen supply, while acute hypoxia results from temporary closing or blockage of a tumor blood vessel. Figure adapted from [32].

It is shown that up to 50–60% of locally advanced solid tumors can have hypoxic or anoxic areas that are heterogeneously distributed within the tumor mass [33]. In order to adapt to the hypoxic environment, the tumor cells activate the hypoxia-inducible factor 1 (HIF-1). This is a transcription factor that facilitates oxygen delivery and adaptation to oxygen deprivation by regulating the expression of certain genes [31]. In normal cells, HIF-1α is kept at a low level because it is degraded, but under hypoxic conditions, HIF-1α becomes stabilized and promote transcription of target genes that for instance can lead to upregulation of angiogenic factors [34]. HIF-1 activation also correlates with promotion of metastasis and promotion of further metabolic imbalances, which are key steps in tumor progression.

Tumor hypoxia plays an important role in cancer treatment. Well-oxygenated cells are more sensitive to ionizing radiation than hypoxic cells, as the oxygen makes the DNA damage produced by free radicals permanent. However, in the absence of

oxygen, the damage can be repaired. This is known as the oxygen effect [31]. The enhancement of biological effect of ionizing radiation due to the presence of oxygen is defined by the oxygen enhancement ratio (OER):

$$\text{OER} = \frac{\text{dose to produce a given effect without oxygen}}{\text{dose to produce the same effect with oxygen}}. \tag{2.6}$$

Hypoxia can also influence tumor cell sensitivity to chemotherapy [26, 30]. There will be a decreased drug delivery to the hypoxic cells, as they lie far away from nutritive blood vessels. Also, the majority of anticancer drugs are only effective against rapidly proliferating cells, and hypoxic cells tend to grow more slowly.

2.2.3 Rectal cancer

Tumors located in the lower 15 centimetres of the rectum are classified as rectal tumors [35, 36]. An anatomical illustration of the intestines is shown in figure 2.9. Rectal cancer usually begins as a polyp on the inner lining of the rectum, and then grows slowly over a period of several years [37]. Once cancer forms, it can grow into the rectum wall and invade nearby lymph nodes. The cancer cells can also penetrate blood vessels and spread to other organs and tissues. The risk of developing rectal cancer increases with age, and the median age at diagnosis in Norway is 69 years [38]. There are no clear reasons why people develop rectal cancer, but lifestyle factors including smoking, physical activity and diet, seem to play a role [39]. This may explain why the incidence of rectal cancer is highest in Western countries.

Typical symptoms of rectal cancer are change in stool habits, bowel pain, rectal bleeding, and findings of polyps by endoscopy. According to the guidelines provided by The Norwegian Directorate of Health, a patient that presents with any of these symptoms is referred to further examinations commonly including endoscopy with biopsy [35]. If the patient is diagnosed with rectal cancer, radiological imaging is performed for preoperative investigation of the tumor. This is crucial for choosing the right treatment strategy and making an accurate prognosis. The staging of rectal cancer is done according to the tumor node metastasis (TNM) system presented in table 2.1 [41]. T_2 weighted and diffusion weighted MRI are recommended for localizing and staging of the primary tumor (T), and for assessing the involvement

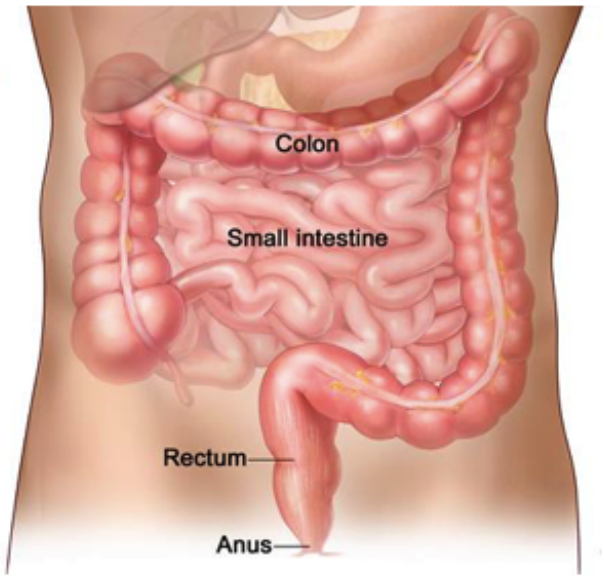

Figure 2.9: An anatomical illustration of the intestines, showing the location of the rectum and the colon. Figure adapted from [40].

of regional lymph nodes (N). Figure 2.10 shows an axial T_2 weighted MR image with the delineated rectal tumor. Distant metastasis (M) is most commonly found in the lungs and liver, and is preferably evaluated with CT scans of the chest and abdomen.

The main treatment of rectal cancer is surgical removal of the primary tumor and nearby lymph nodes [35, 36]. Total mesorectal excision (TME) surgery is considered the gold standard rectal cancer surgery, as it largely reduces the local recurrence rate compared to conventional techniques [42]. TME surgery involves complete removal of the mesorectum, which is the perirectal fat that surrounds the rectum. This ensures a larger circumferential resection margin, which has been shown to have a significant impact on local recurrence and survival rates [43]. However, the surgery has some potential side effects. If the cancer infiltrates the anal sphincter or the pelvic floor, the patient might need a permanent colostomy [1]. Patients can also experience difficulties related to defecation, urination and sexual function.

For patients with locally advanced rectal cancer (LARC), defined as stage T3-4 or N+ according to the TNM system, it can be beneficial to perform preoperative CRT, which is a combination of chemotherapy and radiation therapy. About 30-40% of the patients with rectal cancer receive CRT [35]. The purpose is to reduce the the risk of

Table 2.1: Explanation of the different stages in rectal cancer according to the American Joint Committee on Cancer (AJCC) [41].

Primary Tumor (T)		**Regional Lymph Nodes (N)**		**Distant Metastasis (M)**	
TX	Primary tumor cannot be assessed	NX	Regional lymph nodes cannot be assessed	M0	No distant metastasis
T0	No evidence of primary tumor	N0	No regional lymph node metastasis	M1	Distant metastasis
T1	Tumor invades submucosa	N1	Metastasis in 1-3 regional lymph nodes		
T2	Tumor invades muscularis propria	N2	Metastasis in 4 or more regional lymph nodes		
T3	Tumor invades through the muscularis propria into pericolorectal tissues				
T4a	Tumor penetrates to the surface of the visceral peritoneum				
T4b	Tumor directly invades or is adherent to other organs or structures				

local recurrence by shrinking the tumor before surgery, and make it easier to remove. The radiation field includes the tumor and mesorectum, and also regional lymph node regions that are not removed by surgery. A conventional radiotherapy regime (2 Gy×25 fractions) with chemotherapy is usually used, but a short-course regimen (5 Gy×5 fractions) is an option for elderly patients and patients with reduced general condition. MRI is used after the CRT to evaluate how the tumor has responded, and TME surgery is normally scheduled 6-8 weeks after completion of CRT. After surgery, the TN stage is reevaluated based on a pathological examination of the resected tumor specimen, and a histologic treatment response is assessed by using the tumor regression grade (TRG) system presented in table 2.2 [44]. If the tumor responds very well to CRT, the patient may not need surgery, and a watch-and-wait approach is considered.

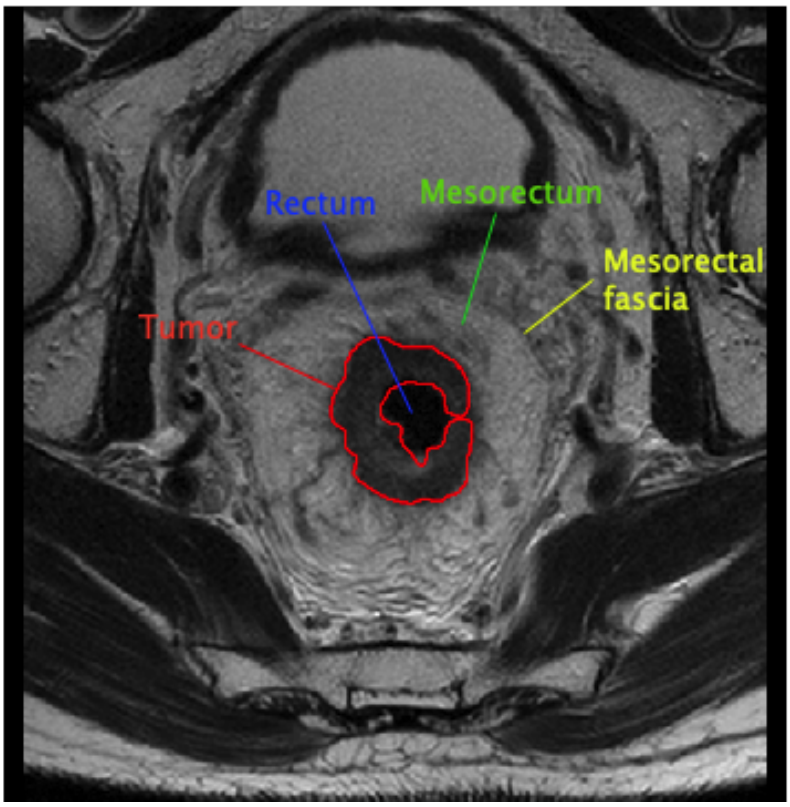

Figure 2.10: Visualization of rectal cancer in an axial T_2 weighted MR image. The tumor delineation, rectum, mesorectum and mesorectal fascia are denoted.

Table 2.2: Tumor regression grading according to the College of American Pathologists (CAP) [44].

	Tumor regression grade
TRG0	No viable cancer cells (complete regression)
TRG1	Single cells or small groups of cancer cells (moderate response)
TRG2	Residual cancer outgrown by fibrosis (minimal response)
TRG3	Minimal or no tumor killed or extensive residual cancer (poor response)

The response to CRT in LARC differs among individual tumors. However, if one could assess the aggressiveness of the tumor before starting the treatment, it would be possible to predict the response to CRT, and make a more individualised treatment approach by for instance escalating the dose for aggressive tumors [45, 46]. DSC-MRI can be a valuable tool for this purpose, as it provides information about hypoxia and abnormal vasculature, which are characteristics related to tumor ag-

gressiveness. Syversen used DSC-MRI data from the OxyTarget study to investigate if R_2^* measurements could predict CRT outcome [8, 9]. She found that the tumoral median area under the curve (AUC) of the normalized R_2^* time course (R_2^*-AUC) obtained from DSC-MRI was significantly associated with CRT response in rectal cancer patients, where a high R_2^*-AUC value was related to poor response. These findings indicate that tumor regions of high R_2^*-AUC values may benefit from a radiation dose escalation.

2.3 Radiobiology

Radiobiology is the study of the effects of ionizing radiation on biologic systems [22, 31]. Ionizing radiation has sufficient energy to eject one or more orbital electrons from the atom or molecule, and is characterized by the localized release of large amounts of energy. DNA is the most critical target for radiation-induced cell killing, as it is central to all cellular functions and is only present in two copies [47]. The DNA can be damaged by direct or indirect action of the radiation. In direct action the radiation interacts directly with the critical target in the cell. This process is dominant for radiations with high linear energy transfer (LET), such as neutrons or protons. The radiation may also interact with other atoms or molecules in the cell (mainly water) to produce free radicals that are able to damage the DNA through diffusion. This is called indirect action of radiation, and is the most common process of DNA damage by low LET radiations, such as x-rays.

Radiation-induced cell damage can be divided into lethal, sublethal and potentially lethal damage [31, 48]. Lethal damage is irreparable and leads to cell death, while sublethal damage can be repaired under normal circumstances. Potentially lethal damage causes cell death under ordinary circumstances, but can be repaired if post-irradiation conditions are suboptimal for growth. The aim of radiotherapy is to deliver a sufficient dose of radiation to the tumor, while limiting the biological consequences for normal tissues. The relationship between the probability of tumor control and the likelihood of normal tissue damage is expressed by the therapeutic ratio, defined as the percentage of tumor control that can be achieved for a given level of normal tissue complications. This concept can be illustrated by comparing the dose-response relationships, as seen in figure 2.11.

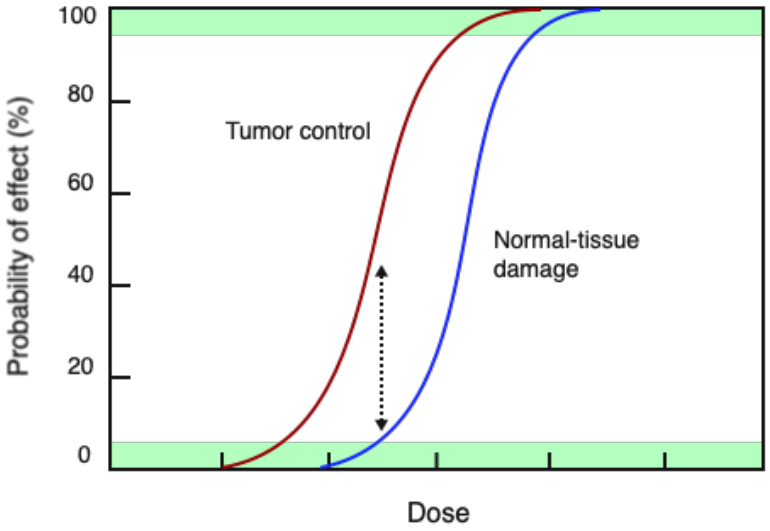

Figure 2.11: Dose–response relationships for both TCP and normal tissue complication probability (NTCP). The upper green area represents the desirable probability of tumor control, while the lower green area represents the acceptable risk of normal tissue complication. The dashed arrow indicates the therapeutic ratio. Well separated curves improves the therapeutic ratio, and lead to a more favorable trade-off between tumor control and toxicity.

The difference between normal tissue and tumor response is enhanced by dose fractionation, which is common practice in modern radiotherapy. It is particularly five mechanisms that influence the outcome of fractionated radiotherapy, and account for the greater sparing of normal tissues compared to tumors. These are known as the five R's of radiobiology, and include repair, reoxygenation, redistribution, repopulation and intrinsic radiosensitivity [31, 49]. Normal tissue is spared when dividing a dose into several fractions due to repair of sublethal damage between the doses, and repopulation of cells. Dose fractionation will simultaneously increase the damage to the tumor, because of reoxygenation of hypoxic cells and redistribution of cells into the radiosensitive phases of the cell cycle.

2.4 Tumor response modelling

A cell survival curve describes the relationship between the radiation dose and the fraction of irradiated cells that survive [31, 48]. Several models have been proposed to define the shape of cell survival curves, but today it is most common to use the linear-quadratic (LQ) model, illustrated in figure 2.12. The LQ model is based on

the fact that chromosome aberrations, or lethal damage, result from the interaction of two separate breaks. According to this model, the breaks can be produced either by a single ionizing event or by two separate events. The cell survival is therefore assumed to be dependent on two factors, one linear component proportional to the dose, and one quadratic component proportional to the square of the dose. Using the LQ model, the expression for the survival fraction of cells irradiated with n fractions of dose d is given by:

$$S^n = e^{-\alpha nd - \beta nd^2} = e^{-\alpha nd(1+\frac{\beta}{\alpha}d)}, \tag{2.7}$$

where α and β are the probabilities of inducing chromosomal aberrations by a single ionizing particle and by two separate ionizing particles, respectively. The α/β-ratio gives the dose at which the two contributions to cell killing are equal.

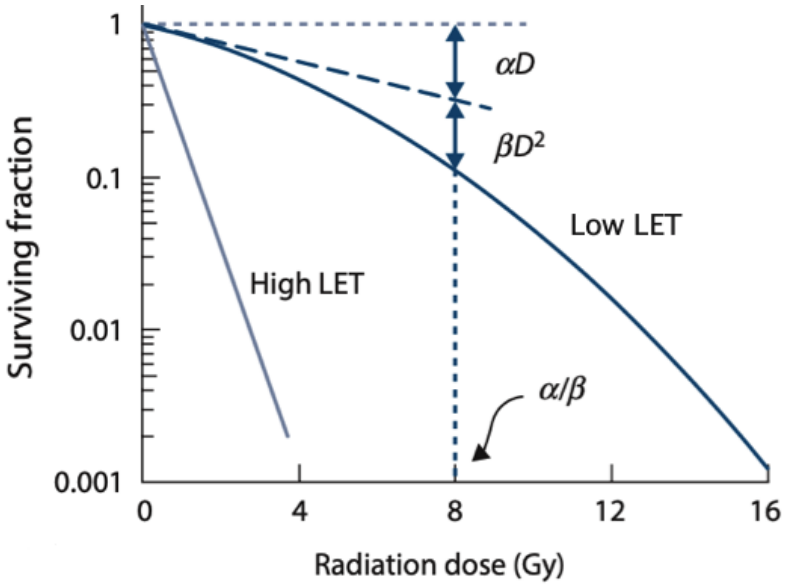

Figure 2.12: Typical cell survival curves for high LET and low LET radiation, showing the LQ relationship between cell survival and radiation dose. At low doses, chromosomal aberrations most likely result from a single electron, and the survival curve appear linear. At higher doses, the two chromosome breaks may also result from two separate electrons. If the quadratic component dominates, the survival curve becomes more curved. This is typical for low LET radiation. Figure adapted from [47].

The radiation effects on tissues are commonly divided into acute and late effects [31, 48]. Acute effects occur within a few hours or days after irradiation in rapidly

proliferating tissues, such as the skin and most tumors. Late effects first appear after a delay of months or years, and are usually more severe as they mainly occur in slowly proliferating tissues, such as the kidney, heart, lung and central nervous system. Early responding tissues typically have a high α/β-ratio of about 10 Gy, making them sensitive to total radiation dose. Late responding tissues tend to have a smaller α/β-ratio of about 2 Gy, and a curvier survival curve. They have increased survival at low doses, and benefit a lot more from fractionation than early responding tissues.

2.4.1 Tumor control probability

Tumor response modelling is commonly based on the LQ model [28, 47, 50]. The expected number of surviving clonogenic cells can be expressed by using equation (2.7):

$$N_s = N_0 S^n = N_0 e^{-\alpha n d(1+\frac{\beta}{\alpha}d)}, \tag{2.8}$$

where N_0 is the initial number of clonogenic cells. The number of surviving clonogens, X, is then approximately Poisson distributed:

$$P(X = x; N_s) = \frac{e^{-N_s} N_s^x}{x!}. \tag{2.9}$$

The TCP corresponds to the probability that no clonogenic cells survive, given that the average number of clonogens per tumor after irradiation is N_s, and is found by setting $x = 0$ in equation (2.9):

$$TCP = P(X = 0; N_s) = e^{-N_s}. \tag{2.10}$$

By combining equation (2.8) and (2.10), and using that $N_0 = \rho_0 V$, the TCP can be expressed as:

$$TCP = e^{-\rho_0 V S^n} = e^{-\rho_0 V e^{-\alpha n d(1+\frac{\beta}{\alpha}d)}}, \tag{2.11}$$

where ρ_0 is the initial tumor cell density and V is the tumor volume. It has been shown that most tumors have non-uniform clonogenic cell density, but conventionally ρ_0 is assumed to be homogeneous [5, 50]. For a non-uniform dose distribution, the tumor can be divided into a number of independent subvolumes. Within each of these volumes, the dose d_i can be considered locally uniform. The TCP for an individual subvolume is given by:

$$TCP_i = e^{-\rho_{0,i} V_i e^{-\alpha_i n d_i (1+\frac{\beta_i}{\alpha_i} d_i)}}, \tag{2.12}$$

where V_i is the volume, $\rho_{0,i}$ is the initial cell density, and α_i and β_i is the radiobiologic factors of the i-th subvolume. Finally, the TCP for the whole tumor is the product of each subvolume's TCP:

$$TCP = \prod_{i=1}^{N} TCP_i, \tag{2.13}$$

where N is the number of subvolumes. TCP modelling gives a good description of the main characteristics of radiation response, but should be used with caution [51, 52]. The TCP value should primarily be used as a relative measure to compare different treatment techniques, such as fractionation schemes or dose escalation.

2.5 Radiotherapy

2.5.1 Definitions of volumes

It is important to use clear definitions for volumes related to both tumor and normal tissues in radiotherapy treatment planning to ensure comparable and reproducible clinical results. The International Commission on Radiation Units and Measurements has defined the following volumes [53]:

- Gross tumor volume (GTV)
- Clinical target volume (CTV)
- Planning target volume (PTV)
- Organs at risk (OAR)

The GTV is an anatomical volume, which can be described as the visible extent of malignant growth. The CTV is a volume containing GTV and/or areas with a certain probability of subclinical disease relevant to treatment. Delineations of CTV are mainly based on clinical experience and guidelines. The PTV includes the CTV plus an additional margin to compensate for uncertainties related to organ motions, patient positioning and intra-treatment variations. The PTV is defined to ensure that the prescribed dose is delivered to the CTV with an acceptable probability, when taking into account all possible geometrical uncertainties. OARs are organs or other normal structures that need to be spared because of possible side effects, and will therefore influence the treatment planning if located near the tumor.

Computed tomography (CT) is considered the primary modality for volume definition and dose calculation in radiotherapy treatment planning [54, 55]. MRI is commonly performed for staging, and is therefore available as a visual aid when delineating target volumes. Due to its superior soft tissue contrast, MR-based treatment planning is of increasing interest [56].

2.5.2 Dose painting

Tumors have traditionally been irradiated with a uniform dose distribution [57]. However, most tumors have a spatial variation in radiation sensitivity due to varying levels of oxygen supply, cell proliferation and density within the tumor mass. Dose painting is a radiotherapy technique where a non-uniform dose distribution is prescribed and delivered to the tumor [58, 59]. The idea is to increase the dose in regions recognized as more radioresistant, in order to improve local control for each individual tumor. Subvolumes that may benefit from a dose escalation can be identified by assessing radiobiological information obtained from functional imaging. The concept of delivering a heterogeneous dose distribution to the tumor was first studied soon after the development of intensity-modulated radiation therapy (IMRT) [60]. Recent advances in functional imaging, such as MRI and PET, allow a more precise targeting of subvolumes in the tumor, and make dose painting more feasible [61].

The first step in dose painting is to find a reliable imaging biomarker that provide information about tumor biology and radiosensitivity [7, 62, 63]. The prescribed

dose distribution is then based on maps that geographically represent the imaging biomarker across the tumor volume by using one of two approaches, as seen in figure 2.13. In DPBN, a specific dose is assigned for each voxel inside the tumor based on the voxel intensity of the corresponding functional image of the tumor. Voxel-based dose prescription will, in theory, provide a highly individualized treatment. However, it requires high precision in imaging and dose delivery.

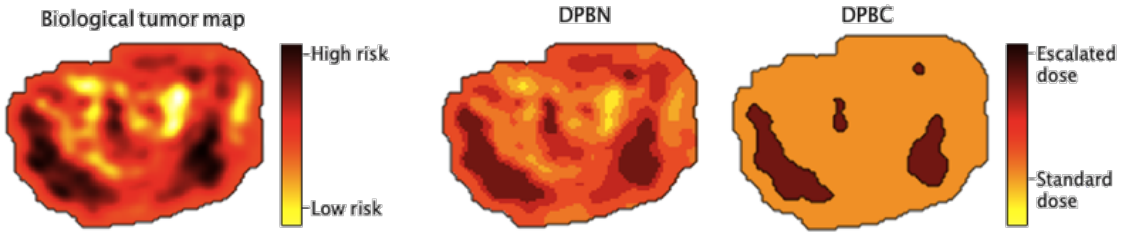

Figure 2.13: A biomarker is measured and geographically mapped across the tumor. For DPBN, the dose is assigned voxel by voxel according to the biological tumor map. DPBC uses a threshold value to segment tumor subvolumes with high risk, and prescribes an escalated dose level to these areas.

In DPBC, which is the main focus of this thesis, the tumor is divided into radioresistant and radiosensitive regions based on a threshold value. The radioresistant subvolumes are then assigned an additional uniformly distributed dose escalation, while the radiation dose to the sensitive parts of the tumor is kept at the standard level. For selective boosting of subvolumes, a potential increase in TCP will partly be due to an increased integral tumor dose, making it difficult to compare the approach to conventional treatment planning [57]. It may, however, be useful to compare dose painting with a uniform dose boost to the whole tumor.

In the following, it is assumed that for DPBC, the radiosensitive regions of the tumor are irradiated with a conventional fractionation dose d_s, and resistant subvolumes are irradiated with a fractionation dose $d_r = bd_s$, where $b \geq 1$ is the dose boost factor. A uniformly escalated dose that would produce an equal integral tumor dose as used in DPBC, can be calculated as [64]:

$$d_u = d_s\left(\frac{V_S + bV_R}{V_S + V_R}\right) \tag{2.14}$$

where V_S and V_R are the volumes of the sensitive and resistant areas of the tumor, respectively. The TCP can then be found by setting $d_i = d_u$ in equation (2.12) for all subvolumes. Figure 2.14 illustrates how d_u, d_s and d_r are related.

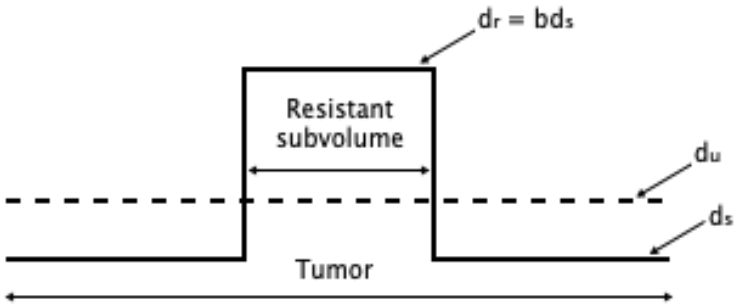

Figure 2.14: Schematic illustration of the conventional tumor dose d_s, the escalated dose d_r, and the uniformly escalated dose d_u. Inspired by [64].

3 Methods and materials

All patient data and images analyzed in this thesis were obtained from the OxyTarget study, which aimed to develop new fMRI protocols for assessing tumor aggressiveness in rectal cancer patients [8].

This thesis builds on a previous thesis by Karina Lund Rød, which also used clinical data from the OxyTarget study. She investigated how to create two-dimensional DPBC prescriptions based on pre-CRT R_2^*-AUC tumor maps, and found by TCP modelling that these prescriptions enhanced the TCP compared to conventional radiotherapy, regardless of tumor response to CRT [65].

3.1 Patients

35 patients diagnosed with LARC were included in this thesis. All patients underwent diagnostic MRI and CT before treatment to stage the tumors according to the TNM system, and were then treated with preoperative CRT. A radiotherapy treatment of 2×25 Gy was given to most patients (n = 30), but other fractionation regimens were also used on a few patients. The chemotherapeutic drug Xeloda® was used in most cases (n = 24), although some patients received FLOX and FLV. 6-8 weeks after completion of the CRT schedule, the patients underwent surgery. The TN stage was assessed again by pathological examination of the resected specimen, and the tumor response was determined by using the TRG system. Patient and tumor characteristics are shown in table 3.1.

3.2 MRI acquisition

The MR images were acquired on a 1.5T Philips Achieva system (Philips Healthcare, Best, The Netherlands) using NOVA Dual HP gradients (33 mT/m maximum gradient amplitude, 180 T/m/s slew rate) and a five-channel cardiac coil with parallel imaging capabilities. The patients were given glucagon (1 mg/mL, 1 mL intramuscularly) and Buscopan® (20 mg/mL, 1 mL intravenously) prior to and during the examination to reduce bowel movement.

High-resolution T_2-weighted images were acquired by a FSE sequence, and DSC

Table 3.1: Information about patients and tumor classification. The data is given in number of patients (percentage), except for age which is given in years (range).

Number of patients	**35**
Male	26
Female	9
Median age (years)	**63 (41-79)**
Male	63 (41-78)
Female	57 (49-79)
Tumor regression grade	
TRG0	4 (11.4%)
TRG1	9 (25.7%)
TRG2	14 (40.0%)
TRG3	8 (22.9%)
TNM	
T2	2 (5.70%)
T3	16 (45.7%)
T4a	5 (14.3%)
T4b	12 (34.3%)
N0	11 (31.4%)
N1	13 (37.1%)
N2	11 (31.4%)
M0	29 (82.9%)
M1	6 (17.1%)

imaging data was obtained by using a 3D T_1-weighted EPI sequence with three echoes. DWI images were also acquired by a EPI sequence, with b-values 0, 25, 50, 100, 500, 1000 and 1300 s/mm^2. The imaging parameters for the sequences are included in table 3.2. The T_2-weighted images were used for tumor staging in all patients, in addition to delineation of regions of interest (ROI). The delineation was done by an experienced radiologist. The DSC images were used to calculate R_2^* voxelwise by using equation (2.3), and store them as R_2^* maps. The DWI images were used to calculate ADC maps.

Table 3.2: Imaging parameters used for the acquired MR sequences.

	T_2-weighted MRI	**DWI**	**DSC-MRI**
Slice thickness (mm)	2.5	4	10
Number of slices	21 - 37	14	12 - 22
TR (ms)	2386 - 4122	3125	37 - 45
TE (ms)	80	75	4.6
Field of view (mm^2)	180×180	160×160	180×180
Acquisition matrix	224×220 - 256×254	128×128	92×90
Flip angle	90°	90°	28°
Number of excitations	3 - 6	6	-
Echo train length	20	57	-
EPI factor	-	-	9
Echo spacing (ms)	-	-	9.2
Temporal resolution	-	-	2 s/imaging volume
Time points/slice	-	-	60

3.3 Preparatory analysis

All subsequent analyses were performed by using Python, except for some statistical analyses done in the programming language "R". All scripts are attached in appendix A. The preparatory analysis carried out in order to investigate DPBC for rectal cancer patients was based on MATLAB scripts written by Karina Lund Rød (A.1 - A.6) [65].

First, the T_2-weighted images and the R_2^* maps were sorted according to slice position in 3D and 4D matrices, respectively (A.1 - A.2). The x-, y-, and z-direction represented the first three dimensions, and time was the fourth dimension for the DSC images. The tumor ROIs were delineated on the T_2-weighted images, and received in the NifTI format. The ROIs therefore needed to be adapted to fit the resolution format of the DSC data (A.3). R_2^*-AUC tumor maps were then generated from the R_2^* maps (A.4). This was done by storing the R_2^*-values for each time point in voxelwise arrays. The arrays were normalized by subtracting the mean value of the baseline images, so that the array values represented change in R_2^* from baseline,

ΔR_2^*. R_2^*-AUC was then found for each voxel inside the ROI by plotting the arrays as a function of time, and calculating the integral. The average of all ΔR_2^* curves for one of the tumors is shown in figure 3.1. The integral was calculated from 0 to 525±25 s, depending on the time points used for the image acquisition.

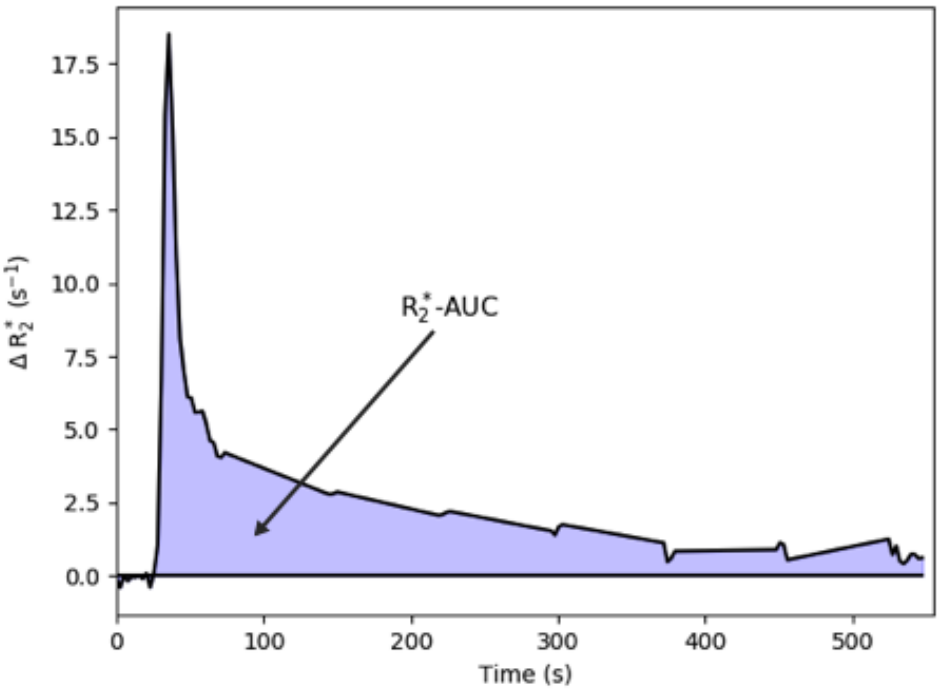

Figure 3.1: ΔR_2^* plotted as a function of time for the dynamic sequence. R_2^*-AUC, the area under the curve marked in blue, was found by integrating the function from 0 to 525±25 s.

Before using the R_2^*-AUC maps for DPBC, noise filtration and spatial smoothing were performed (A.5 - A.6). Noise filtration was done by discarding the lowest and highest 2.5% of the values for each tumor, which was found by calculating the 2.5th and 97.5th percentiles of the R_2^*-AUC distribution. Spatial smoothing was done to simulate the effect of inter-fractional tumor movement, and performed by using a Gaussian filter from the scikit image processing tool in Python. Figure 3.2 visualizes the effect of pre-processing the R_2^*-AUC maps. It can be seen that the noise filtration led to a removal of probable outliers, and that the tumor volume was slightly increased due to the spatial smoothing.

In total 4 patients were excluded during the preparatory analysis. Two of the patients were excluded when calculating the R_2^*-AUC tumor maps, as their number

of baseline images could not be found. One patient was excluded due to their outlying median R_2^*-AUC, and one patient was excluded since the resistant volume covered more than 2/3 of the tumor.

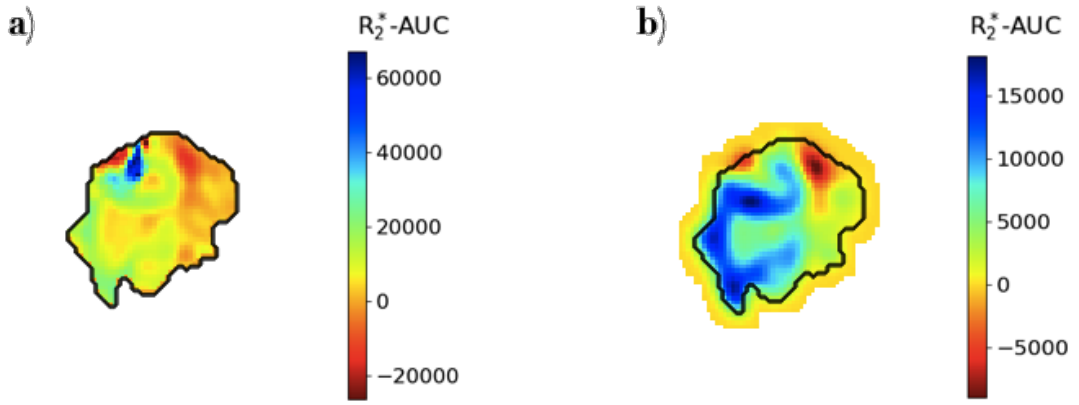

Figure 3.2: R_2^*-AUC tumor maps for DPBC. a) Before pre-processing. b) After noise filtration and spatial smoothing. The original ROI contour is added to visualize the difference between the tumor volumes.

3.3.1 Statistical analysis

Statistical analyses often assume that the data is normally distributed. Considering the relatively small sample size of this project, the data was not expected to pass this requirement. The non-parametric Mann-Whitney U-test does not require large normally distributed samples, and was therefore used in this thesis for statistical analysis. The null hypothesis (H_0) is that the two independent samples being compared come from the same distribution, while the alternative hypothesis (H_1) is that their distributions differ [66]. The p-value is the probability of observing a test statistic that is as extreme as or more extreme than the one observed, assuming H_0 is true. The null hypothesis is rejected when the p-value is smaller than the significance level. For this thesis, the significance level was set to 0.05.

A boxplot can be useful to compare data from several groups, and to visualize the result of an statistical analysis. The box extends from the first quartile to the third quartile of the data, with a line showing the median. The whiskers show the range of the data, and represent values that are found a certain distance away from the box edge. Values outside these are classified as outliers.

3.4 Dose painting by contours

3.4.1 Problem setup

The creation of R_2^*-AUC-based DPBC dose prescription maps was based on the setup illustrated in figure 3.3. The approach was to divide the tumor into radioresistant and radiosensitive regions based on a threshold value derived from the R_2^*-AUC maps, termed R_2^*-AUC_{CUT}. Subvolumes consisting of voxels with R_2^*-AUC above R_2^*-AUC_{CUT} formed the radioresistant compartment, R, as high R_2^*-AUC has been related to limited radiocurability. The remaining radiosensitive compartment of the tumor, S, consisting of voxels with R_2^*-AUC below R_2^*-AUC_{CUT}, was assumed to respond well to standard radiation doses.

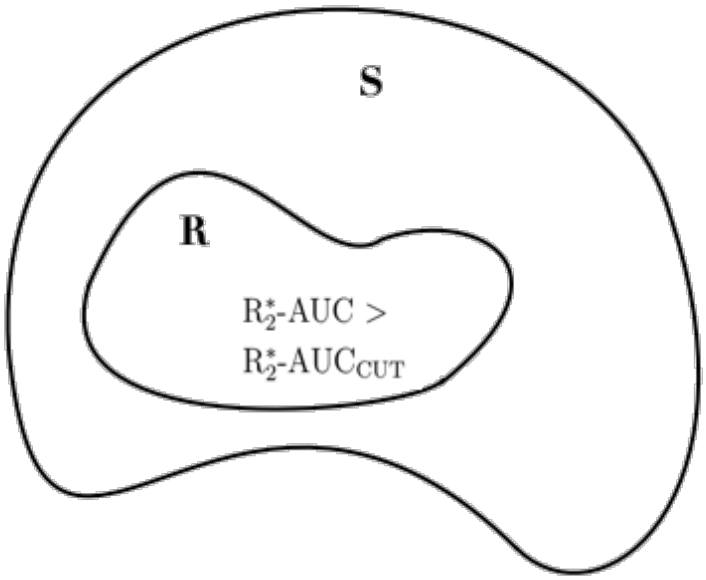

Figure 3.3: Illustration of how the DPBC planning was carried out. The radioresistant subvolume, R, was found by segmenting tumor voxels with R_2^*-AUC above R_2^*-AUC_{CUT}. The remaining tumor voxels formed the radiosensitive compartment, S. S is assumed to obtain good tumor control with standard radiation dose, while R is assumed to require a dose escalation to obtain the same tumor control.

An R_2^*-AUC_{CUT} value of 2574 is used in further analyses, and was derived by Rød [65]. She applied a percentile screening technique to find out if any percentiles of the R_2^*-AUC distribution were more strongly associated with the TRG than the median. This was done by using the Mann-Whitney U-test to assess the relationship of each

percentile to the TRG.

3.4.2 Generation of DPBC maps

DPBC maps were generated by using R_2^*-AUC_{CUT} to divide the tumor volume into R and S (A.7). First, a 3D matrix with the same shape as the R_2^*-AUC map was made for each patient to store the corresponding DPBC map. All values in the R_2^*-AUC map were then evaluated voxel by voxel, to determine which values were above and below R_2^*-AUC_{CUT}. This information was used to group the voxels into R and S, and DPBC maps were created by assigning two different total radiation dose levels to these. Figure 3.4a shows a slice from one of the preliminary DPBC maps, which were stored for each patient.

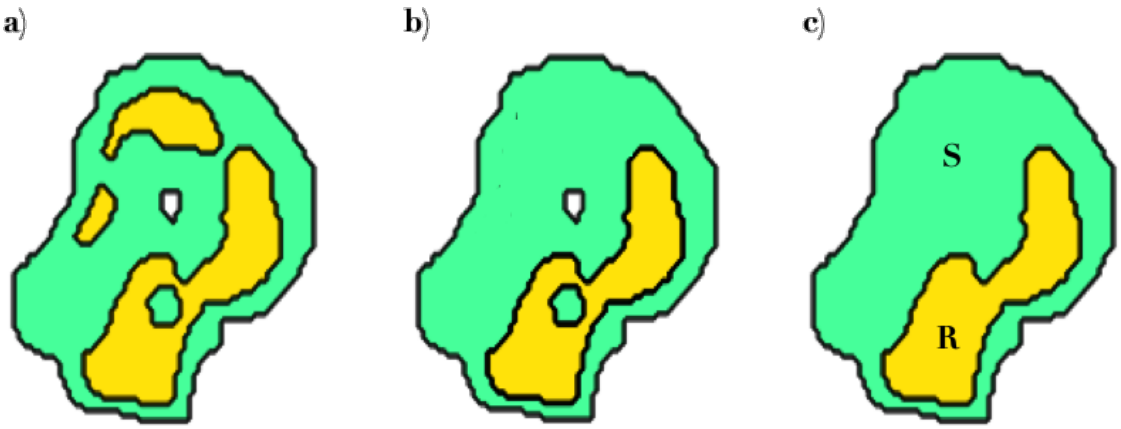

Figure 3.4: Visualization of the methodology used for generation of R_2^*-AUC-based DPBC maps. a) Preliminary DPBC map where all voxel values above R_2^*-AUC_{CUT} add to R. b) All subvolumes smaller than a certain size are neglected and incorporated into S. c) Final DPBC map where small clusters are included in the dominant volume.

Further analyses aimed to make the model more realistic. To be able to implement the DPBC maps in radiotherapy treatment planning, there are some physical limitations that must be taken into account. The minimum volume that can be used in dose painting was estimated by a medical physicist to be a sphere with diameter of 1 cm, depending on the dose level difference in S and R. All subvolumes smaller than 1 cm^3 were therefore neglected and considered as a part of S, as seen in figure 3.4b. This was done by calculating the amount of voxels that corresponded to 1

cm^3, and then using an image processing tool in python, called skimage, to remove the small regions. 29 of the patients had subvolumes larger than 0.5 cm^3, and 16 of the patients had subvolumes larger than 1 cm^3.

Some of the subvolumes had clusters of voxels with R_2^*-AUC below R_2^*-AUC_{CUT}. A cluster size limit was therefore defined so that clusters consisting of fewer than a certain number of voxels were included in R. Furthermore, some of the tumors had small "holes". These were considered a part of the tumor if they were smaller than the cluster size limit. The final compartmentalization of R and S were then set, as shown in figure 3.4c, and the number of voxels in each region could be found.

Statistical analysis was performed to assess the relationship between the volume of R and TRG by using the Mann-Whitney U-test (A.10-A.11). An array was made for each level of TRG, containing the volume of R for each patient in this group. The difference between these arrays could then be assessed by using the Mann-Whitney U-test. The specific statistical tests were done in programming language "R", because of its extensive tool set for this purpose. The tests were performed using a cluster size limit of 50, and a subvolume limit of 0, 0.5 and 1 cm^3. Boxplots were made for visualization of the result.

3.5 TCP modelling

The potential advantage of the DPBC plans were assessed by using TCP modelling (A.8). All computations were based on the LQ model, as discussed in section 2.4. First, the individual TCP for R and S were calculated by using equation (2.12). To perform these calculations, model parameters including the α/β-ratio, tumor cell density, volumes of R and S, as well as radiation dose information for the two respective compartments, were needed. These parameters are summarized in figure 3.5.

The α and β values used for oxygenated conditions were first chosen based on previous studies, and are included in table 3.3. Suwinski et al. estimated in total two α/β values for rectal cancer, one with and one without accounting for repopulation [67]. A third α/β, found by Chvetsov et al., was also tested to account for completely oxygenated conditions [64]. This value was, however, not specific for rectal cancer

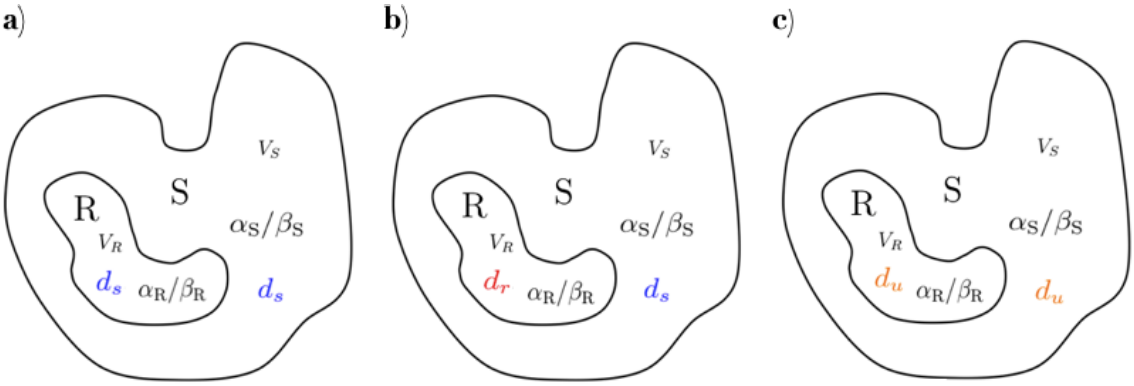

Figure 3.5: Illustration of the model parameters used to calculate TCP. a) Standard plan with a uniform dose distribution. b) DPBC plan with escalated dose to R. c) Uniform dose boost with total dose equal to the DPBC plan.

due to a lack of relevant literature. α_R/β_R, the radiobiological ratio used for hypoxic conditions, was calculated by relating it to α_S/β_S via typical OER values:

$$\alpha_R = \frac{\alpha_S}{\text{OER}}, \tag{3.1}$$

$$\beta_R = \frac{\beta_S}{\text{OER}^2}. \tag{3.2}$$

Similar formulas have been used in TCP modelling studies that include hypoxic subvolumes [5, 59, 64]. The TCP calculations were performed using an OER of 1.75 and 2.7, also in agreement with previous studies [5, 64].

Table 3.3: α_S and β_S values estimated by Suwinski et al. and Chvetsov et al. [64, 67]. The two first estimates are specific to rectal cancer, and the last is typical for lung cancer.

Estimate type	α_S (Gy^{-1})	β_S (Gy^{-2})	α_S/β_S (Gy)
No repopulation	0.339	0.067	5.06
Repopulation	0.335	0.030	11.2
Complete oxygenation	0.450	0.039	11.5

A literature search revealed that several TCP studies varied the value of α to fit the observed results [5, 68]. A second approach based on this method was therefore

investigated. The α value was fitted to an estimate of the TCP for the patient cohort when using a standard dose and an OER of 1.75. The cohort TCP was predicted based on the percentage of patients with TRG0-1, as they were assumed to obtain tumor control.

The clonogenic density was first assumed to be a constant value of 10^6 cells/cm^3 across the tumor, based on previous findings [50, 69]. The volumes of R and S were found by calculating the volume of a single voxel, and then multiplying this volume with the number of voxels in each region. The fraction dose d_s was set to 2 Gy, and the number of fractions to 25, similar to conventional radiotherapy for rectal cancer. The fraction dose applied to R was determined by the dose boost factor, b, described in section 2.5.2. A literature search was performed to find out which values of b that may be relevant for clinical application. The review by Van Wickle et al. addressed methods of delivering escalated radiotherapy boost in rectal cancer, and provided a summary of the studies covered [70]. Most of these studies used a total dose escalation of 60 Gy to the entire GTV, which corresponds to $b = 1.2$. However, the total dose will be smaller when only the most aggressive subvolumes are boosted compared to a uniform GTV boost, thus it may be feasible with larger values of b. Simulations were run using b-values ranging from 1 to 3.

The individual TCP calculated for R and S were finally combined in an overall TCP for the DPBC plans using equation (2.13). Only the patients with subvolumes larger than 1 cm^3 were considered. The TCP was also computed for a uniform dose boost for comparison. The uniform dose boosts corresponding to the total dose of the DPBC plans were calculated by using equation (2.14). The TCP for each patient in addition to the average TCP was then plotted against various b-values for both treatment strategies. A 95% confidence interval for the average TCP was also plotted.

3.6 Estimation of cell densities from ADC maps

Previous studies have showed correlation between the ADC and the cell density in tissues [5, 71]. Based on this research, ADC maps were used to estimate the average tumor cell density for all patients with subvolumes larger than 1 cm^3 (A.9). Casares-Magaz et al. translated ADC maps into cell densities, and investigated how

these ADC map-based cell densities affected the TCP [5]. They considered three different approaches to relate the ADC values with cell densities voxel-by-voxel: a linear, a binary and a sigmoid relation. The sigmoid relation was most relevant for this thesis, and can be written as:

$$\rho = \left(9.9\left(1 - \frac{1}{1 + e^{\frac{1.3-\mathrm{ADC}}{0.1}}}\right) + 0.1\right)10^6 \text{ cells/cm}^3, \tag{3.3}$$

where the ADC value is given in 10^{-3} mm^2/s. ADC maps were calculated based on DWI with b-values 100, 500, 1000 s/mm^2, and had to be adapted to fit the resolution of the DPBC plans.

First, new DPBC maps were generated based on more accurate tumor ROIs that were resampled from the T_2 weighted images to the R_2^* image grid. One of the patients was excluded from further analyses since the new DPBC map no longer revealed any subvolumes larger than 1 cm^3. The contours defining the tumor and the resistant subvolumes were saved as a NifTI file for each patient, and resampled back to the T_2 weighted image. To calculate the ADC values in the regions defined from the DPBC maps, the contours were resampled to the DWI grid. The contours could also have been resampled directly from the R_2^* maps to the DWI, however, the original ROIs on the T_2 weighted images were used as a reference to check that everything seemed as expected. The resampling was done by using Insight Toolkit (ITK), which is an open-source library that provides software tools for image analysis [72]. Nearest neighbor interpolation was chosen as interpolator to preserve the integer values of the contour labels. Figure 3.6 shows one of the calculated ADC maps, adapted to the corresponding DPBC map.

Average ADC values were found for the tumor, the resistant and the sensitive regions, and the corresponding cell densities were estimated by applying equation (3.3). Boxplots were used to show the difference in cell density for the different regions for patients with TRG0-3. The ADC-based cell densities were also included in the TCP modelling, and compared with the TCP for a constant cell density of 10^6 and 10^7 cells/cm^3. The comparisons were done using the same DPBC maps.

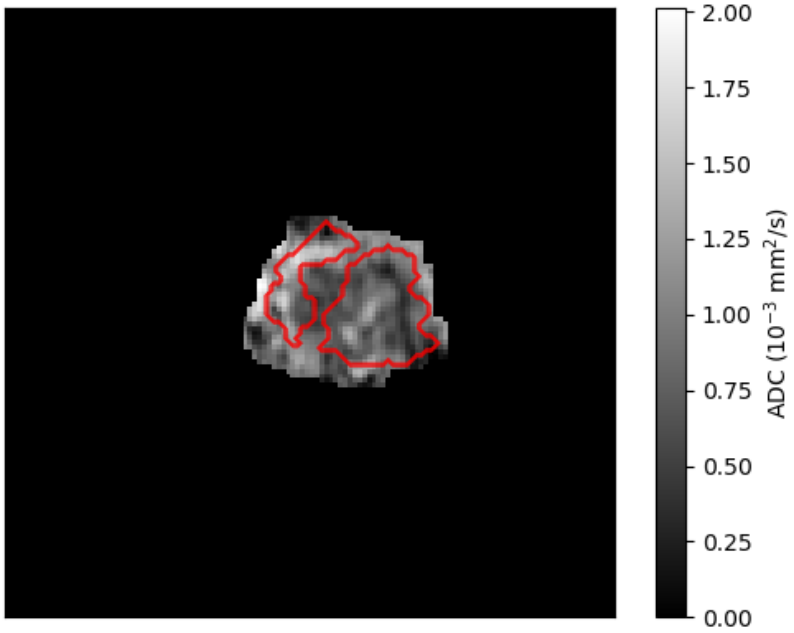

Figure 3.6: One slice of the calculated ADC maps is shown together with red contours that represents the radioresistant regions. ADC values were only calculated inside the tumor.

3.7 Clinical implementation of DPBC

To evaluate the DPBC plans further, it was of interest to incorporate the plans into RayStation to generate dose volume histograms (DVHs). DVHs are valuable tools in radiotherapy treatment planning, as they show the dose coverage to both the tumor and OARs. Since the TCP modelling does not consider normal tissues, it is especially interesting to look at the DVH for OARs, and if it changes with the DPBC strategy.

In order to incorporate the plans into RayStation, the DPBC plans first had to be saved as NifTI files. Then the contours were adapted to fit the resolution format of the T_2 weighted images that were going to be used in the radiotherapy planning. This was done by using the same approach as for the ADC maps. The adapted NifTI files were then converted to radiotherapy structures to be able to recognize the contours in RayStation. Figure 3.7 shows an example of a T_2 weighted image together with the DPBC plan. Furthermore, pseudo-CTs have to be generated from the MR images in order to obtain electron density information for dose calculations.

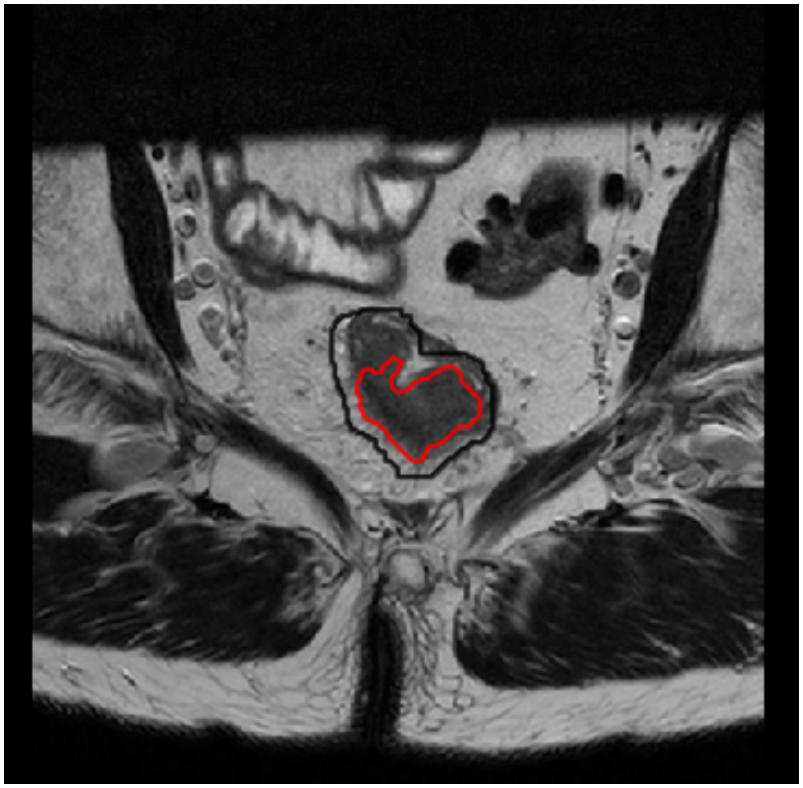

Figure 3.7: One slice of a DPBC plan is shown together with the corresponding T_2 weighted image. The black contour represents the tumor, and the red contour represents the radioresistant region.

4 Results

4.1 DPBC maps

Figure 4.1 shows the R_2^*-AUC tumor map, along with the corresponding DPBC map for one slice of a tumor. The contour of the boost subvolume is added to both maps. Figure 4.2 shows all slices of the DPBC map for the same tumor.

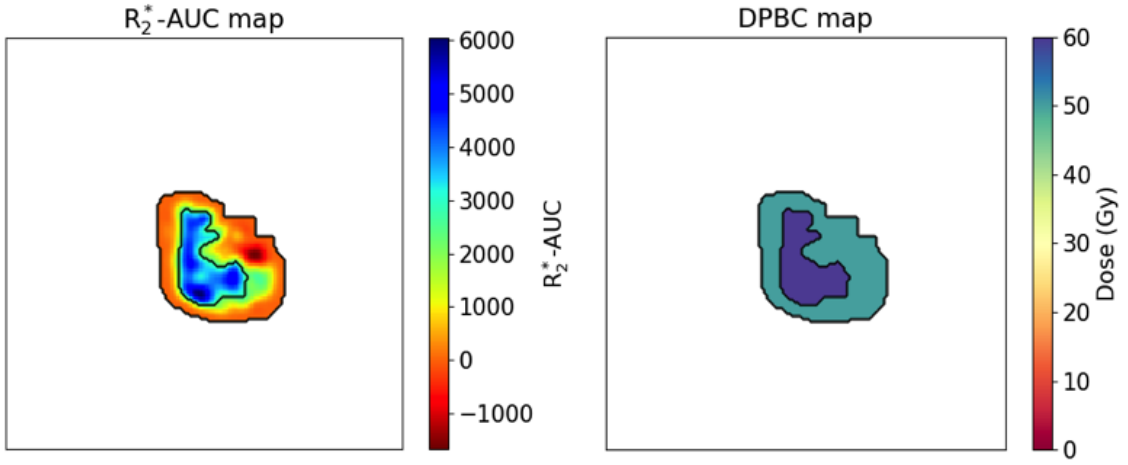

Figure 4.1: R_2^*-AUC tumor map and the corresponding DPBC map for one slice of a tumor. The total radiation dose to R and S are 60 Gy and 50 Gy, respectively.

Figure 4.2: The DPBC map for one of the patients, showing the dose distribution for the tumor slice by slice. The two first and last slices did not contain any tumor volume, and were therefore not included in the figure.

4.1.1 Statistical analysis

Statistical analysis using the Mann-Whitney U-test was performed to assess the relationship between TRG and the volume of R before removing any of the subvolumes, when subvolumes smaller than 0.5 cm^3 have been removed, and when subvolumes smaller than 1 cm^3 have been removed. Boxplots visualizing the results are shown in figure 4.3. The same trend is seen for each subvolume limit, indicating larger subvolumes for the poor responders (TRG2-3) compared to the good responders (TRG0-1). The specific median values and p-values can be found in appendix B.

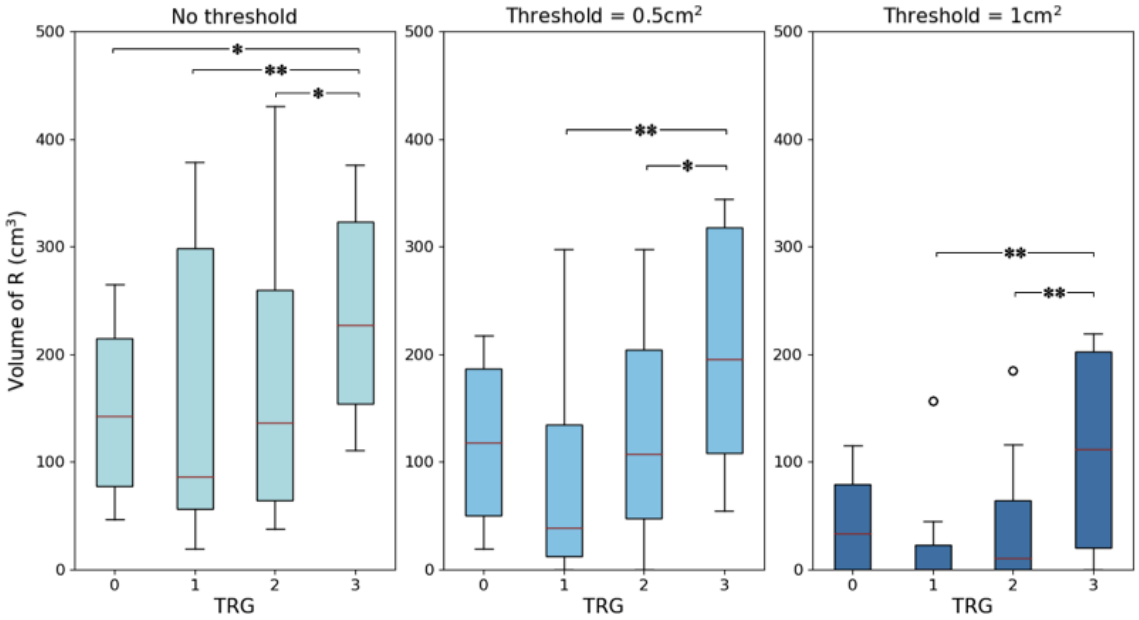

Figure 4.3: Boxplots showing the volume of R for patients with TRG0-3, using a subvolume limit of 0, 0.5 and 1 cm^3. *: Difference significant at significance level 0.05. **: Difference significant at significance level 0.01.

4.2 TCP modelling

The TCP modelling was first done with the α and β values found in the literature. Figure 4.4 shows the average TCP for all patients with subvolumes larger than 1 cm^3, using the three alternatives of α/β and an OER of 1.75 and 2.7. The TCP modelling was then done for α values fitted to the cohort TCP. 5 of 16 patients with subvolumes larger than 1 cm^3 had TRG0-1, thus the mean TCP for a standard dose was predicted to be 31.25%. Figure 4.5 shows the average TCP for the fitted α, using the three alternatives of α/β-ratio and an OER of 1.75 and 2.7.

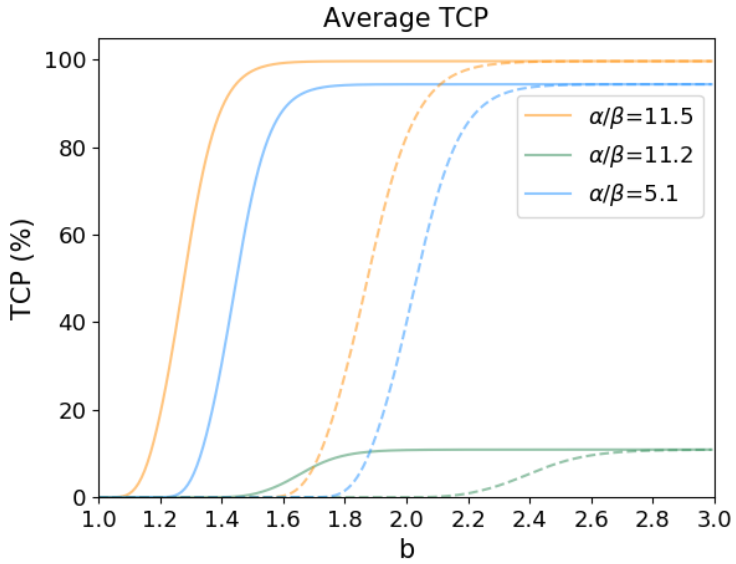

Figure 4.4: The average TCP for the DPBC plans as a function of b for the three alternatives of α/β. The solid lines represent an OER of 1.75, and the dashed lines represent an OER of 2.7.

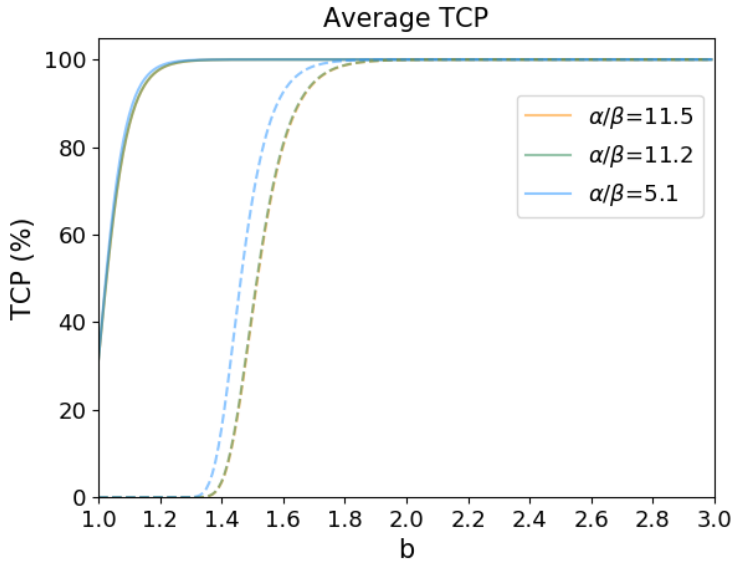

Figure 4.5: The average TCP for the DPBC plans as a function of b for the three alternatives of α/β, when α is fitted to the cohort TCP. The solid lines represent an OER of 1.75, and the dashed lines represent an OER of 2.7. The orange and green lines are overlapping.

The TCP was also computed for a uniform dose boost, and compared with the DPBC plans, using an OER of 1.75 and $\alpha/\beta = 11.5$. Figure 4.6a) and b) shows

the individual and average TCP, respectively, for both treatment planning strategies before the value of α was fitted. It is seen that the TCP is very low even at high dose boost factors. Figure 4.7 shows the same as figure 4.6, except with a fitted α value. Here, more realistic TCP values are predicted for lower doses. Table 4.1 presents the TCP for each patient, in addition to the individual TCP for the sensitive and resistant regions for both treatment planning strategies when using a b-value of 1.2, and a fitted α value.

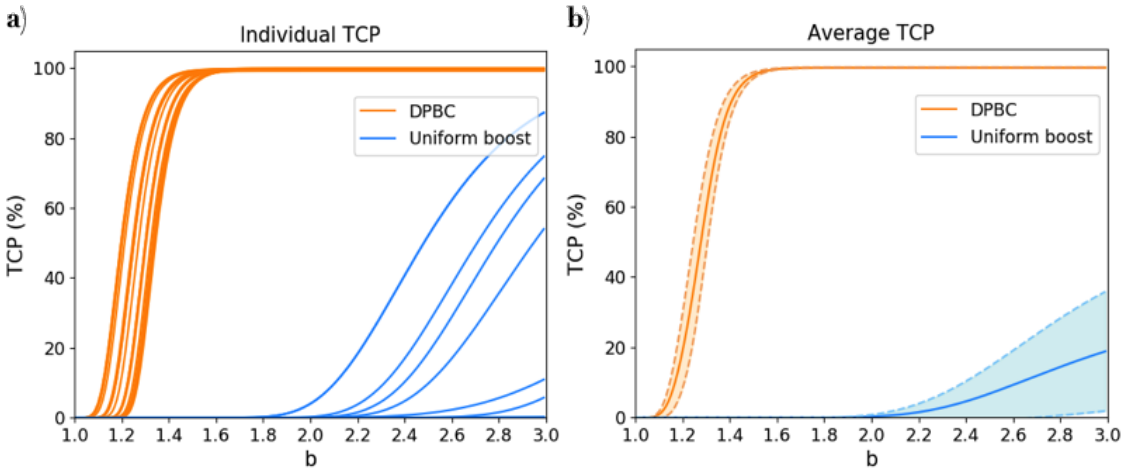

Figure 4.6: a) The individual TCP for each patient as a function of b, for both the DPBC plans and the corresponding uniform dose boost. b) The average TCP as a function of b together with a 95% confidence interval.

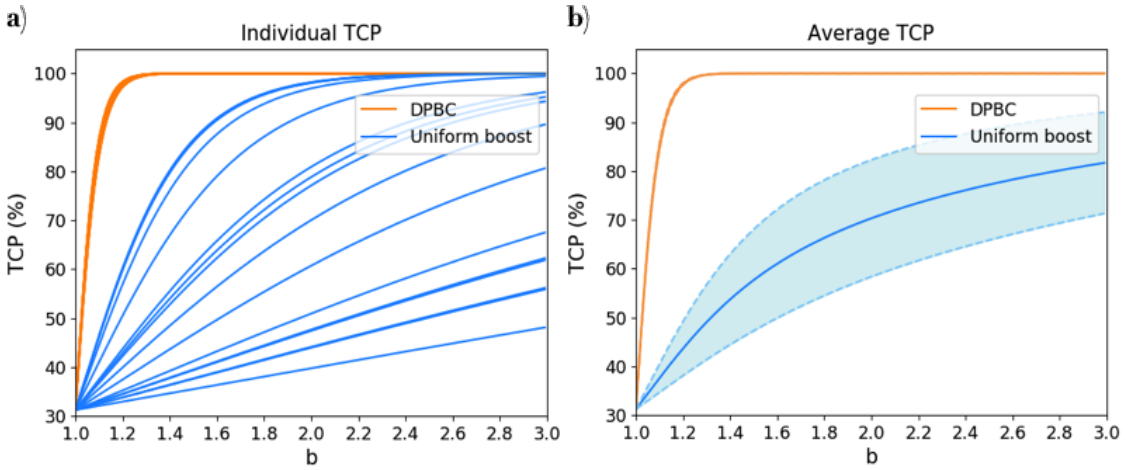

Figure 4.7: a) The individual TCP for each patient as a function of b, for both the DPBC plans and the corresponding uniform dose boost when α is fitted to the cohort TCP. b) The average TCP as a function of b together with a 95% confidence interval.

Table 4.1: The TCP(%) for each patient, in addition to the individual TCP for the sensitive and resistant regions for DPBC and a uniform dose boost. The modelling was done with an OER of 1.75, $\alpha/\beta = 11.5$ and b=1.2.

		DPBC			Uniform dose boost		
Patient	TRG	Tumor	S	R	Tumor	S	R
1	1	97.61	100.0	97.61	34.5	100.0	34.5
2	2	97.66	100.0	97.66	37.46	100.0	37.46
3	2	98.25	100.0	98.25	56.9	100.0	56.9
4	3	98.31	100.0	98.31	59.89	100.0	59.89
5	1	98.18	100.0	98.18	42.23	100.0	42.23
6	0	97.81	100.0	97.81	39.93	100.0	39.93
7	3	98.28	100.0	98.28	50.5	100.0	50.5
8	3	98.23	100.0	98.23	59.83	100.0	59.83
9	2	97.65	100.0	97.65	33.79	100.0	33.79
10	2	97.31	100.0	97.31	33.82	100.0	33.83
11	1	97.21	100.0	97.22	34.55	100.0	34.55
12	2	97.17	100.0	97.17	35.24	100.0	35.24
13	3	97.63	100.0	97.63	43.72	100.0	43.72
14	0	98.05	100.0	98.05	42.88	100.0	42.88
15	3	97.16	100.0	97.16	32.95	100.0	32.95
16	2	98.02	100.0	98.02	60.2	100.0	60.2

4.3 Estimation of cell densities from ADC maps

The average ADC values and the estimated cell densities for all of the patients are presented in table 4.2. Figure 4.8 shows the average cell density for the tumor, the sensitive region and the resistant region for patients with different scores of TRG.

4.3.1 TCP modelling

The TCP for the DPBC plans were modelled with the ADC-based cell densities for S and R, and compared with the TCP based on the constant cell density first assumed. As the estimated cell densities were close to 10^7 cells/cm^3, the TCP was

Table 4.2: The average ADC values for the tumor, the resistant and the sensitive regions, together with the estimated cell densities for all of the patients.

		ADC value (10^{-3} mm^2/s)			Cell density (10^7 cells/cm^3)		
Patient	TRG	Tumor	S	R	Tumor	S	R
1	1	0.785	0.783	0.878	1.083	1.083	1.075
2	2	0.865	0.863	0.886	1.076	1.077	1.074
3	2	0.662	0.659	0.686	1.087	1.087	1.087
4	3	0.555	0.552	0.562	1.088	1.088	1.088
5	1	1.186	1.192	1.113	0.849	0.838	0.957
6	0	0.737	0.741	0.651	1.085	1.085	1.088
7	3	1.382	1.387	1.352	0.402	0.391	0.468
8	3	0.888	0.92	0.828	1.073	1.067	1.08
9	2	1.17	1.175	0.914	0.877	0.869	1.069
10	2	0.83	0.822	0.996	1.08	1.081	1.044
11	1	1.243	1.25	1.133	0.731	0.715	0.932
12	2	0.963	0.968	0.757	1.056	1.054	1.085
13	3	1.154	1.166	1.055	0.902	0.884	1.01
14	0	1.046	1.068	0.834	1.017	1.0	1.08
15	2	1.187	1.247	0.993	0.847	0.722	1.045

also modelled for a constant cell density with this value. The comparisons were done using a fitted α, an OER of 1.75 and $\alpha/\beta = 11.5$. Figure 4.9a) and b) show the individual and average TCP, respectively, for constant cell densities of 10^6 and 10^7 cells/cm^3 and for the cell densities estimated from ADC maps.

4.4 Clinical implementation of DPBC

RayStation was not able to import the radiotherapy structures converted from the NifTI files that contained the DPBC plans. The problem was related to the DICOM header of the radiotherapy structure files, where some of the tags not were correctly linked to the T_2 weighted MR images. The details of the problem were forwarded to RaySearch, but no solution was reached during the course of this thesis.

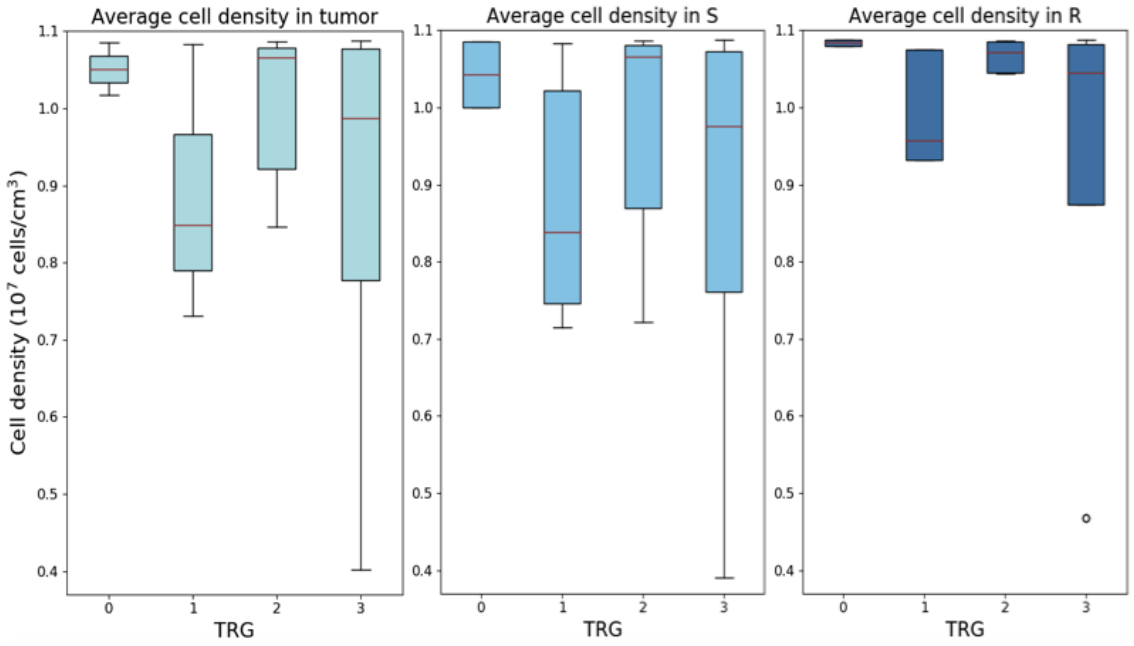

Figure 4.8: Boxplots showing the average cell density for the tumor, the sensitive region and the resistant region for patients with TRG0-3.

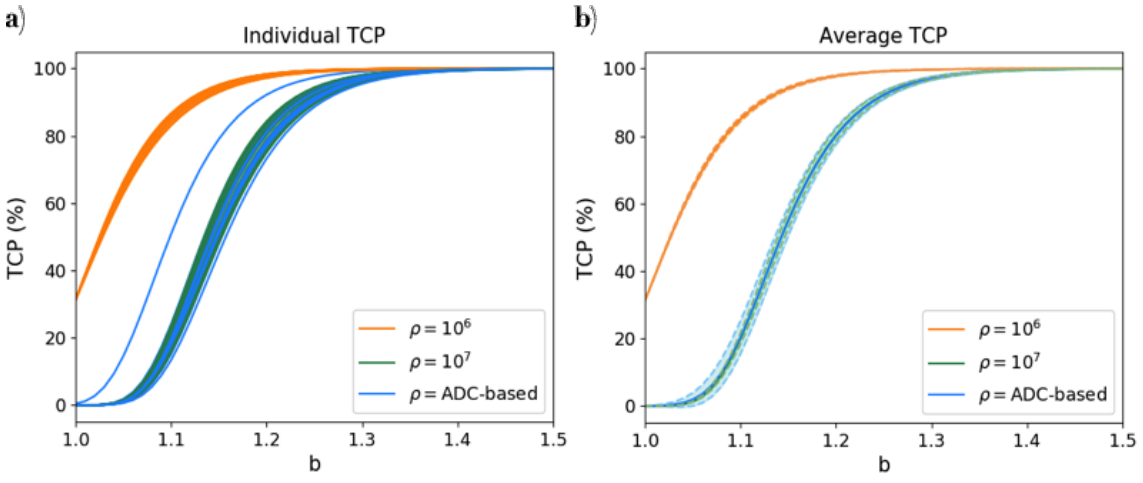

Figure 4.9: a) The individual TCP for each patient for constant cell densities of 10^6 and 10^7 cells/cm^3, in addition to the TCP for cell densities estimated from ADC maps, plotted as a function of b. b) The average TCP as a function of b together with a 95% confidence interval.

5 Discussion

5.1 Methods

5.1.1 Preparatory analysis

The preparatory analysis carried out in order to investigate DPBC was based on the methods implemented by Rød [65]. The tumor ROIs were adapted to fit the resolution format of the DSC images by finding the T_2 weighed MR slices that were closest in position to the DSC slices, and then downscaling these. This approach is simple and sufficient for the analyses done in this thesis, but resampling should be considered for future work for higher accuracy. Uncertainties related to the generation and filtration of the R_2^*-AUC maps are outside the scope of this work, and discussed in detail by Rød [65].

5.1.2 Generation of DPBC maps

DPBC is sensitive to the threshold value used to divide the tumor into a resistant and a sensitive part, and it is difficult to find an optimal threshold that neither overestimates or underestimates the boost volume. The threshold value, $R_2^*\text{-AUC}_{\text{CUT}}$, used in this thesis was derived by Rød [65]. She used a percentile screening method to find out which parts of the R_2^*-AUC distribution that were significantly associated with TRG. $R_2^*\text{-AUC}_{\text{CUT}}$ was then set as the global percentile of the R_2^*-AUC distribution corresponding to a percentile showing strong association with TRG.

Three-dimensional DPBC maps were generated based on this threshold, and further work consisted of making the DPBC plans clinically feasible. The minimum volume of the resistant regions that can be boosted in dose painting depends on the ability to produce steep enough dose gradients [28]. Too small target volumes can either cause the resistant volume to receive a lower dose, or cause the surrounding sensitive volume to be irradiated with a higher dose than prescribed [73, 74]. As external photon beams have finite dose gradients, the desired steepness may be problematic to achieve with photon irradiation. This has motivated the investigation of dose painting with particle therapy, as irradiation of heavy charged particles allows steeper dose gradients [75, 76, 77].

The minimal subvolume that can be accurately boosted in dose painting was estimated by a medical physicist at St. Olavs hospital to be a sphere with diameter of 1 cm. All resistant volumes smaller than 1 cm^3 were therefore neglected and considered as a part of S. Small clusters of voxels belonging to the sensitive compartment within the boost subvolume, or small holes in the tumor, were included in the dominant region for the same reasons. The approach used for removing the small subvolumes did not consider the size of each direction of the region. Some of the subvolumes may therefore be too narrow for DPBC. However, only 16 of the patients ended up with resistant regions after this approach, and if stricter requirements were set there would be even fewer patients to analyse.

5.1.3 TCP modelling

There were several uncertainties related to the TCP calculations, mainly due to model simplifications and uncertainties regarding the model parameters. Important factors in a fractionated treatment course, such as tumor cell repopulation, repair, redistribution and reoxygenation were not incorporated into the LQ-based Poisson TCP model. Repopulation and repair of clonogenic cells between the fractions may lead to a lower TCP. The damage to the tumor will, however, at the same time increase due to reoxygenation of hypoxic cells, and redistribution of cells into the radiosensitive phases of the cell cycle.

The α/β ratios used for the sensitive compartment was chosen based on previous studies [64, 67]. However, only one of the studies was specific for rectal cancer. The limited literature about the α/β ratio in rectal cancer may indicate that precise knowledge about is lacking. The α/β ratio in the resistant region was found by directly relating it to the α/β ratio in the sensitive region via the OER. This is a common method for finding the α/β ratio in hypoxic regions, that assumes fully oxygenated conditions for the sensitive region. This assumption may not hold, as the α/β values were based on a population average. The TCP modelling was first done with the suggested literature values for α. However, previous TCP studies tend to adjust the α value to match the observed results [5, 68]. This method was therefore also investigated by fitting the α value to the TCP for the patient cohort used in this thesis. The cohort TCP was predicted based on TRG, assuming that

patients with TRG0-1 would obtain tumor control.

The TCP was calculated for various dose levels to the resistant subvolumes to make it possible to observe how the TCP depended on the boost factor. Literature suggested a uniform dose escalation of 60 Gy, which corresponds to a boost factor of 1.2 [70]. It may, however, be feasible to use higher doses when only the subvolumes are boosted. The DPBC plans have a higher integral tumor dose than conventional treatment planning. This can make it difficult to compare them, since a potential increase in the TCP for DPBC will partly be due to the higher total dose. The DPBC plans were therefore compared to a uniform dose boost with equal total dose. It could have been interesting to examine whether the TCP is dependent on the location of the resistant subvolumes. However, the current TCP model only accounts for the volume of the different regions, not their position.

5.1.4 Estimation of cell densities from ADC maps

A uniform cell density has been the typical approach in TCP modelling, even though it has been shown that most tumors have non-uniform clonogenic cell density [5, 50]. The TCP was therefore first calculated using a constant cell density across the tumor, with a value in agreement with previous TCP modelling studies [50, 69]. However, it may be more accurate to estimate the cell density based on functional imaging. Casares-Magaz et al. used ADC maps to calculate the cell density of the tumor, and investigated how the ADC-based cell densities affected the TCP [5]. Based on this research, ADC maps were used to estimate the average tumor cell density in addition to the average cell density in the resistant and in the sensitive region for all patients included in the TCP modelling. There are, however, some uncertainties related to this approach. The model used to relate the ADC values to cell densities was mainly based on TCP studies of prostate cancer [5]. The conversion may therefore not be very representative for the rectal cancer data used in this thesis, as the density of clonogenic cells vary for different cancer types.

5.1.5 Clinical implementation of DPBC

The TCP value should primarily be used as a relative measure to compare different treatment techniques, as it does not for instance take OARs into consideration. To

evaluate the DPBC plans further, it was therefore of interest to incorporate them into a treatment planning system. Generation of DVHs would be useful to ensure that the desired dose is given to the target volumes, and that the dose boosts do not increase the risks of normal tissue toxicity.

Implementation of the DPBC plans into RayStation involved several processing steps with associated uncertainties. First, the contours from the DPBC plans had to be saved as NifTI files, and adapted to the resolution format of the T_2 weighted MR images used in the treatment planning. Then these files needed to be converted to radiotherapy structures for Raystation to be able to recognize them as contours. RayStation was, however, not able to import these structures, as some of the tags in the DICOM header were not correctly linked to the planning MR images. RaySearch is currently trying to fix this problem.

5.2 Results

5.2.1 DPBC maps

DPBC, or subvolume boosting seems to be the most common approach related to dose painting in previous studies [78, 79, 80, 81]. There may be several reasons for this. First, it is easier to make dose plans in DPBC compared to DPBN, where more advanced methods is needed to compute and prescribe heterogeneous doses across the tumor. DPBC plans are also easier to integrate into conventional treatment planning systems and clinical workflows. Additionally, DPBC is more robust to spatial errors. This factor is especially important for rectal cancer patients, where the risk of bowel movement is high. The downside to DPBC is that it only assumes two sets of characteristics, one that represents the aggressive regions of the tumor, and one that represents the rest of the tumor. In reality, tumor biology characteristics such as the OER, the cell density and the α/β ratio, changes continuously across the tumor. Also, a large contrast in dose levels between the two regions would make it hard to produce steep enough dose gradients. However, this is related to the concept of DPBC. DPBN should be used if more parameter levels are desired.

Statistical testing was done to assess the relationship between the patients' TRG and their volume of R. The aim was to obtain information about whether the tumor

volume adding to the radiation resistant region was larger for the poor responders compared to the good responders. The statistical test was performed before any of the R subvolumes were incorporated into S, when subvolumes smaller than 0.5 cm^3 were removed, and finally, after all subvolumes smaller than 1 cm^3 were disregarded. The volume of R decreased noticeably with increasing subvolume limit, but the same trend was seen for each limit. Patients with TRG3 had significantly larger R volume compared to patients with TRG2 and TRG1 for all subvolume limits. A significant difference was also seen between TRG3 and TRG0 before removing any of the R volumes. Patients with TRG0 were expected to have the lowest volume of R, but this was not the case. This may be related to the small number of patients in each TRG group. Only two patients were in the TRG0 group, which means that outliers have greater impact and can cause unexpected results.

5.2.2 TCP modelling

The TCP was first calculated using the suggested α and β values from the literature. The most favorable results were then seen for an α/β ratio of 11.5 Gy. This was expected, since the ratio represented completely oxygenated conditions in the sensitive region. The least favorable results were seen for the α/β ratio of 11.2 Gy, despite the similar value. However, the results are consistent with the assumption that this α/β ratio accounts for repopulation, which introduces a loss in the efficiency of fractionated radiotherapy. Intermediate results were obtained for the other α/β specific to rectal cancer, which did not account for repopulation. This was also expected.

The gain in TCP was found for different dose boost levels to get an idea of how much the dose had to be escalated to obtain sufficient tumor control. When using an OER of 1.75, the TCP reached a maximum close to 100% approximately at b=1.5 for α/β=11.5 Gy. For α/β=5.1 Gy, the maximum TCP was slightly lower, and for α/β=11.2, the TCP did not get any higher than about 10%. When using an OER of 2.7, a noticeably higher dose boost was needed to reach the maximum TCP. Overall, the TCPs seemed to be quite low, particularly for high dose boost factors. This indicated that the TCP model was incorrect, or that one or more parameters needed to be adjusted.

The TCP modelling was therefore also done by fitting the α value to the cohort TCP for a standard dose (b=1). Figure 4.5 shows that with this approach, the model predicted tumor control for all the α/β ratios at b=1.2 and 1.8 for an OER of 1.75 and 2.7, respectively. A b-value of 1.2 is suitable for clinical application, and is consistent with the dose boosts used in other studies [70]. When different α/β values were used, the model predicted very similar TCPs compared to the first approach, where the choice of α/β had a large impact on the results, and was a major source of uncertainty.

The TCP was also calculated for a uniform dose boost to the whole tumor with equal total dose as the corresponding DPBC plan. Before fitting the α value to the cohort TCP, the TCPs for a uniform dose boost were remarkably low compared to the TCPs for DPBC. Twice as high dose as used in conventional radiotherapy was needed to get TCP values larger than 0. By fitting the α value, the TCP modelling predicted more reliable values, and it was therefore decided to use this approach in further analyses.

The TCPs for the uniform dose boost strategy were still noticeably lower compared to the corresponding DPBC plans. This is mainly because the resistant subvolumes were assigned a too low dose to obtain tumor control in these regions. Since the total TCP was found by multiplying the individual TCP for the different regions, a low TCP for the resistant region will affect the total result even if it only accounts for a small part of the tumor. The dose to the sensitive region was slightly increased for a uniform dose boost compared to DPBC, but as seen in table 4.1, the TCP for the sensitive region was already 100% for each patient, thus escalating the dose would not influence the total TCP. These findings are consistent with previous research, and indicate that hypoxia targeted dose painting may be more favorable than to uniformly increase the total dose to the whole tumor [57].

From figure 4.7 it is seen that the patients obtained larger individual differences for a uniform dose boost than for DPBC. This is mainly related to the varying volume of the resistant regions. According to equation (2.12), patients with larger resistant regions will obtain a lower TCP compared to patients that have smaller subvolumes. However, for DPBC, all patients quickly reached a maximum TCP as the dose to the

resistant region was high enough to obtain tumor control regardless of the volume.

5.2.3 ADC-based cell densities

Cell densities were estimated based on average ADC values for the tumor, the resistant and the sensitive regions. The model used to relate them was based on ADC values ranging from 0.5 to 2.5 $\cdot 10^{-3}$ mm^2/s and corresponding cell densities ranging from 10^5 to 10^7 cells/cm^3. However, the average ADC values found in the present work ranged from 0.555 to 1.382 $\cdot 10^{-3}$ mm^2/s. The conversion was therefore not so sensitive for the data used in this thesis, and the estimated cell densities ended up being shifted towards higher values of the scale. Prostate cancer is known to be highly heterogeneous, with a lower density of clonogenic cells across the prostate compared to other forms of cancer [82]. Therefore, it may still be reasonable to assume that rectal tumors have higher cell densities.

Figure 4.8 revealed some difference in the cell density between the sensitive and the resistant part of the tumor. The average cell density in the resistant regions seemed to be slightly higher than for the rest of the tumor, and may further confirm that these regions are more aggressive. Moreover, it was of interest to investigate whether the cell density was higher for the poor responders compared to the good responders. However, no clear trend was observed between the cell densities for different TRG groups. This might be related to the small number of patients in each group, as previously mentioned.

The ADC-based cell densities were included in the TCP modelling, and compared to the TCPs based on a constant cell density of 10^6 cells/cm^3. The TCPs based on the cell densities from ADC maps were lower for all patients, which was expected since the cell densities were close to 10^7 cells/cm^3. The difference was largest when using low dose boost factors, and evened out with increasing boost. The overall implication is that a cell density of 10^6 cells/cm^3 may be too low and hence overestimate the TCP. It was also of interest to model the TCP for a constant cell density of 10^7 cells/cm^3 to investigate if there were any differences compared to the TCP for ADC-based cell densities.

The average TCP with a constant cell density of 10^7 cells/cm^3 was almost identical

to the average TCP with ADC-based cell densities. However, the variation in TCP between patients was larger for ADC-based cell densities than for both of the constant cell densities. This may imply that patient-specific cell densities can predict the outcome more accurately for each patient, and may be helpful to further individualize the treatment. On the other hand, the average TCP values indicate that setting a constant cell density of 10^7 cells/cm^3 across the tumor may be sufficient. It would have been interesting to adapt the model to fit data from rectal cancer, but the lack of literature on rectal cancer makes this difficult.

5.3 Clinical implications

The presence of hypoxic regions is known to influence the effect of radiation, and can be difficult to treat with conventional radiotherapy [83]. Dose painting has the potential to overcome regions with increased radiation resistance, and improve the local tumor control. A major advantage of dose painting compared to a uniform escalation to the whole tumor, is that the small boost volumes make it possible to prescribe high dose levels to these without increasing the risks of normal tissue toxicity [4]. Another benefit with dose painting is that the resistant regions are found based on quantitative values, and therefore the variability related to manual contouring is reduced. As the DPBC plans only consist of two dose levels, they also have the potential to easily be integrated into conventional treatment planning systems and clinical workflows [84].

There are, however, some challenges related to the clinical realization of dose painting. The first step is to find a reliable imaging biomarker that provides information about tumor biology and radiosensitivity. R_2^*-AUC has been found to be significantly associated with the CRT outcome in rectal cancer patients, but has not yet been shown to be directly related to a relevant biological mechanism. Furthermore, it is important to image the patient in exact treatment position, so that the R_2^*-AUC maps are representative for the tumor biology at the time of radiotherapy. The boost volume may change during the treatment course due to reoxygenation or organ motion. Replanning during the treatment should therefore be considered if repeated MR images during the course of radiotherapy are available.

Radiotherapy treatment planning generally requires a planning CT to obtain elec-

tron density information for dose calculations [7]. Dose painting based on MRI may therefore be more compatible with MR-only radiotherapy to reduce errors related to image fusion. Clinical implementation of dose painting plans still requires robust and accurate image registration tools, including resampling of the R_2^*-AUC maps to the dose planning grid [4].

Dose painting is a relatively new radiotherapy approach that has shown promising results. However, the variety of different and potentially relevant imaging techniques and biomarkers makes it possible to investigate a number of different dose painting strategies. The majority of studies regarding hypoxia targeted dose painting have based the visualization of hypoxia on PET tracers [78, 80, 81]. When it comes to rectal cancer, there are several dose boost trials, but few includes a dose painting approach [70]. This makes it challenging to compare the results.

5.4 Future work

DPBC based on R_2^*-AUC maps is an experimental methodology with room for improvement in several areas. Before dose painting can be clinically implemented, the radiobiological targets that most likely will benefit from a dose escalation have to be identified. First, it should therefore be investigated whether R_2^*-AUC is directly associated with hypoxia, and how to optimally define the hypoxic subvolumes.

The modelling parameters used in the TCP modelling should also be looked into more closely, as should the correlation between ADC values and cell densities for rectal cancer. The image processing that was done in order to match the original tumor ROIs from the T_2 weighted images to the R_2^* image grid, should be performed for each patient to get more accurate DPBC maps. Currently, the resampling was only done for the analyses involving ADC maps. Also, different software tools were used for the resampling than for the rest of the analyses. If possible, the resampling should be integrated into the DPBC model to simplify the workflow and save time.

The primary area for future work is to continue the incorporation of the DPBC plans into RayStation. If the dose plans were to be used in the clinic, they have to be compatible with the treatment planning system. Also, the ability to generate DVHs is useful to evaluate if the desired dose is given to the target volumes, and if

the doses to OARs are kept low. It also makes it possible to further compare the DPBC plans with the corresponding conventional and uniform dose boost plans.

6 Conclusion

This thesis investigated the potential advantage of DPBC prescriptions based on R_2^*-AUC tumor maps in rectal cancer. TCP modelling showed enhanced tumor control for the DPBC maps compared to a uniform boost to the whole tumor. Clinically, this suggests that DPBC has the potential to overcome radioresistant regions, and increase the probability of a good radiotherapy treatment outcome. It is, however, crucial to continue the work on including the DPBC plans into a treatment planning system to investigate the impact on OARs.

ADC maps were used to calculate non-uniform, patient-specific cell densities in an attempt to individualise the TCP modelling further. TCP modelling showed similar results when using a constant cell density of 10^7 cells/cm^3 compared to using ADC-based cell densities. This indicates that it may be sufficient to assume a constant cell density across the tumor, which makes future clinical implementation simpler. The conversion used to translate ADC values to cell densities should, however, be adapted more closely to rectal cancer to further examine this.

References

[1] G. F. Weber, R. Rosenberg, J. E. Murphy, C. M. zum Büschenfelde, and H. Friess, "Multimodal treatment strategies for locally advanced rectal cancer," *Expert Review of Anticancer Therapy*, vol. 12, no. 4, p. 481–494, 2012.

[2] World Health Organization, "WHO report on cancer: Setting priorities, investing wisely and providing care for all," Geneva: World Health Organization; 2020.

[3] P. Vaupel, "Tumor microenvironmental physiology and its implications for radiation oncology," *Seminars in Radiation Oncology*, vol. 14, no. 3, p. 198–206, 2004.

[4] D. Thorwarth, "Biologically adapted radiation therapy," *Zeitschrift für Medizinische Physik*, vol. 28, no. 3, pp. 177–183, 2018.

[5] O. Casares-Magaz, U. van der Heide, J. Rørvik, P. Steenbergen, and L. Muren, "A tumour control probability model for radiotherapy of prostate cancer using magnetic resonance imaging-based apparent diffusion coefficient maps," *Radiotherapy and Oncology*, vol. 119, no. 1, p. 111–116, 2016.

[6] E. Malinen, Å. Søvik, D. Hristov, Ø. S. Bruland, and D. R. Olsen, "Adapting radiotherapy to hypoxic tumours," *Phys. Med. Biol.*, vol. 51, p. 4903–4921, 2006.

[7] R. Alonzi, "Functional radiotherapy targeting using focused dose escalation," *Clinical Oncology*, vol. 27, no. 10, p. 601–617, 2015.

[8] Functional MRI of Hypoxia-mediated Rectal Cancer Aggressiveness (OxyTarget). 2013, retrieved 21.02.2020. [Online]. Available at `https://clinicaltrials.gov/ct2/show/NCT01816607`.

[9] I. F. Syversen, "*Prediction of chemoradiotherapy response in rectal cancer using static and dynamic R2* MRI measurements.*" Project thesis, NTNU, 2017.

[10] F. Julbø, "*Phantom MR imaging for MR-only radiotherapy: identifying optimal sequences and acquisition parameters.*" Project thesis, NTNU, 2019.

[11] C. Westbrook, C. K. Roth, and J. Talbot, *MRI in practice*. Wiley-Blackwell, 4th ed., 2011.

[12] M. D. Guimaraes, A. Schuch, B. Hochhegger, J. L. Gross, R. Chojniak, and E. Marchior, "Functional magnetic resonance imaging in oncology: State of the art," *Radiologia Brasileira*, vol. 47, no. 2, p. 101–111, 2014.

[13] R. B. Buxton, *Introduction to Functional Magnetic Resonance Imaging: Principles and Techniques*. Cambridge University Press, 2002.

[14] E. Grøvik, *Multimodal Dynamic MRI for Structural and Functional Assessment of Cancer*. PhD thesis, University of Oslo, 2017.

[15] M. A. Schmidt and G. S. Payne, "Radio therapy planning using MRI," *Physics in Medicine and Biology*, vol. 60, no. 22, p. R323–R361, 2015.

[16] G.-H. Jahng, K.-L. Li, L. Ostergaard, and F. Calamante, "Perfusion magnetic resonance imaging: A comprehensive update on principles and techniques," *Korean Journal of Radiology*, vol. 15, no. 5, p. 554–577, 2014.

[17] Questions and answers in MRI. Echo-Planar Imaging (EPI). Retrieved 12.02.2020. [Online]. Available at `http://mriquestions.com/echo-planar-imaging.html`.

[18] M. A. Schmidt and G. S. Payne, "Dynamic multi-echo DCE- and DSC-MRI in rectal cancer: Low primary tumor K^{trans} and $\Delta R_2{}^*$ peak are significantly associated with lymph node metastasis," *Journal of Magnetic Resonance Imaging*, vol. 46, no. 1, p. 194–206, 2017.

[19] V. Baliyan, C. J. Das, R. Sharma, and A. K. Gupta, "Diffusion weighted imaging: Technique and applications," *World journal of radiology*, vol. 8, no. 9, p. 785–798, 2016.

[20] A. R. Padhani, G. Liu, D. Mu-Koh, T. L. Chenevert, H. C. Thoeny, T. Takahara, A. Dzik-Jurasz, B. D. Ross, M. V. Cauteren, D. Collins, D. A. Hammoud, G. J. S. Rustin, B. Taouli, and P. Choyke, "Diffusion-weighted magnetic resonance imaging as a cancer biomarker: Consensus and recommendations," *Neoplasia*, vol. 11, no. 2, pp. 102–125, 2009.

[21] L. Monguzzia, D. Ippolitoa, D. P. Bernasconic, C. Tratteneroa, S. Galimbertica, and S. Sironia, "Locally advanced rectal cancer: Value of ADC mapping in prediction of tumor response to radiochemotherapy," *European Journal of Radiology*, vol. 82, no. 2, p. 234–240, 2013.

[22] L. L. Gunderson and J. E. Tepper, *Clinical Radiation Oncology*. Elsevier, 2011.

[23] D. Hanahan and R. A. Weinberg, "The hallmarks of cancer," *Cell*, vol. 100, no. 1, p. 57–70, 2000.

[24] D. Hanahan and R. A. Weinberg, "The hallmarks of cancer: The next generation," *Cell*, vol. 144, no. 5, pp. 646–674, 2011.

[25] J. C. Forster, W. M. Harriss-Phillips, M. J. J. Douglass, and E. Bezak, "A review of the development of tumor vasculature and its effects on the tumor microenvironment," *Hypoxia*, vol. 5, pp. 21–32, 2017.

[26] O. Trédan, C. M. Galmarini, K. Patel, and I. F. Tannock, "Drug resistance and the solid tumor microenvironment," *Journal of the National Cancer Institute*, vol. 99, no. 19, p. 1441–1454, 2007.

[27] M. B. Schaaf, A. D. Garg, and P. Agostinis, "Defining the role of the tumor vasculature in antitumor immunity and immunotherapy," *Cell Death & Disease*, vol. 9, no. 115, 2018.

[28] J. Rødal, *On Functional Imaging and Treatment Planning for Biologically Adapted Radiotherapy*. PhD thesis, NTNU and Oslo University Hospital, 2012.

[29] K. A. Miles, "Tumour angiogenesis and its relation to contrast enhancement on computed tomography: a review," *European Journal of Radiology*, vol. 30, no. 3, pp. 198–205, 1999.

[30] J. M. Brown, "Exploiting the hypoxic cancer cell: mechanisms and therapeutic strategies," *Molecular Medicine Today*, vol. 6, no. 4, pp. 157–162, 2000.

[31] E. J. Hall and A. J. Giaccia, *Radiobiology for the radiologist*. Lippincott Williams & Wilkins, 2011.

[32] Oncohema Key. Dose-Response Modifiers in Radiation Therapy. Retrieved 06.03.2020. [Online]. Available at `https://oncohemakey.com/dose-response-modifiers-in-radiation-therapy/`.

[33] P. Vaupel and A. Mayer, "Hypoxia and anemia: effects on tumor biology and treatment resistancet," *Transfusion Clinique et Biologique*, vol. 12, no. 1, pp. 5–10, 2005.

[34] S. A. Hendry, R. H. Farnsworth, B. Solomon, M. G. Achen, S. A. Stacker, and S. B. Fox, "The role of the tumor vasculature in the host immune response: Implications for therapeutic strategies targeting the tumor microenvironment," *Front. Immunol.*, vol. 7, p. 621, 2016.

[35] The Norwegian Directorate of Health, "Nasjonalt handlingsprogram med retningslinjer for diagnostikk, behandling og oppfølging av kreft i tykktarm og endetarm," 2019.

[36] R. Glynne-Jones, L. Wyrwicz, E. Tiret, G. Brown, C. Rödel, A. Cervantes, and D. Arnold, "Rectal cancer: ESMO clinical practice guidelines for diagnosis, treatment and follow-up†," *Annals of Oncology*, vol. 28, no. 4, p. iv22–iv40, 2017.

[37] American Cancer Society, "Colorectal cancer facts & figures 2017-2019," 2017.

[38] Cancer Registry of Norway, "Cancer in Norway 2018 - Cancer incidence, mortality, survival and prevalence in Norway," 2019.

[39] H. Kirkegaard, N. F. Johnsen, J. Christensen, K. Frederiksen, K. Overvad, and A. Tjønneland, "Association of adherence to lifestyle recommendations and risk of colorectal cancer: a prospective danish cohort study," *BMJ*, vol. 341, p. c5504, 2010.

[40] National Cancer Institute. Colon Cancer Treatment – Patient Version. Retrieved 19.03.2020. [Online]. Available at `https://www.cancer.gov/types/colorectal/patient/colon-treatment-pdq`.

[41] American Joint Committee on Cancer, *AJCC Cancer Staging Manual*. Springer, 7th ed., 2010.

[42] C. A. Maurer, P. Renzulli, C. Kull, S. A. Käser, L. Mazzucchelli, A. Ulrich, and M. W. Büchler, "The impact of the introduction of total mesorectal excision on local recurrence rate and survival in rectal cancer: Long-term results," *Annals of Surgical Oncology*, vol. 18, no. 7, p. 1899–1906, 2011.

[43] D. A. Wibe, P. R. Rendedal, E. Svensson, J. Norstein, T. J. Eide, H. E. Myrvold, and O. Søreide, "Prognostic significance of the circumferential resection margin following total mesorectal excision for rectal cancer," *BJS*, vol. 89, no. 3, pp. 327–334, 2002.

[44] Y. Zhu, Y. Sun, S. Hu, Y. Jiang, J. Yue, X. Xue, L. Yang, and L. Xue, "Comparison of five tumor regression grading systems for gastric adenocarcinoma after neoadjuvant chemotherapy: a retrospective study of 192 cases from national cancer center in china," *BMC Gastroenterology*, vol. 17, no. 41, 2017.

[45] K. M. Bakke, K. H. Hole, S. Dueland, K. K. Grøholt, K. Flatmark, A. H. Ree, T. Seierstad, and K. R. Redalen, "Diffusion-weighted magnetic resonance imaging of rectal cancer: tumour volume and perfusion fraction predict chemoradiotherapy response and survival," *Acta Oncologica*, vol. 56, no. 6, p. 813–818, 2017.

[46] J. Yu, N. Li, X. Wang, H. Ren, W. Wang, S. Wang, Y. Song, Y. Liu, Y. Li, X. Zhou, A. Luo, Z. Liu, and J. Jin, "Circulating serum microrna-345 correlates with unfavorable pathological response to preoperative chemoradiotherapy in locally advanced rectal cancer," *Oncotarget*, vol. 7, no. 39, p. 64233–64243, 2016.

[47] M. C. Joiner and A. J. van der Kogel, *Basic Clinical Radiobiology*. CRC Press, 5th ed., 2019.

[48] N. Suntharalingam, E. Podgorsak, , and J. Hendry, "Basic Radiobiology," in *Radiation Oncology Physics: A Handbook for Teachers and Students*, p. 485–504, IAEA, 2005.

[49] H. R. Withers, "The Four R's of Radiotherapy," *Advances in Radiation Biology*, vol. 5, pp. 241–271, 1975.

[50] S. Webb and A. E. Nahum, "A model for calculating tumour control probability in radiotherapy including the effects of inhomogeneous distributions of dose and clonogenic cell density," *Physics in Medicine and Biology*, vol. 38, no. 6, p. 653–666, 1993.

[51] C. P. Karger, "Biological models in treatment planning," in *New Technologies in Radiation Oncology*, p. 221–235, Springer, 2006.

[52] F. Tommasino, A. Nahum, and L. Cella, "Increasing the power of tumour control and normal tissue complication probability modelling in radiotherapy: recent trends and current issues," *Translational Cancer Research*, vol. 6, no. 5, p. S807–S821, 2017.

[53] "3. Definition of volumes," *Journal of the International Commission on Radiation Units and Measurements*, vol. 14, no. 2, p. 55–63, 2014.

[54] M. Brændengen, M. G. Guren, and B. Glimelius, "Target volume definition in rectal cancer: What is the best imaging modality," *Current Colorectal Cancer Reports*, vol. 9, no. 2, p. 116–125, 2013.

[55] M. Brændengen, K. Hansson, C. Radu, A. Siegbahn, H. Jacobsson, and B. Glimelius, "Delineation of gross tumor volume (GTV) for radiation treatment planning of locally advanced rectal cancer using information from MRI or FDG-PET/CT: A prospective study," *Current Colorectal Cancer Reports*, vol. 81, no. 4, pp. e439–e445, 2011.

[56] J. Jonsson, T. Nyholm, and K. Söderkvist, "The rationale for MR-only treatment planning for external radiotherapy," *Clin Transl Radiat Oncol*, vol. 18, p. 60–65, 2019.

[57] Å. Søvik, E. Malinen, Ø. S. Bruland, S. M. Bentzen, and D. R. Olsen, "Optimization of tumour control probability in hypoxic tumours by radiation dose redistribution: A modelling study," *Physics in Medicine and Biology*, vol. 52, no. 2, pp. 499–513, 2006.

[58] S. M. Bentzen and V. Gregoire, "Molecular imaging-based dose painting: A novel paradigm for radiation therapy prescription," *Seminars in Radiation Oncology*, vol. 21, no. 2, pp. 101–110, 2011.

[59] A. Gago-Arias, B. Sánchez-Nieto, I. Espinoza, C. P. Karger, and J. Pardo-Montero, "Impact of different biologically-adapted radiotherapy strategies on tumor control evaluated with a tumor response model," *PLoS ONE*, vol. 13, no. 4, 2018.

[60] C. C. Ling, J. Humm, S. Larson, H. Amols, Z. Fuks, S. Leibel, and J. A. Koutcher, "Towards multidimensional radiotherapy (MD-CRT): biological imaging and biological conformality," *International Journal of Radiation Oncology, Biology, Physics*, vol. 47, no. 3, p. 551–560, 2000.

[61] O. J. Gurney-Champion, F. Mahmood, M. van Schie, R. Julian, B. George, M. E. P. Philippens, U. A. van der Heide, D. Thorwarth, and K. R. Redalen, "Quantitative imaging for radiotherapy purposes," *Radiotherapy and Oncology*, vol. 146, pp. 66–75, 2020.

[62] R. J. D. Prestwich, S. Vaidyanathan, and A. F. Scarsbrook, "Functional imaging biomarkers: Potential to guide an individualised approach to radiotherapy," *Clinical Oncology*, vol. 27, no. 10, p. 588–600, 2015.

[63] J. E. Bayouth, T. L. Casavant, M. M. Graham, M. Sonka, M. Muruganandham, and J. M. Buatti, "Image-based biomarkers in clinical practice," *Seminars in Radiation Oncology*, vol. 21, no. 2, pp. 157–166, 2011.

[64] A. V. Chvetsov, J. G. Rajendran, J. Zeng, S. A. Patel, S. R. Bowen, and E. Y. Kim, "Theoretical effectiveness of cell survival in fractionated radiotherapy with hypoxia-targeted dose escalation," *Medical Physics*, vol. 44, no. 5, pp. 1975–1982, 2017.

[65] K. L. Rød, "Simulations of dose painting based on functional MRI in rectal cancer," Master's thesis, NTNU, 2019.

[66] N. Nachar, "The mann-whitney u: A test for assessing whether two independent samples come from the same distribution," *Tutorials in Quantitative Methods for Psychology*, vol. 4, no. 1, pp. 13–20, 2008.

[67] R. Suwinski, I. Wzietek, R. Tarnawski, A. Namysl-Kaletka, M. Kryj, A. Chmielarz, and J. Wydmaǹski, "Moderately low alpha/beta ratio for rectal cancer may best explain the outcome of three fractionation schedules of pre-

operative radiotherapy," *International Journal of Radiation Oncology, Biology, Physics*, vol. 69, no. 3, p. 793–799, 2007.

[68] F. M. Buffa, C. West, K. Byrne, J. V. Moore, and A. E. Nahum, "Radiation response and cure rate of human colon adenocarcinoma spheroids of different size: the significance of hypoxia on tumor control modelling," *International Journal of Radiation Oncology, Biology, Physics*, vol. 49, no. 4, pp. 1109–1118, 2001.

[69] S. Walsh and W. van der Putten, "A TCP model for external beam treatment of intermediate-risk prostate cancer," *Medical Physics*, vol. 40, no. 3, p. 031709, 2013.

[70] J. D. V. Wickle, E. S. Paulson, J. C. Landry, B. A. Erickson, and W. A. Hall, "Adaptive radiation dose escalation in rectal adenocarcinoma: a review," *Journal of Gastrointestinal Oncology*, vol. 8, no. 5, p. 902–914, 2017.

[71] A. Surov, H. J. Meyer, and A. Wienke, "Correlation between apparent diffusion coefficient (ADC) and cellularity is different in several tumors: a meta-analysis," *Oncotarget*, vol. 8, no. 35, p. 59492–59499, 2017.

[72] M. McCormicka, X. Liu, J. Jomier, C. Marion, and L. Ibanez, "ITK: enabling reproducible research and open science," *Front Neuroinform*, vol. 8, no. 13, 2014.

[73] D. Berwouts, L. A. M. Olteanu, F. Duprez, T. Vercauteren, W. D. Gersema, W. D. Nevea, C. V. de Wiele, and I. Madani, "Three-phase adaptive dose-painting-by-numbers for head-and-neck cancer: initial results of the phase I clinical trial," *Radiotherapy and Oncology*, vol. 107, no. 3, pp. 310–316, 2013.

[74] K. Håkansson, L. Specht, M. C. Aznar, J. H. Rasmussen, S. M. Bentzen, and I. R. Vogelius, "Prescribing and evaluating target dose in dose-painting treatment plans," *Acta Oncologica*, vol. 53, no. 9, pp. 1251–1256, 2014.

[75] M. Durantea, R. Orecchia, and J. S. Loeffler, "Charged-particle therapy in cancer: clinical uses and future perspectives," *Nature Reviews Clinical Oncology*, vol. 14, p. 483–495, 2017.

[76] N. Bassler, O. Jäkel, C. S. Søndergaard, and J. B. Petersen, "Dose- and LET-painting with particle therapy," *Acta Oncologica*, vol. 49, no. 7, pp. 1170–1176, 2010.

[77] E. Malinen and Å. Søvik, "Dose or 'LET' painting – What is optimal in particle therapy of hypoxic tumors?," *Acta Oncologica*, vol. 54, no. 9, p. 1614–1622, 2015.

[78] I. Madani, W. Duthoy, C. Derie, W. D. Gersem, T. Boterberg, M. Saerens, F. Jacobs, V. Grégoire, M. Lonneux, L. Vakaet, B. Vanderstraeten, W. Bauters, K. Bonte, H. Thieren, and W. D. Neve, "Positron emission tomography-guided, focal-dose escalation using intensity-modulated radiotherapy for head and neck cancer," *International Journal of Radiation Oncology*Biology*Physics*, vol. 68, no. 1, pp. 126–135, 2007.

[79] I. M. Lips, U. A. van der Heide, K. Haustermans, E. N. van Lin, F. Pos, S. P. Franken, A. N. Kotte, C. H. van Gils, and M. van Vulpen, "Single blind randomized phase III trial to investigate the benefit of a focal lesion ablative microboost in prostate cancer (FLAME-trial): study protocol for a randomized controlled trial," *Trials*, vol. 12, no. 255, 2011.

[80] W. van Elmpt, D. D. Ruysscher, A. van der Salm, A. Lakeman, J. van der Stoep, D. Emans, E. Damen, M. Öllers, J.-J. Sonke, and J. Belderbos, "The PET-boost randomised phase II dose-escalation trial in non-small cell lung cancer," *Radiotherapy and Oncology*, vol. 104, no. 1, pp. 67–71, 2012.

[81] S. Welz, D. Mönnich, C. Pfannenberg, K. Nikolaou, M. Reimold, C. L. Fougère, G. Reischl, P.-S. Mauz, F. Paulsen, M. Alber, C. Belka, D. Zips, and D. Thorwarth, "Prognostic value of dynamic hypoxia pet in head and neck cancer: Results from a planned interim analysis of a randomized phase II hypoxia-image guided dose escalation trial," *Radiotherapy and Oncology*, vol. 124, no. 3, pp. 526–532, 2017.

[82] Y. P. Yu and J.-H. Luo, "Pathological factors evaluating prostate cancer," *Histology and histopathology*, vol. 22, no. 11, pp. 1291–1300, 2007.

[83] H. Harada, "How can we overcome tumor hypoxia in radiation therapy?," *Journal of radiation research*, vol. 52, no. 5, pp. 545–556, 2011.

[84] M. Gérard, A. Corroyer-Dulmont, P. Lesueur, S. Collet, M. Chérel, M. Bourgeois, D. Stefan, E. J. Limkin, C. Perrio, J.-S. Guillamo, B. Dubray, M. Bernaudin, J. Thariat, and S. Valable, "Hypoxia imaging and adaptive radiotherapy: A state-of-the-art approach in the management of glioma," *Front med*, vol. 6, no. 117, 2019.

A Code

A.1 sortT2.py

```
1
2 #This script sorts the T2-weighted images (received in DICOM format) for each patient in
3 #the z-direction. These are the MR images used for TN staging and delineation of
4 #tumor ROIs. The script is based on MATLAB scripts written by Karina Rød.
5
6 import numpy as np
7 import os
8 import pydicom
9 import matplotlib.pyplot as plt
10
11 #path towards the OxyTarget data folder
12 filePath = '/Users/frida/Documents/Fysmat 5. klasse/Masteroppgave/MR_data/'
13
14 #patients that will be analysed (patient 126 have been excluded)
15 patientList = [24, 27, 32, 41, 43, 44, 47, 49, 50, 51, 52, 55, 56, 67, 74, 79, 80, 87,
       89, 90, 96, 107, 116, 120, 121, 125, 128, 131, 138, 146, 150, 153, 154, 170]
16
17 nPatients = len( patientList )
18
19 #Loop that goes over all patients that are going to be analysed
20 for patient in patientList :
21     i = 0
22     #Make a list over all the image files and count them
23     imList = []
24     for file in os.listdir ( filePath + "OxyTarget_" + str(patient) + "/T2"):
25         if file.endswith(".dcm"):
26             imList.append(os.path.join( filePath + "OxyTarget_" + str(patient) + "/T2"
      ,file))
27         i+=1
28
29     nImT2 = len(imList)
30
31     #Ref file
32     RefDs = pydicom.dcmread(imList[0])
33
34     #Load dimensions
35     ConstPixelDims = (int(RefDs.Rows), int(RefDs.Columns), nImT2)
36
37     #Load spacing values (in mm)
38     ConstPixelSpacing = (float(RefDs.PixelSpacing[0]), float(RefDs.PixelSpacing[1]),
       float(RefDs.SliceThickness))
39
40     #Array to store all T2 images
41     imT2 = np.zeros(ConstPixelDims, dtype=RefDs.pixel_array.dtype)
```

```
42
43      #List to store z values
44      zValueT2 = np.zeros(nImT2)
45
46      i = 0
47      #Loop through all the DICOM files to get z-values
48      for file in imList:
49          #Read the file
50          ds = pydicom.dcmread(file)
51          #Puts slice position into a list
52          zValueT2[i] = ds.ImagePositionPatient[2]
53          i+=1
54
55      #Sorts the slices
56      sort_zindex = np.argsort(zValueT2)
57      sort_zvalues = np.sort(zValueT2)
58
59      i = 0
60      #Loop through all the DICOM files:
61      for file in imList:
62          #Read the file
63          ds = pydicom.dcmread(file)
64          #Store the raw image data in sorted order
65          imT2[:, :, np.where(sort_zindex==i)[0][0]] = ds.pixel_array
66          i+=1
67
68      #Saving variables to a .npz-file in the patient's T2 folder
69      np.savez(filePath + "OxyTarget_" + str(patient) + "/T2/3Dmatrix", imT2=imT2,
        zValueT2=sort_zvalues, nSlicesT2=nImT2, nImT2=nImT2)
```

A.2 sortDynamic.py

```
1
2  #This script sorts the dynamic images obtained with the DSC sequence (received
3  #in DICOM format). These are the maps of the R2* values. Since the data set is
4  #4D, the images are sorted with respect to position and acquisition time. The
5  #script is based on MATLAB scripts written by Karina Rød.
6
7  import numpy as np
8  import os
9  import pydicom
10 import matplotlib.pyplot as plt
11
12 #path towards the OxyTarget data folder
13 filePath = '/Users/frida/Documents/Fysmat 5. klasse/Masteroppgave/MR_data/'
14
15 #patients that will be analysed
16 patientList = [24, 27, 32, 41, 43, 44, 47, 49, 50, 51, 52, 55, 56, 67, 74, 79, 80, 87,
       89, 90, 96, 107, 116, 120, 121, 125, 128, 131, 138, 146, 150, 153, 154, 170]
```

```
17
18 nPatients = len( patientList )
19
20 #Loop that goes over all patients that are going to be analysed
21 for patient in patientList :
22     i = 0
23     #Make a list over all the image files
24     imList = []
25     for file in os. listdir ( filePath + "OxyTarget_" + str(patient) + "/R2Star"):
26         if file .endswith(".dcm"):
27             imList.append(os.path. join ( filePath + "OxyTarget_"
28             + str( patient ) + "/R2Star", file ))
29         i+=1
30
31     #Number of image files
32     nIm = len(imList)
33
34     #Ref file
35     RefDs = pydicom.dcmread(imList[80])
36
37     #Load dimensions
38     ConstPixelDims = (int(RefDs.Rows), int(RefDs.Columns), nIm)
39
40     #Load spacing values (in mm)
41     ConstPixelSpacing = (float(RefDs.PixelSpacing[0]) , float (RefDs.PixelSpacing[1]) ,
       float (RefDs. SliceThickness ))
42
43     #Array to store acquisition time values
44     acqTimeValue = np.zeros(nIm)
45
46     #Array to store z values
47     zValue = np.zeros(nIm)
48
49     #Array to store image data from all files
50     im = np.zeros(ConstPixelDims, dtype=RefDs. pixel_array .dtype)
51
52     i = 0
53     #Loop through all the DICOM files
54     for file in imList:
55         #Read the file
56         ds = pydicom.dcmread(file)
57         #Image needs to be multiplied with a scaling factor to get
58         #the correct R2* value
59         scalingFactor = ds[0x00771001].value
60         #Puts slice position and acquisition times into arrays
61         zValue[i] = ds.ImagePositionPatient [2]
62         acqTimeValue[i] = ds.AcquisitionTime
63         #Puts image data into 3D array
64         im[:, :, i] = ds. pixel_array * scalingFactor
```

```
        i+=1

    #make 2D array with z-values in 1. row and time-values in 2.
    #row to sort the files
    zAndTime = np.zeros((2,nIm))
    zAndTime[0,:]=zValue
    zAndTime[1,:]=acqTimeValue

    #Find the indices that sorts the images in the order where all
    #images with the lowest z value come first, and these are
    #sorted by acqusition time internally, and so on
    sortIndex = np.lexsort((zAndTime[1,:],zAndTime[0,:]))

    #number of acquisition time values
    nAt = len(set(acqTimeValue))

    #number of slices
    nSlices = round(nIm/nAt)

    #sort the image files
    sortedIm = im[:,:, sortIndex]

    #reshape the array to 4D; the first two dimensions are image
    #data, the 3. is z-values and the 4. is acquisition times
    im4D = np.reshape(sortedIm,(ConstPixelDims[0],ConstPixelDims[1], nSlices,nAt))

    #sort zValue
    zValue_set = set(zValue)
    zValue_new = np.sort(list(zValue_set))

    #sort acqTimeValue
    acqTimeValue_set = set(acqTimeValue)
    acqTimeValue_new = np.sort(list(acqTimeValue_set))

    #Saving variables to a .npz-file in the patient's R2* folder
    np.savez(filePath + "OxyTarget_" + str(patient) + "/R2Star/4Dmatrix", im=im4D,
    nAt=nAt, nSlices=nSlices, nIm=nIm, zValue = zValue_new, acqTimeValue =
    acqTimeValue_new)
```

A.3 dynamicROIs.py

```

#This script uploads the tumor ROIs and adapt them to fit the DSC data format.
#The script is based on MATLAB scripts written by Karina Rød.

import numpy as np
import pydicom
import matplotlib.pyplot as plt
import nibabel as nib
```

```
9
10 #path towards the OxyTarget data folder
11 filePath = '/Users/frida/Documents/Fysmat 5. klasse/Masteroppgave/MR_data/'
12
13 #patients that will be analysed
14 patientList = [24, 27, 32, 41, 43, 44, 47, 49, 50, 51, 52, 55, 56, 67, 74, 79, 80, 87,
       89, 90, 96, 107, 116, 120, 121, 125, 128, 131, 138, 146, 150, 153, 154, 170]
15
16 #Patients that have subvolumes larger than 1cm3
17 patientList2 = [41, 44, 47, 49, 55, 56, 80, 89, 96, 116, 121, 125, 128, 131, 138, 170]
18
19 nPatients = len( patientList )
20
21 #Loop that goes over all patients that are going to be analysed
22 for patient in patientList :
23     i=0
24     #Load the sorted DSC images (R2*maps) and T2 images
25     loadFileT2 = np.load( filePath +"OxyTarget_"+str(patient)+"/T2/3Dmatrix.npz")
26     loadFileR2 = np.load( filePath +"OxyTarget_"+str(patient)+"/R2Star/4Dmatrix.npz")
27     imT2 = loadFileT2["imT2"]
28     nImT2 = loadFileT2["nImT2"]
29     im = loadFileR2["im"]
30     nSlices = loadFileR2["nSlices"]
31     zValueT2 = loadFileT2["zValueT2"]
32     zValue = loadFileR2["zValue"]
33
34     #Load the ROI from the NIfTI file in the binary folder; Prefix "an"
35     #denotes the initials of the radiologist that delineated the ROIs
36     nii = nib.load( filePath +"OxyTarget_"+str(patient)+'/binary/an/tumour.nii')
37     #get image data
38     ROI = nii.get_fdata()
39     #get the right dimensions and scaling
40     ROI = ROI/1000
41     ROI = np.swapaxes( ROI, 0, 1)
42     xPixels = ROI.shape[0]
43     yPixels = ROI.shape[1]
44     nSlicesT2 = ROI.shape[2]
45
46     #For these patients the ROI slices are in the opposite order,
47     #so they have to be reversed
48     if (patient == 32) or (patient == 74) or (patient == 79) or (patient == 96):
49         copy = np.copy(ROI)
50         i = 0
51         for s in range(nSlicesT2-1,-1,-1):
52             ROI[:,:, i] = copy[:,:, s]
53             i += 1
54
55     #Adapting the ROI to fit the DSC format
56     dynamicROI = np.zeros((256, 256, nSlices))
```

```
    z_vals = [] #The 12 z-values from T2W used for DSC

    for z in range(nSlices):
        s = 0
        minimum = 10
        for i in range(nSlicesT2):
            #find T2 slice that is closest in position to DSC slice
            if (np.abs(zValue[z] - zValueT2[i]) < minimum):
                minimum = abs(zValue[z] - zValueT2[i])
                s = i #choose ROI for T2 image i
        z_vals.append(s)

        if (minimum < 4):
            for x in range(256):
                for y in range(256):
                    if ((ROI[2*x+1,2*y+1,s] == 1) or (ROI[2*x,2*y+1,s] == 1) or
                    (ROI[2*x+1,2*y,s] == 1) or (ROI[2*x,2*y,s] == 1)):
                        dynamicROI[x,y,z] = 1

    #Dynamic ROI made by resampling (Only done for patients in patientList2)
    nii = nib.load(filePath + "OxyTarget_" + str(patient) + '/gtv1_onR2star.nii')
    adaptedROI = nii.get_fdata()
    #Must swap to get right dimentions
    adaptedROI_swaped = np.swapaxes(adaptedROI, 0, 1)

    #Saving variables to a .npz-file in the patients' folder
    np.savez(filePath + "OxyTarget_" + str(patient) + "/dynamicROI", dynamicROI=
    dynamicROI, xPixels=xPixels, yPixels=yPixels, z_vals=z_vals, adaptedROI_swaped=
    adaptedROI_swaped)
```

A.4 dynamicR2star.py

```

#This script is used to plot normalised voxel-by-voxel R2* timecourses using
#the DSC-derived images(R2*-maps), for all voxels inside ROIs. Then, R2*-AUC
#is calculated voxel-by-voxel, and a map is generated for each dynamic slice.
#The script is based on MATLAB scripts written by Karina Rød.

import numpy as np
import matplotlib.pyplot as plt

#path towards the OxyTarget data folder
filePath = '/Users/frida/Documents/Fysmat 5. klasse/Masteroppgave/MR_data/'

#patients that will be analysed (126 and 154 have been excluded as
#the number of baseline images could not be found)
patientList = [24, 27, 32, 41, 43, 44, 47, 49, 50, 51, 52, 55, 56, 67, 74, 79, 80, 87,
    89, 90, 96, 107, 116, 120, 121, 125, 128, 131, 138, 146, 150, 153, 170]

```

```
#Patients that have subvolumes larger than 1cm3
patientList2 = [41, 44, 47, 49, 55, 56, 80, 89, 96, 116, 121, 125, 128, 131, 138, 170]

nPatients = len( patientList )

#the number of baseline images for each patient (found by counting manually)
nBaselineImages=[12, 13, 12, 12, 10, 16, 10, 10, 6, 7, 11, 10, 14, 13, 9, 15, 15, 15,
    15, 15, 14, 15, 15, 18, 14, 16, 14, 12, 18, 16, 12, 15, 17];
nBaselineImages2=[16, 10, 10, 14, 15, 14, 15, 16, 14, 12, 17]

#Loop that goes over all patients that are going to be analysed
patientNr = 0
for patient in patientList :
    #load R2* and ROI data
    loadFileR2 = np.load( filePath +"OxyTarget_"+str(patient)+"/R2Star/4Dmatrix.npz")
    loadFileROI = np.load( filePath +"OxyTarget_"+str(patient)+"/dynamicROI.npz")
    im = loadFileR2["im"]
    nSlices = loadFileR2["nSlices"]
    nAt = loadFileR2["nAt"]
    acqTimeValue = loadFileR2["acqTimeValue"]
    dynamicROI = loadFileROI["dynamicROI"]
    adaptedROI = loadFileROI["adaptedROI_swaped"]

    #Make a 3D matrix that holds the peak R2* values
    R2StarPeakEnhancedMap = np.zeros((256,256,nSlices))

    #Make a 3D matrix that holds voxel-vise R2*-AUC values
    AUCmap = np.zeros((256,256,nSlices))
    R2StarPeakEnhancedValues = []
    AUCvalues = []
    curveAverage = np.zeros((256*256,nAt))
    index = 0
    negativeValuesDynamic = 0

    #change from acquisition time to seconds
    t = np.zeros(60)
    for i in range(60):
        h = np.floor(acqTimeValue[i] * 0.0001)
        m = np.floor((acqTimeValue[i] - (h*10000)) * 0.01)
        s = np.floor(acqTimeValue[i]-h * 10000-m * 100)
        t[i] = h*60*60 + m*60 + s +(acqTimeValue[i]-np.floor(acqTimeValue[i]))
    t = t - t[0]

    for s in range( nSlices ):
        tAUC = []
        tVal = t[0]
        tIndex = 0

        #Finding AUC in this interval
```

```
        AUCinterval = 525;
        if (np.amax(t) < AUCinterval):
            tAUC = t
        else:
            while (tVal < AUCinterval):
                tAUC.append(t[tIndex])
                tIndex += 1
                tVal = t[tIndex]

        for x in range(256):
            for y in range(256):
                #only perform calculations inside ROI
                if (dynamicROI[x,y,s] == 1): #use adaptedROI for patientList2
                    Sum = 0
                    #use nBaselineImages2 for patientList2
                    for i in range(nBaselineImages[patientNr]):
                        #Sum R2* for all baseline images
                        Sum = Sum + im[x,y,s,i]
                    baseline = Sum/nBaselineImages[patientNr]

                    #Normalization of curves by substracting baseline
                    pixelArray = np.squeeze(im[x,y,s,:]) - baseline

                    #Finding the maximum value of Delta-R2*
                    maximum = np.amax(pixelArray)

                    #only interested in positive R2*-peak
                    if (maximum > 0):
                        R2StarPeakEnhancedMap[x,y,s] = maximum
                        R2StarPeakEnhancedValues.append(maximum)
                        pixelArrayAUC = np.zeros(len(tAUC))

                        for it in range(len(pixelArrayAUC)):
                            pixelArrayAUC[it] = pixelArray[it]
                        #finding R2*-AUC using composite trapezoidal rule
                        AUCvalues.append(np.trapz(pixelArrayAUC,
                        x=tAUC))

                        AUCmap[x,y,s] = AUCvalues[index]
                        curveAverage[index,:] = pixelArray
                        index += 1

                    elif (maximum < 0):
                        negativeValuesDynamic =
                        negativeValuesDynamic + 1

    #Plot the average of all delta-R2* curves for the patient

    #Saving variables to a .npz-file in the patient's R2* folder
```

```
114     np.savez( filePath  + "OxyTarget_" + str(patient) + "/R2Star/R2StarAUCMap",
        AUCvalues=AUCvalues, AUCmap=AUCmap, negativeValuesDynamic=
        negativeValuesDynamic, t=t, tAUC=tAUC )
115
116     patientNr += 1
```

A.5 filterR2StarAUCmaps.py

```
1
2  #This script is used to filter unphysiological high and low values (noise)
3  #from the parametric R2*-AUC maps generated in dynamicR2Star.py. R2*-AUC
4  #values lying below the 2.5 percentile or above the 97.5 percentile are
5  #assumed to fall within this category and are discarded for each patient.
6  #The script is based on MATLAB scripts written by Karina Rød.
7
8  import numpy as np
9  import matplotlib.pyplot as plt
10 import cv2
11
12 #path towards the OxyTarget data folder
13 filePath = '/Users/frida/Documents/Fysmat 5. klasse/Masteroppgave/MR_data/'
14
15 patientList = [24, 27, 32, 41, 43, 44, 47, 49, 50, 51, 52, 55, 56, 67, 74, 79, 80, 87,
       89, 90, 96, 107, 116, 120, 121, 125, 128, 131, 138, 146, 150, 153, 170]
16
17 #Patients that have subvolumes larger than 1cm3
18 patientList2 = [41, 44, 47, 49, 55, 56, 80, 89, 96, 116, 121, 125, 128, 131, 138, 170]
19
20 nPatients = len( patientList )
21
22 #Loop that goes over all patients that are going to be analysed
23 for patient in patientList:
24     #load R2* AUC maps
25     loadFileR2map = np.load(filePath + "OxyTarget_" + str(patient) + "/R2Star/
       R2StarAUCMap.npz")
26     #load values
27     AUCvalues = loadFileR2map["AUCvalues"]
28     AUCmap = loadFileR2map["AUCmap"]
29     t = loadFileR2map["t"]
30     tAUC = loadFileR2map["tAUC"]
31     xRes = AUCmap.shape[0]
32     yRes = AUCmap.shape[1]
33     nSlices = AUCmap.shape[2]
34
35     #find 2.5 and 97.5 percentile of the R2*-AUC map by using numpy build-in function
36     pc = 2.5;
37     L = np.percentile(AUCvalues,pc)
38     H = np.percentile(AUCvalues,100-pc)
39
```

```
    #matrix for storing filtered maps
    AUCmap_corr = np.zeros((xRes,yRes,nSlices))

    #Loop through all R2*-AUC maps
    for s in range( nSlices ):
        for x in range(256):
            for y in range(256):
                AUCmap_corr[x,y,s] = AUCmap[x,y,s]
                #Remove low and high values
                if (AUCmap_corr[x,y,s]<L or AUCmap_corr[x,y,s]>H):
                    AUCmap_corr[x,y,s] = 0;

    #Reshape the 3D matrix into a 1D array with the filtered
    #R2*-AUC spectrum
    fAUCvalues = np.reshape(AUCmap_corr, xRes*yRes*nSlices, order='F')

    #Remove pixels with no R2*-AUC information
    fAUCvalues = fAUCvalues[fAUCvalues != 0]

    #check that total fAUC values is 95 % of original AUC array
    if ( (len(fAUCvalues) < 0.949*(len(AUCvalues))) or
    (len(fAUCvalues) > 0.951*(len(AUCvalues)))):
        print(' Filtration  not in concordance with requirements')

    #saving variables to a .npz-file in the patients' DPBC folder
    np.savez( filePath  + "OxyTarget_" + str(patient) + "/DPBC/AUCmap_filtered",
    AUCmap_corr=AUCmap_corr, nSlices=nSlices, xRes=xRes, yRes=yRes, fAUCvalues=
    fAUCvalues)
```

A.6 gaussian2d.py

```

#This script is used to perform a Gaussian 2D smoothing of the R2*-AUC maps,
#whose upper and lower 2.5 th percentiles are already filtered
#(filterR2StarAUCmaps.py). Smoothing with a Gaussian kernel is done to
#account for interfractional tumor motion (uncertainty). The script is based
#on MATLAB scripts written by Karina Rød.

import numpy as np
import matplotlib.pyplot as plt
import skimage

#path towards the OxyTarget data folder
filePath  = '/Users/frida/Documents/Fysmat 5. klasse/Masteroppgave/MR_data/'

patientList  = [24, 27, 32, 41, 43, 44, 47, 49, 50, 51, 52, 55, 56, 67, 74, 79, 80, 87,
      89, 90, 96, 107, 116, 120, 121, 125, 128, 131, 138, 146, 150, 153, 170]
nPatients  = len( patientList )

```

```
#Patients that have subvolumes larger than 1cm3
patientList2 = [41, 44, 47, 49, 55, 56, 80, 89, 96, 116, 121, 125, 128, 131, 138, 170]

#Loop that goes over all patients that are going to be analysed
for patient in patientList :
    #load R2* AUC maps
    loadFileR2map = np.load(filePath + "OxyTarget_" + str(patient) + "/R2Star/R2StarAUCMap.npz")
    loadFileR2map_filtered = np.load( filePath + "OxyTarget_" + str(patient) + "/DPBC/AUCmap_filtered.npz")

    #load values
    AUCvalues = loadFileR2map["AUCvalues"]
    AUCmap = loadFileR2map["AUCmap"]
    t = loadFileR2map["t"]
    tAUC = loadFileR2map["tAUC"]
    AUCmap_corr = loadFileR2map_filtered ["AUCmap_corr"]
    nSlices = loadFileR2map_filtered ["nSlices"]
    xRes = loadFileR2map_filtered ["xRes"]
    yRes = loadFileR2map_filtered ["yRes"]
    fAUCvalues = loadFileR2map_filtered ["fAUCvalues"]

    #Resolution info
    FOV = 180*180
    FOVx = 180
    FOVy = 180
    acqMatrix = 92*90
    wx = FOVx/92 #in-plane resolution in x direction
    wy = FOVy/90 #in-plane y resolution in y direction

    #PTV margin as estimated by Kleijnen et al. for GTV motion within
    #five weeks of CRT:
    LR=6.8 # PTV margin in left/right direction in mm
    AP=10.8 # PTV margin in anterior/posterior direction in mm

    #specifies the full-width at half maximum (FWHM) of the Gaussian
    #smoothing kernel in mm as the mean of the PTV margins, so an
    #isotropic kernel can be used

    FWHM = np.round(np.mean([LR,AP]),0) #round to nearest integer

    sigma_y = FWHM/(2.3548*wy) #2 mm
    sigma_x = FWHM/(2.3548*wx) #1.96mm

    #sigma in x and y direction differ only by hundreds: round to 2mm
    sigma = sigma_y
    filterSize = 2*np.ceil(2*sigma)+1

    #create 3D matrix for the R2*-AUC maps smoothed with a Gaussian kernel
```

```
    GFAUCmap = np.zeros((xRes,yRes,nSlices))

    #Loop through all slices and apply the 2D Gaussian filter to the R2*-AUC maps
    for s in range( nSlices ):
        GFAUCmap[:,:,s] = skimage. filters .gaussian(AUCmap_corr[:,:,s], sigma=sigma,
        truncate=2.0)

    #Reshape the 3D matrix into a 1D array with whole tumor R2*-AUC values
    gsAUCvalues = np.reshape(GFAUCmap, xRes*yRes*nSlices, order='F')

    #Remove pixels with no R2*-AUC information
    gsAUCvalues= gsAUCvalues[gsAUCvalues != 0]

    #Saving variables to a .npz-file in the patient's DPBC folder
    np.savez( filePath + "OxyTarget_" + str(patient) + "/DPBC/AUCmap_Gfiltered",
    GFAUCmap = GFAUCmap, gsAUCvalues = gsAUCvalues)
```

A.7 DPBCmaps.py

```

#This script generates DPBC dose maps by using the threshold R2*-AUC value
#found by Karina Rød to assign a dose escalation to the resistant subvolumes.

import numpy as np
import matplotlib.pyplot as plt
from matplotlib import rcParams
import cv2
import skimage.morphology
import nibabel as nib

#threshold values found by Karina
GlobalCUT_R2StarAUC_A = 1.9028e+03
GlobalCUT_R2StarAUC_B = 2.1655e+03
GlobalCUT_R2StarAUC_C = 2574

#path towards the OxyTarget data folder
filePath = '/Users/frida/Documents/Fysmat 5. klasse/Masteroppgave/MR_data/'

#patients that will be analysed (Patient 27 and 74 have been excluded due to
#extremal R2*-AUC values)
patientList = [24, 32, 41, 43, 44, 47, 49, 50, 51, 52, 55, 56, 67, 79, 80, 87, 89, 90,
    96, 107, 116, 120, 121, 125, 128, 131, 138, 146, 150, 153, 170]
#Patients that have subvolumes larger than 1cm3
patientList2 = [41, 44, 47, 49, 55, 56, 80, 89, 96, 116, 121, 125, 128, 131, 138, 170]

nPatients = len( patientList )

#Calculate the volume of each voxel
FOV = 180*180  #mm2
```

```
AcqMatrix = 92*90
sliceThck = 10 #mm
pixelSize = (FOV/AcqMatrix)/100 #cm2
voxelVolum = (sliceThck *(FOV/AcqMatrix))/1000 #cm3

#minimum achievable region size in diameter (cm)
min_diameter = 1

#minimum achievable region size (number of pixels in a circle with min_diameter cm)
threshold = (min_diameter/pixelSize)**2*(np.pi/4)

#make small clusters belong to the dominant subvolume if smaller than this threshold
threshold_clusters = 50
ind = 0

#Loop that goes over all patients that are going to be analysed
for patient in patientList :
    #load variables from files
    loadFileR2map_filtered = np.load( filePath + "OxyTarget_" + str(patient) + "/
    DPBC/AUCmap_filtered.npz")
    nSlices = loadFileR2map_filtered ["nSlices"]

    loadFileR2map_Gfiltered = np.load( filePath + "OxyTarget_" + str(patient) + "/
    DPBC/AUCmap_Gfiltered.npz")
    GFAUCmap = loadFileR2map_Gfiltered["GFAUCmap"]

    #Only needed for visualization of dose maps on T2 images
    loadT2im = np.load(filePath + "OxyTarget_" + str(patient) + "/T2/3Dmatrix.npz")
    T2im = loadT2im["imT2"]
    loadDynamicROI = np.load(filePath+"OxyTarget_"+str(patient)+"/dynamicROI.npz")
    z_vals = loadDynamicROI["z_vals"]

    #Define that ROI voxels with R2*-AUC above threshold form the resistant
    #compartment, R, and voxels below form the sensitive compartment, S.

    #Set two different dose levels for S and R
    D_S = 50 #Total dose to S
    b = 1.2 #Dose boost factor
    D_R = 50*b #Total dose to R

    #3D matrix that holds preliminary dose prescription maps
    doseMap_a = np.zeros((256,256,nSlices))
    #Store dose maps when removing small subvolumes
    doseMap_b = np.zeros((256,256,nSlices))
    #Store dose maps when removing small subvolumes and fill small clusters
    doseMap_c = np.zeros((256,256,nSlices))
    #Store the region of the whole tumor (ROI)
    ROI = np.zeros((256,256, nSlices ))
    #Store the regions with R2*-AUC below threshold
```

```
    S_regs = np.zeros((256,256, nSlices))
    #Store the regions with R2*-AUC above threshold
    R_regs = np.zeros((256,256, nSlices))
    #Arrays to help contouring the dose maps
    contouring_a = np.zeros((256,256, nSlices))
    contouring_c = np.zeros((256,256, nSlices))

    no_S_a = 0 #number of all pixels with value below threshold in tumor
    no_R_a = 0 #number of all pixels with value above threshold in tumor
    no_ROI = 0 #number of pixels inside ROI

    #Loop through every pixel-value (R2* AUC) to check if it is above or
    #below the threshold
    for s in range(nSlices):
        for x in range(256):
            for y in range(256):
                if ((GFAUCmap[x,y,s]) != 0): #check only inside ROI
                    if (GFAUCmap[x,y,s] > GlobalCUT_R2StarAUC_C):
                        doseMap_a[x,y,s] = D_R
                        R_regs[x,y,s] = 1
                        S_regs[x,y,s] = 0
                        contouring_a[x,y,s] = 0
                        no_R_a += 1
                    else:
                        doseMap_a[x,y,s] = D_S
                        R_regs[x,y,s] = 0
                        S_regs[x,y,s] = 1
                        contouring_a[x,y,s] = 1
                        no_S_a += 1
                    ROI[x,y,s] = 1
                    no_ROI += 1
                else:
                    #useful for nice plotting
                    GFAUCmap[x,y,s] = np.nan
                    doseMap_a[x,y,s] = np.nan

    #Want to cut hypoxic regions smaller than a threshold and fill small clusters inside the
    #dominant subvolume to make the dose plans clinically feasible

    #no voxels contributing to R when small regions removed
    no_R_b = 0
    #no voxels contributing to S when small regions removed and clusters are filled (temp)
    no_S_c_temp = 0
    #no voxels contributing to R when small regions removed and clusters are filled
    no_R_c = 0

    for s in range(nSlices):
        #Cut hypoxic regions smaller than a threshold
        img = np.array(R_regs[:,:,s], dtype=np.uint8)
```

```
        _, binary = cv2.threshold(img, 0, 1, cv2.THRESH_BINARY)
        binary = np.array(binary, dtype=np.bool)
        remove_small_R = skimage.morphology.remove_small_objects
        (binary, min_size = threshold, connectivity =3)

        #Make small S clusters inside R with volume less than
        #threshold_clusters a part of R
        filled_R = ~ skimage.morphology.remove_small_objects
        (~remove_small_R, min_size = threshold_clusters )

        #Make small holes in S with volume less than threshold_clusters a part of S
        img = np.array(S_regs [:,:, s], dtype=np.uint8)
        _, binary = cv2.threshold(img, 0, 1, cv2.THRESH_BINARY)
        binary = np.array(binary, dtype=np.bool)
        filled_S = ~ skimage.morphology.remove_small_objects
        (~binary, min_size = threshold_clusters )

        #Make dose maps
        for x in range(256):
            for y in range(256):
                #make dose map b
                if (ROI[x,y,s] == 1):
                    doseMap_b[x,y,s] = D_S
                else:
                    doseMap_b[x,y,s] = np.nan
                if (remove_small_R[x,y] == 1):
                    doseMap_b[x,y,s] = D_R
                    #counting all voxels contributing to R for dose map b
                    no_R_b += 1

                #make final dose map c
                if (ROI[x,y,s] == 1 or filled_S [x,y] == 1):
                    doseMap_c[x,y,s] = D_S
                    #temporary voxels contributing to S for dose map c
                    no_S_c_temp += 1
                    contouring_c [x,y,s] = 1
                else:
                    doseMap_c[x,y,s] = np.nan

                if ( filled_R [x,y] == 1):
                    doseMap_c[x,y,s] = D_R
                    #counting all voxels contributing to R for dose map c
                    no_R_c += 1
    no_S_b = no_ROI - no_R_b
    no_S_c = no_S_c_temp - no_R_c

    #Save variables
    #different sizes of min_diameter need to be run and saved separately
    np.savez( filePath + "OxyTarget_" + str(patient) + "/DPBC/DPBC_3d", ROI = ROI,
```

```
    doseMap_a = doseMap_a, doseMap = doseMap_c, no_S_a = no_S_a, no_R_a = no_R_a,
    no_R_b = no_R_b, no_S_b = no_S_b, no_R_c = no_R_c, no_S_c = no_S_c)

    #Must make dosemap "binary" to save it as a nifti file for planning in Raystation.
    #Value 1 represent the tumor and value 2 represent the subvolumes.
    binary_dosemap = np.zeros((256,256, nSlices ))
    for s in range( nSlices ):
        for x in range(256):
            for y in range(256):
                if (doseMap_c[x,y,s]==D_S):
                    binary_dosemap[x,y,s]=1
                if (doseMap_c[x,y,s]==D_R):
                    binary_dosemap[x,y,s]=2

    #Must swap back to original
    binary_dosemap_swaped = np.swapaxes(binary_dosemap, 0, 1)
    #Get the right header information from a reference nifti file
    nii_ref = nib.load( filePath + "OxyTarget_" + str(patient) + '/gtv1_onR2star.nii')
    header_ref = nii_ref.header.copy()
    #Save binary_dosemap as nifti file along with reference header
    doseMap_nifti = nib.Nifti1Image(binary_dosemap_swaped, None, header=header_ref)
    doseMap_nifti.to_filename("Contours_"+str(patient))

    #Plot dose maps
```

A.8 TCP.py

```

#This script calculates the TCP for DPBC plans and uniform dose boost

import numpy as np
import matplotlib.pyplot as plt
import scipy.optimize
from scipy.stats import sem, t

filePath = '/Users/frida/Documents/Fysmat 5. klasse/Masteroppgave/MR_data/'

patientList = [24, 32, 41, 43, 44, 47, 49, 50, 51, 52, 55, 56, 67, 79, 80, 87, 89, 90,
    96, 107, 116, 120, 121, 125, 128, 131, 138, 146, 150, 153, 170]

#Patients that still have regions with hypoxia when min diameter = 1 cm (16)
patientList2 = [41, 44, 47, 49, 55, 56, 80, 89, 96, 116, 121, 125, 128, 131, 138, 170]

#Patients that still have regions with hypoxia when min diameter = 0.5 cm (29)
patientList3 = [24, 32, 41, 43, 44, 47, 49, 50, 51, 55, 56, 79, 80, 87, 89, 90, 96,
    107, 116, 120, 121, 125, 128, 131, 138, 146, 150, 153, 170]

nPatients = len( patientList2 )

```

```
b_values = np.around(np.arange(1,2,0.01), decimals=3)

#The volume of each voxel
FOV = 180*180 #mm2
AcqMatrix = 92*90
sliceThck = 10 #mm
voxelVolmm = sliceThck * (FOV/AcqMatrix) #mm3
voxelVolcm = voxelVolmm/1000 #cm^3

#3 different alpha/beta ratio in S found from literature
aS_list = [0.339, 0.335, 0.450]
bS_list = [0.067, 0.030, 0.039]
ab_list = [0.339/0.067, 0.335/0.030, 0.450/0.039]

#Matrices used to plot b-value vs TCP
TCP_DPBC_matrix = np.zeros((len(b_values), nPatients))
TCP_uniform_matrix = np.zeros((len(b_values), nPatients))

plt.figure()
i=0
for patient in patientList2:
    StandardTCPList = []
    DPBC_TCPList = []
    TCP_uniform = []

    loadFile = np.load(filePath+"OxyTarget_"+str(patient)+"/DPBC/DPBC_3d.npz")
    S = loadFile["no_S_c"] #no pixels contributing to S when small regions removed
    R = loadFile["no_R_c"] #no pixels contributing to R when small regions removed

    #Define parameters for TCP modelling
    dS = 2      #fractional doses to S
    n = 25      #total fractions

    #Assumed cell densities in R and S (cells/cm^3)
    rhoS = 10**6
    rhoR = 10**6

    OER = 1.75

    #Alpha/beta ratio in S found from literature
    aS = aS_list[2]
    bS = bS_list[2]
    ab = ab_list[2]

    #Define alpha/beta ratio in R via OER
    aR = aS/OER
    bR = bS/(OER**2)
    abR = aR/bR

```

```
    Vs = S * voxelVolcm #volume of S
    Vr = R * voxelVolcm #volume of R

    #find alpha value that fits the cohort TCP for standard dose
    TCP_cohort = 5/16

    def F(alpha):
        return TCP_cohort - np.exp(-rhoS * Vs * np.exp(-n * alpha * dS *(1 + dS/ab))
    ) * np.exp(-rhoR * Vr * np.exp(-n * alpha/OER * dS *(1 + dS/abR)))

    alpha = scipy.optimize.broyden1(F, 0.5)
    aS = alpha

    for b in b_values:

        OER = 1.75
        aR = aS/OER
        dR = dS*b #fractional doses to R

        #Calculate the TCP for the DPBC plan
        #TCP for S (equation 2.12)
        constS = n * aS * dS *(1 + dS/ab)
        SFs = np.exp(-constS) #Surviving fraction
        TCPs = np.exp(-rhoS * Vs * SFs)
        #TCP for R (equation 2.12)
        constR = n * aR * dR *(1 + dR/abR)
        SFr = np.exp(-constR);
        TCPr = np.exp(-rhoR * Vr * SFr)
        #Total TCP for the DPBC plan (equation 2.13)
        TCP_DPBC = TCPs * TCPr
        DPBC_TCPList.append(TCP_DPBC * 100)

        #Calculate TCP for R for the standard plan
        #gives standard dose to R
        constR_std = n * aR * dS *(1 + dS/abR)
        SF_r_std= np.exp(-constR_std)
        TCP_r_STD = np.exp(-rhoR * Vr * SF_r_std)
        #TCP for standard RT scheduling (equation 2.13)
        TCP_STD = TCPs * TCP_r_STD
        StandardTCPList.append(TCP_STD * 100)

        #Calculate TCP for S and R uniform dose boost
        #Uniformly escalated dose (equation 2.14)
        d_u = dS * ((Vs + b * Vr)/(Vs + Vr))
        #Survival fraction
        SF_s_uniform = np.exp(-n * aS * d_u *(1 + d_u/ab))
        SF_r_uniform = np.exp(-n * aR * d_u *(1 + d_u/abR))
        #Calculate TCP for R and S
        TCP_s_uniform = np.exp(-rhoS * Vs * SF_s_uniform)
```

```
118             TCP_r_uniform = np.exp(-rhoR * Vr * SF_r_uniform)
119
120             #TCP for uniform dose boost
121             TCP_u = TCP_s_uniform * TCP_r_uniform
122             TCP_uniform.append(TCP_u * 100)
123
124         #Store data in matrix
125         TCP_DPBC_matrix[:,i] = DPBC_TCPList
126         TCP_uniform_matrix[:,i] = TCP_uniform
127         i+=1
128
129         #Plot TCP for each patient
130
131 #Find average values for TCP for each b-value
132 average_TCP_DPBC = np.mean(TCP_DPBC_matrix, axis=1)
133 average_TCP_uniform= np.mean(TCP_uniform_matrix, axis=1)
134
135 #Plot average TCP + confidence interval
```

A.9 CellDensityFromADC.py

```
1
2 #This script calculates the cell density from average ADC values based on a model
3 #created by Casares-Magaz et al. The TCP for the DPBC plans are calculated with
4 #ADC-based cell densities and compared with the TCP based on constant densities.
5
6 import numpy as np
7 import matplotlib.pyplot as plt
8 from matplotlib import rcParams
9 import nibabel as nib
10
11 filePath = '/Users/frida/Documents/Fysmat 5. klasse/Masteroppgave/MR_data/'
12
13 #Need to exclude 138 as this patient no longer has subvolume larger than 1 cm^3
14 #due to adapted ROI
15 patientList = [41, 44, 47, 49, 55, 56, 80, 89, 96, 116, 121, 125, 128, 131, 170]
16 TRG = [1, 2, 2, 3, 1, 0, 3, 3, 2, 2, 1, 2, 3, 0, 2]
17
18 nPatients = len( patientList )
19
20 #Alpha and beta values found in the litterature
21 aS_list = [0.339, 0.335, 0.450]
22 bS_list = [0.067, 0.030, 0.039]
23
24 #Alpha/beta ratio in S
25 aS = aS_list [2]
26 bS = bS_list [2]
27 ab = aS/bS
28
```

```
#boost factor values
b_values = np.around(np.arange(1,1.51,0.01),3)

#Average ADC in whole tumor
ADC_tumor_list = [7.849e-04, 8.649e-04, 6.624e-04, 5.548e-04, 1.186e-03,
                  7.375e-04, 1.382e-03, 8.885e-04, 1.170e-03, 8.302e-04,
                  1.243e-03, 9.630e-04, 1.154e-03, 1.046e-03, 1.187e-03]
#Average ADC in R
ADC_R_list = [8.778e-04, 8.857e-04, 6.863e-04, 5.624e-04, 1.113e-03,
              6.505e-04, 1.352e-03, 8.277e-04, 9.139e-04, 9.964e-04,
              1.133e-03, 7.567e-04, 1.055e-03, 8.344e-04, 9.933e-04]
#Average ADC in S
ADC_S_list = [7.826e-04, 8.628e-04, 6.587e-04, 5.525e-04, 1.192e-03,
              7.411e-04, 1.387e-03, 9.199e-04, 1.175e-03, 8.219e-04,
              1.250e-03, 9.680e-04, 1.166e-03, 1.068e-03, 1.247e-03]

#Lists for storing the cell densities for each patient
rhoR_list = []
rhoS_list = []
rho_list = []

#Calculate the cell density based on equation 3.3
for i in range(nPatients):
    rho_S = (9.9*(1 - 1/(1+np.exp((1.3-ADC_S_list[i]*10**3)/0.1)) + 0.1))*10**6
    rho_R = 9.9*(1 - 1/(1+np.exp((1.3-ADC_R_list[i]*10**3)/0.1)) + 0.1)*10**6
    rho = 9.9*(1 - 1/(1+np.exp((1.3-ADC_tumor_list[i]*10**3)/0.1)) + 0.1)*10**6

    rhoS_list.append(rho_S)
    rhoR_list.append(rho_R)
    rho_list.append(rho)

#Matrices used for plotting and to find average TCP
TCP_ADCbased_matrix = np.zeros((len(b_values), nPatients))
TCP_assumed_matrix = np.zeros((len(b_values), nPatients))
TCP_assumed2_matrix = np.zeros((len(b_values), nPatients))

i=0
plt.figure()
for patient in patientList:

    #Save cell densities for making box plot
    rho_tumor = np.round(rho_list[i]/10**7, 3)
    rho_S = np.round(rhoS_list[i]/10**7, 3)
    rho_R = np.round(rhoR_list[i]/10**7, 3)
    np.savez(filePath + "OxyTarget_" + str(patient) + "/celldensities", rho_R=rho_R,
    rho_S=rho_S, rho_tumor=rho_tumor)

    #Store the TCP for each b-value when cell density is assumed to be a constant
    value of 10^6
```

```
    TCP_assumed = []
    #Store the TCP for each b-value when cell density is assumed to be a constant value of 10^7
    TCP_assumed2 = []
    #Store the TCP for each b-value when cell density is based on ADC values
    TCP_ADCbased = []

    loadFile = np.load( filePath +"OxyTarget_"+str(patient)+"/DPBC/DPBC_3d.npz")
    S = loadFile["no_S_c"] #number of pixels contributing to S when small regions removed
    R = loadFile["no_R_c"] #number of pixels contributing to R when small regions removed

    OER = 1.75

    #Alpha/beta ratio in R
    aR = aS/OER
    bR = bS/(OER**2)
    abR = aR/bR

    #Fractional doses to S
    dS = 2
    n = 25

    #Assumed cell density in R and S ( cells /cm^3)
    rhoS = 10**6
    rhoR = 10**6

    #Calculate the volume of each voxel
    FOV = 180*180 #mm2
    AcqMatrix = 92*90
    sliceThck = 10 #mm
    voxelVolmm = sliceThck * (FOV/AcqMatrix) #mm3
    voxelVolcm = voxelVolmm/1000 #cm^3

    Vs = S * voxelVolcm #volume of S
    Vr = R * voxelVolcm #volume of R

    #find alpha value that fits the cohort TCP for standard dose
    TCP_cohort = 5/16

    def F(alpha):
        return TCP_cohort - np.exp(-rhoS * Vs * np.exp(-n * alpha * dS *(1 + dS/ab)) ) * np.exp(-rhoR * Vr * np.exp(-n * alpha/OER * dS *(1 + dS/abR)))

    alpha = scipy.optimize.broyden1(F, 0.5)
    aS = alpha

    #Assumed cell density in R and S ( cells /cm^3)
```

```
    rhoS_2 = 10**7
    rhoR_2 = 10**7

    #Calculated cell density in R and S from ADC maps
    rhoR_ADCbased = rhoR_list[i]
    rhoS_ADCbased = rhoS_list[i]
    #Average cell density in tumor
    rho_ADCbased = rho_list[i]

    for b in b_values:

        OER = 1.75
        aR = aS/OER
        dR = dS*b

        #Surviving fraction for S
        constS = n * aS * dS *(1 + dS/(ab))
        SFs = np.exp(-constS)

        #Surviving fraction for R
        constR = n * aR * dR *(1 + dR/(abR))
        SFr = np.exp(-constR)

        #TCP for S with assumed cell density of 10^6
        TCPs = np.exp(-rhoS * Vs * SFs)

        #TCP for R with assumed cell density of 10^6
        TCPr = np.exp(-rhoR * Vr * SFr)

        #TCP for S with ADC-based cell density
        TCP_ADCbased_S = np.exp(-rhoS_ADCbased * Vs * SFs)

        #TCP for R with ADC-based cell density
        TCP_ADCbased_R = np.exp(-rhoR_ADCbased * Vr * SFr)

        #TCP for S with assumed cell density of 10^7
        TCP_assumed2_S = np.exp(-rhoS_2 * Vs * SFs)

        #TCP for R with assumed cell density of 10^7
        TCP_assumed2_R = np.exp(-rhoR_2 * Vr * SFr)

        #TCP for the tumor with assumed cell density of 10^6
        TCP_1 = TCPs * TCPr
        TCP_assumed.append(TCP_1*100)

        #TCP for the tumor with ADC-based cell density
        TCP_2 = TCP_ADCbased_R * TCP_ADCbased_S
        TCP_ADCbased.append(TCP_2*100)
```

```
171             #TCP for the tumor with assumed cell density of 10^67
172             TCP_3 = TCP_assumed2_R * TCP_assumed2_S
173             TCP_assumed2.append(TCP_3*100)
174
175         #Store data in matrix to find average TCP
176         TCP_ADCbased_matrix[:,i] = TCP_ADCbased
177         TCP_assumed_matrix[:,i] = TCP_assumed
178         TCP_assumed2_matrix[:,i] = TCP_assumed2
179         i+=1
180
181         #Plot TCP for each patient
182
183 #Find average values for TCP for each b-value
184 average_TCP_ADCbased = np.mean(TCP_ADCbased_matrix, axis=1)
185 average_TCP_assumed = np.mean(TCP_assumed_matrix, axis=1)
186 average_TCP_assumed2= np.mean(TCP_assumed2_matrix, axis=1)
187
188 #Plot average TCP + confidence interval
```

A.10 Boxplot.py

```
1  """
2  This script make box plots to visualize the relationship
3  between the volume of R and TRG, and the relationship between
4   cell density and TRG. Statistical testing was done for TRG
5  vs R done in programming language "R".
6  """
7
8  import numpy as np
9  import matplotlib.pyplot as plt
10
11  filePath = '/Users/frida/Documents/Fysmat 5. klasse/Masteroppgave/MR_data/'
12
13  patientList = [24, 32, 41, 43, 44, 47, 49, 50, 51, 52, 55, 56, 67, 79, 80, 87, 89, 90,
        96, 107, 116, 120, 121, 125, 128, 131, 138, 146, 150, 153, 170]
14 TRG_list = [2, 2, 1, 1, 2, 2, 3, 1, 1, 2, 1, 0, 1, 3, 3, 0, 3, 2, 2, 1, 2, 1, 1, 2, 3,
        0, 3, 2, 0, 2, 2]
15
16  patientList2 = [41, 44, 47, 49, 55, 56, 80, 89, 96, 116, 121, 125, 128, 131, 170]
17 TRG_list2 = [1, 2, 2, 3, 1, 0, 3, 3, 2, 2, 1, 2, 3, 0, 2]
18
19 #Found by setting min_diameter=0.5 in DPBCmaps.py
20 R_threshold_05 = [1728, 1458, 6109, 603, 3779, 6877, 8128, 3450, 982, 0, 7604, 4499,
      0, 1385, 8794, 1534, 6493, 5337, 7615, 317, 5186, 133, 1596, 1646, 3510, 5564,
      2757, 142, 485, 515, 3844]
21
22 #Array for each level of TRG to store no. R-voxels for each patient in this group
23 #No threshold
24 R_TRG0 = []
```

```
R_TRG1 = []
R_TRG2 = []
R_TRG3 = []

#Threshold = 0.5 cm^3
R05_TRG0 = []
R05_TRG1 = []
R05_TRG2 = []
R05_TRG3 = []

#Threshold = 1 cm^3
R1_TRG0 = []
R1_TRG1 = []
R1_TRG2 = []
R1_TRG3 = []

#Array for each level of TRG to store the cell density for each patient in this group
#Cell densities for the tumor
tumor_TRG0 = []
tumor_TRG1 = []
tumor_TRG2 = []
tumor_TRG3 = []

#Cell densities for R
RTRG0 = []
RTRG1 = []
RTRG2 = []
RTRG3 = []

#Cell densities for S
S_TRG0 = []
S_TRG1 = []
S_TRG2 = []
S_TRG3 = []

#The volume of each voxel
FOV = 180*180  #mm^2
AcqMatrix = 92*90
sliceThck = 10 #mm
pixelSize = (FOV/AcqMatrix)/100 #cm^2
voxelVolum = (sliceThck *(FOV/AcqMatrix))/1000 #cm^3

for i in range(3):
    #TRG vs R
    index = 0
    for patient in patientList :
        loadFile = np.load( filePath + "OxyTarget_" + str(patient)
        + "/DPBC/DPBC_3d.npz")
        #no pixels contributing to R
```

```
        R = loadFile["no_R_a"]
        #no pixels contributing to R for subvolume limit = 0.5 cm^2
        R_05 = R_threshold_05[index]
        #no pixels contributing to R for subvolume limit = 1 cm^2
        R_1 = loadFile["no_R_c"]

        #Convert to volume (cm^3)
        vol_R = R * voxelVolum
        vol_R_05 = R_05 *voxelVolum
        vol_R_1 = R_1 *voxelVolum

        if (TRG_list[index]==0):
            R_TRG0.append(vol_R)
            R1_TRG0.append(vol_R_1)
            R05_TRG0.append(vol_R_05)

        elif (TRG_list[index]==1):
            R_TRG1.append(vol_R)
            R1_TRG1.append(vol_R_1)
            R05_TRG1.append(vol_R_05)

        elif (TRG_list[index]==2):
            R_TRG2.append(vol_R)
            R1_TRG2.append(vol_R_1)
            R05_TRG2.append(vol_R_05)

        elif (TRG_list[index]==3):
            R_TRG3.append(vol_R)
            R1_TRG3.append(vol_R_1)
            R05_TRG3.append(vol_R_05)

        index += 1

    #TRG vs cell density
    index2=0
    for patient in patientList2 :
        loadCelldensities = np.load( filePath + "OxyTarget_" + str(patient)
        + "/ celldensities .npz")
        rhoR = loadCelldensities ["rho_R"] #Cell density in R
        rhoS = loadCelldensities ["rho_S"] #Cell density in S
        rho = loadCelldensities ["rho_tumor"] #Cell density in tumor

        if (TRG_list2[index2]==0):
            tumor_TRG0.append(rho)
            RTRG0.append(rhoR)
            S_TRG0.append(rhoS)

        elif (TRG_list2[index2]==1):
            tumor_TRG1.append(rho)
```

```
                RTRG1.append(rhoR)
                S_TRG1.append(rhoS)

            elif (TRG_list2[index2]==2):
                tumor_TRG2.append(rho)
                RTRG2.append(rhoR)
                S_TRG2.append(rhoS)

            elif (TRG_list2[index2]==3):
                tumor_TRG3.append(rho)
                RTRG3.append(rhoR)
                S_TRG3.append(rhoS)

            index2 += 1

        #Plot TRG vs R
        #Plot TRG vs cell density

#Save the info for TRG vs R for statistical analysis in programming language "R".
with open("TRGvsR.txt", 'w') as f:
        lists = [R_TRG0, R_TRG1, R_TRG2, R_TRG3, R05_TRG0, R05_TRG1, R05_TRG2,
        R05_TRG3, R1_TRG0, R1_TRG1, R1_TRG2, R1_TRG3]
        names = ['R_TRG0', 'R_TRG1', 'R_TRG2', 'R_TRG3', 'R05_TRG0', 'R05_TRG1', '
        R05_TRG2', 'R05_TRG3', 'R1_TRG0', 'R1_TRG1', 'R1_TRG2', 'R1_TRG3']
        for i in range(len( lists )):
            f.write(names[i])
            for s in lists [i]:
                f.write(" %.4f"%s)
            f.write("\n")
```

A.11 MannWhitneyTest.r

```
#This script loads the lists from TRGvsR.py containing R-volumes
#for each TRG, and use Mann Whitney U-test to test if they differ .
#p-values for each comparison is written to a text file .

# Each line is the name of the list , and then its content
file = readLines("/Users/fredrine/Desktop/TRGvsR.txt")
names = c()
for (i in 1:12){
  names = c(names,as.list( strsplit ( file [i]," ")) [[1]][1])
}
 firstlist = as.numeric(as. list ( strsplit ( file [1]," ")) [[1]][-1])
# The list values are gathered as a list of lists
data = list( firstlist )
for (i in 2:12){
   otherlist = as.numeric(as. list ( strsplit ( file [i]," ")) [[1]][-1])
  data = append(data,list( otherlist ))
}
```

```
names(data) = names

#wilcox.test is equivalent to the Mann Whitney U-test for this data
pvals1 = c()
for (i in 1:3){
  for (j in (i+1):4){
    p = wilcox.test(data[[i]], data[[j]])$p.value
    pvals1 = c(pvals1,paste(names[i]," vs ",names[j],": ",p,sep=""))
  }
}

pvals2 = c()
for (i in 5:7){
  for (j in (i+1):8){
    p = wilcox.test(data[[i]], data[[j]])$p.value
    pvals2 = c(pvals2,paste(names[i]," vs ",names[j],": ",p,sep=""))
  }
}

pvals3 = c()
for (i in 9:11){
  for (j in (i+1):12){
    p = wilcox.test(data[[i]], data[[j]])$p.value
    pvals3 = c(pvals3,paste(names[i]," vs ",names[j],": ",p,sep=""))
  }
}
```

B Comparison of TRG and R

Table B.1: The median R volumes in addition to the results of the Mann-Whitney U-test for the comparison of TRG and the volume of R before removing any of the subvolumes.

	Median R volumes (cm^3)		
Comparison	**Group 1**	**Group 2**	**p-value**
TRG0 vs TRG1	142	86.0	0.795
TRG0 vs TRG2	142	137	1
TRG0 vs TRG3	142	227	0.023
TRG1 vs TRG2	86.0	137	0.263
TRG1 vs TRG3	86.0	227	0.007
TRG2 vs TRG3	137	227	0.013

Table B.2: The median R volumes in addition to the results of the Mann-Whitney U-test for the comparison of TRG and the volume of R when subvolumes smaller than 0.5 cm^3 have been removed.

	Median R volumes (cm^3)		
Comparison	**Group 1**	**Group 2**	**p-value**
TRG0 vs TRG1	118	38.4	0.279
TRG0 vs TRG2	118	108	1
TRG0 vs TRG3	118	196	0.058
TRG1 vs TRG2	38.4	108	0.092
TRG1 vs TRG3	38.4	196	0.000
TRG2 vs TRG3	108	196	0.032

Table B.3: The median R volumes in addition to the results of the Mann-Whitney U-test for the comparison of TRG and the volume of R when subvolumes smaller than 1 cm^3 have been removed.

	Median R volumes (cm^3)		
Comparison	**Group 1**	**Group 2**	**p-value**
TRG0 vs TRG1	33.8	0.0	0.217
TRG0 vs TRG2	33.8	10.4	0.829
TRG0 vs TRG3	33.8	112	0.055
TRG1 vs TRG2	0.0	10.4	0.168
TRG1 vs TRG3	0.0	112	0.000
TRG2 vs TRG3	10.4	112	0.006

Frida Marie Ihle Julbø

MR-based radiotherapy dose painting: modelling studies

NTNU
Norwegian University of
Science and Technology